NTNU

Norwegian University of
Science and Technology

Multiscalar Structural Study of the Brittle Deformation History in the Åna-Sira Anorthosite massif, Rogaland, Southwestern Norway

Anne-Line Kvale Ferstad

Geology
Submission date: May 2017
Supervisor: Giulio Viola, IGP

Norwegian University of Science and Technology
Department of Geoscience and Petroleum

Abstract

The c. 930 Ma Åna-Sira anorthosite massif (ÅS) is a part of the Rogaland Anorthosite Province, situated in the county of Sokndal, Rogaland. In this thesis, multiscalar efforts are aimed at unraveling the spatial and temporal evolution of the highly fractured and faulted basement in the study area. Five prominent lineament systems (N-S, ENE-WSW, NE-SW, WNW-ESE, NW-SE) are distinguished using lineament mapping and give important information about the main spatial distribution of fractures and faults. Lineament maps, together with detailed structural mapping, microstructural analysis and radiometric dating reveal several deformation phases in ÅS. Rapid cooling of the c. 930 Ma old magmatic body generated cooling joints. The intrusion of the Fe-Ti-norite dikes 10 Ma later, exploited the cooling joints generating NW-SE trending structures which were later displaced by NE-SW trending structures. Further deformation was accommodated by NE-SW directed oblique extension leading to the emplacement of Egersund dike swarm and formation of WNW-ESE trending structures c. 616 Ma ago. During the Cambrian, Caledonian contraction caused top-to-SE displacement with folding of NE-SW trending faults that were later reactivated in a brittle fashion with top-to-NW normal faulting due the Caledonian extensional collapse in Devonian. Extensional normal reactivation of the inherited faults occurred during three phases in the Mesozoic generating N-S, WNW-ESE and NE-SW trending structures and development of gouge-rich and brecciated rocks.

Detailed mesoscopic, microstructural and radiometric analysis of the important large-scale NE-SW trending Helleren Fault Zone (HFZ) revealed several different processes leading to strain localization within the fault. Rapid cooling of the anorthosite in the Neoproterozoic caused the formation of cooling joints, allowed for the ingress of fluids and percolation of new minerals, whereby alteration of the anorthosite along the veins weakened the HFZ. When early NW-SE directed, Caledonian shortening (Cambrian) affected the HFZ, strain localized along the cooling joints creating local foliation at the HFZ with a protomylonitic texture implying top-to-SE reverse transfer. Increasing lateral displacement during the Silurian continent-continent collision caused folding of the fault. The latest deformation was accommodated by a shift in the stress field due to the extensional collapse of Caledonian Orogeny, and caused normal top-to-NW brittle faulting of the HFZ. By utilize K/Ar dating of synkinematic illite, the timing of the last temporal evolution of multiply-reactivated brittle-ductile HFZ is constrained. All the ages vary as a function of grain size, whereby ages decrease with decreasing grain size. The results from the radiometric dating display a final fault increment (finest grain size) at the Helleren Fault Zone at 403 ± 10 Ma, related to Caledonian extension and collapse of the orogeny.

Sammendrag

Det c. 930 Ma gamle Åna-Sira anortositt massiv (ÅS) er en del av Rogaland Anortositt Provins og ligger i distriktet Sokndal, Rogaland. I dette prosjektet, ble det tatt i bruk en fler-skala metode for a forstå den romlige og tidsmessige geologiske utviklingen av grunnfjellet som er i høy grad oppsprukket og rommer flere forkastinger. Lineamentkartlegging ble brukt til å kartlegge fem gjennomgående lineament systemer (N-S, ØNØ-VSV, NØ-SV, VNV-ØSØ, NV-SØ), som gå viktig informasjon om den romlige fordelingen av sprekker og forkastinger. Lineamentkartlegging sammen med detaljert strukturell kartlegging, mikrostruktur analyse og radiometrisk datering avslører flere deformasjonsfaser i ÅS. Hurtig nedkjøling av den c. 930 Ma gamle magmatiske kroppen førte til dannelse av nedkjølingsårer. Intrusjonen av Fe-Ti-noritt gangene 10 Ma senere utnyttet disse nedkjølingsårene og utviklet strukturer orientert NV-SØ som senere ble forskjøvet av NØ-SV orienterte strukturer. Videre deformasjon ble dannet av skjev NØ-SV ekstensjon som førte til intrusjonen av Egersund gang kompleks og dannelsen av VNV-ØSØ orienterte strukturer for c. 616 Ma siden. Under Kambrisk tid førte Kaledonisk kontraksjon til topp-til-SØ reversforskyvning med folding av NØ-SV orienterte forkastinger som senere ble reaktivert i det sprø regime med topp-til-NW normal forskyvning, som følge av Kaledonsk ekstensjons-kollaps i Devon. Reaktivering av nedarvede forkastinger skjedde under tre ekstensjonsfaser i Mesozoikum som utviklet N-S, WNW-ESE og NE-SW orienterte strukturer og dannelse av bergarter rike på forkastingsmel og forkastningsbreksje.

Detaljert mesoskopisk, mikrostrukturell og radiometrisk analyse av den betydningsfulle stor-skala NØ-SV orienterte Helleren Forkastings Sone (HFZ) avslører flere forskjellige prosesser som førte til formforandring lokalisert i forkastningen. Hurtig nedkjøling av bergarten i Neoproterozoikum førte til dannelse av nedkjølingsårer som åpnet for innstrømning av fluider og sig av sekundære mineralfaser som førte til omdanning av bergarten langs årene og reduserte bruddstyrken til HFZ. Når den tidlige fasen av Kaledonsk kompresjon påvirket HFZ, ble formforandringen lokalisert langs de nedarvede nedkjølingsårene og lokal foliasjon ble dannet langs disse hvor proto-mylonittisk tekstur viser topp-til-SØ forflytting. Økende lateral forflytting under Silurisk kontinent-kontinent kollisjon førte til folding av forkastningen. Siste deformasjon skjedde som følge av en endring av spenningssituasjon fra kompresjon til ekstensjon og kollaps av orogenesen som førte til topp-til-NV normal bevegelse av HFZ. K/Ar-datering av syn-kinematisk illitt ble brukt til å finne den tidsmessige utviklingen av den sprø-duktile HFZ. Alle aldere som ble funnet varierer som en funksjon av kornstørrelse, hvor alder minker med minkende kornstørrelse. Resultatet av dateringer viser at siste forkastings tilvekst (minste kornstr.) på HFZ skjedde for 403 ± 10 Ma siden og er relatert til Kaledonsk ekstensjon og kollaps av orogenesen.

Acknowledgements

This thesis is the final project of my Mater of Science in Geology at the Department of Geoscience and Petroleum, Norwegian University of Science and Technology (NTNU). It has been funded part by NTNU and NGU.

First of all, I would like to thank my supervisor, Prof. Giulio Viola for his guidance and the feedback he has given me during my masters. Your encouragement and expertise has inspired me to work hard and I have learned a lot from you. In addition, I would like to thank Dr. Espen Torgersen at NGU for always being so helpful and always have time to answer my question and look at my data. Nolwenn Coint, thank you for helping me with petrology.

I would also like to thank Titania AS and geotechnical Engineer Kostas Botsialas for being so welcoming and let me work in the pit and help with accommodation.

Fam. Ferstad and Sondre, thank you for always supporting me and encourage me to do my best. Torbjørn Bartels, thank you for language correction of my text.

These five years at NTNU would not have been the same without my fellow students, Cathinka, Eric, Bård, Odd and Sondre for great company during field trips and long days at the office. Your friendship means a lot to me and thank you for letting me win Curve Fever a couple of times during these years.

Table of content

Table of figures

Abbreviations

An - Anorthite
ÅS – Åna Sira massif
BKSK – Bjerkreim-Sokndal layered intrusion
Bt - Biotite
Cal – Calcite
Chl - Chlorite
Cpx – Clinopyroxene
DEM – Digital Elevation Model
Ep - Epidote
Fsp- Feldspar
FZ- Fault Zone
Hbl – Hornblende
Hem - Hematite
HFZ – Helleren Fault Zone
HSZ – Hardangerfjord Shear zone
Ill – Illite
Ilm – Ilmenite
Kfsp- K-feldspar
Kln – Kaolin
LiDAR – Light detection and ranging
LGF – Lærdal Gjende Fault Complex
LS – Lineament System
LSS – Lower Slip Surface
Mag – Magnetite
Ms – Muscovite
MTFC – Møre-Trøndelag Fault Complex
NSD – Nordfjord-Sogn Detachment Zone
ØFC – Øygarden Fault Complex
Op - Opaque
Pl - Plagioclase
PPL – Plane polarized light
Qtz - Quartz
RAP – Rogaland Anorthosite Province
SEM – Scanning Electron Microscope
Ttn – Titanite
USS – Upper Slip Surface
XPL – Cross polarized light
XRD – X-Ray Diffraction
Zo – Zoisite

1 Introduction and aims of the study

The Neoproterozoic Rogaland Anorthosite Complex has been studied in great detail during the last decades, mostly due to the sheer scientific interest linked to the genesis of anorthosites, their petrology and emplacement mechanisms and the exploitation of its economic Ti-Fe ore deposits (e.g. Pasteels and Michot, 1975; Krause et al., 1985; Demaiffe et al., 1986; Schärer et al., 1996; Boven et al., 2001; Westphal et al., 2003; Bolle et al., 2010). Tectonic and structural insights into the brittle evolution of the area are given by, e.g., Karlsen (1997), Henderson (2001), Henderson (2002) and Montalbano et al. (2016), who investigated fractures and faults related to alteration of the Tellenes ore body and the intrusion of the Egersund dike swarm. Recently, the BASE project, which is a research initiative launched by the Geological Survey of Norway and funded by Det Norske Oljeselskap, Lundin Petroleum, Maersk Oil and Wintershall, has aimed at understanding the interplay between brittle tectonic activity and weathering of the crystalline basement in southwestern Norway. One of the target areas of the project is the Åna-Sira anorthosite, which is a part of the Rogaland Anorthosite Complex and the study area for this thesis. The Åna-Sira anorthosite is well exposed, and is characterized by a generally high fracture density. Its glacially-polished surface and the sparse vegetation (Mangerud et al., 2011) provide excellent exposures of the basement and of its structures, which would otherwise remain less accessible and more elusive.

In this MSc project, multidisciplinary efforts aimed at unravelling the spatial and temporal evolution of the highly fractured and faulted basement exposed in the area and at better understanding how brittle deformation contributed, together with weathering and alteration, to the exposed basement potentially acquiring petrophysical properties of reservoir quality. Most of the weathered sequence atop the fresh basement was removed by glacial erosion, but equivalent rocks are being targeted for oil exploration and production in the North Sea, where a weathered (in the Late Triassic; Fredin et al., 2017) and fractured top-basement is well preserved beneath the Mesozoic sedimentary sequence (Tvedt et al., 2013). This geological framework offers the opportunity to study the basement onshore and use it as a correlative analogue for the offshore domain (Schärer et al., 1996; Smethurst, 2000).

Weathering of crystalline basement may break down the rock due to a plethora of processes activated by interaction with the atmosphere, fluids and living organisms. Weathering processes can be either physical or chemical, where physical processes are most intense in dry

and cold environments, whereas chemical processes dominate in wet and hot climates. However, these may often occur simultaneously and work together to degrade the rock. When a rock is weathered, it may generate a product called saprolite, literally meaning "rotten rock". Complex and diverse processes take place during saprolitization, reflecting the overall climatic conditions, the local morphology and the rock that is saprolitized. In general, though, K-feldspar, plagioclase and biotite are altered and replaced by illite and smectite for low weathering degrees and kaolinite for more extreme alteration (Gilkes et al., 1973; Fredin et al., 2017). Fredin et al. (2017) dated saprolite in three different locations in Southwestern Scandinavia by K-Ar dating of illite formed authigenically during weathering in the deepest part of the saprolitic mantle and constrained a Late Triassic age, which they assigned to a major episode of landscape development at that time. Since similar weathering-ages were found in three different areas in Scandinavia, they conclude that Late Triassic weathering affected a large area. Most of the saprolites have since been removed on-shore due to glacial erosion in Neogene and Pleistocene times (Fredin et al., 2017) but are more widely preserved off-shore due to burial and basin formation. In those environments saprolites represent potential unconventional reservoirs, especially when developed atop a heavily fractured crystalline basement (Fredin et al., 2017).

A couple of kilometers north of the Rogaland Anorthosite Province outcrop rock sequences belonging to the Caledonian nappe system, which have been extensively used to reconstruct the geological and structural evolution of the area starting from the Cambrian (e.g. Bryhni and Sturt, 1985; Eide et al., 1997; Smethurst, 2000; Valle et al., 2002; Fossen and Hurich, 2005; Fossen et al., 2016; Ksienzyk et al., 2016; Scheiber et al., 2016). These studies emphasize the temporal and spatial evolution of major structures during both collisional and extensional phases and providing important factual and conceptual background to this MSc study.

When working in old and multiply deformed terranes, it is important to separate all deformation structures into internally coherent sets, each of which only contains the results of one single deformation episode. To separate the different events, questions such as how many fractures and faults occur, what are their characteristics and when they were imposed on the rock, must be addressed to be able to identify all the events that, starting from a homogenous and undeformed rock at a given time t_0, have led to the present rock structural configuration (Fig. 1-1).

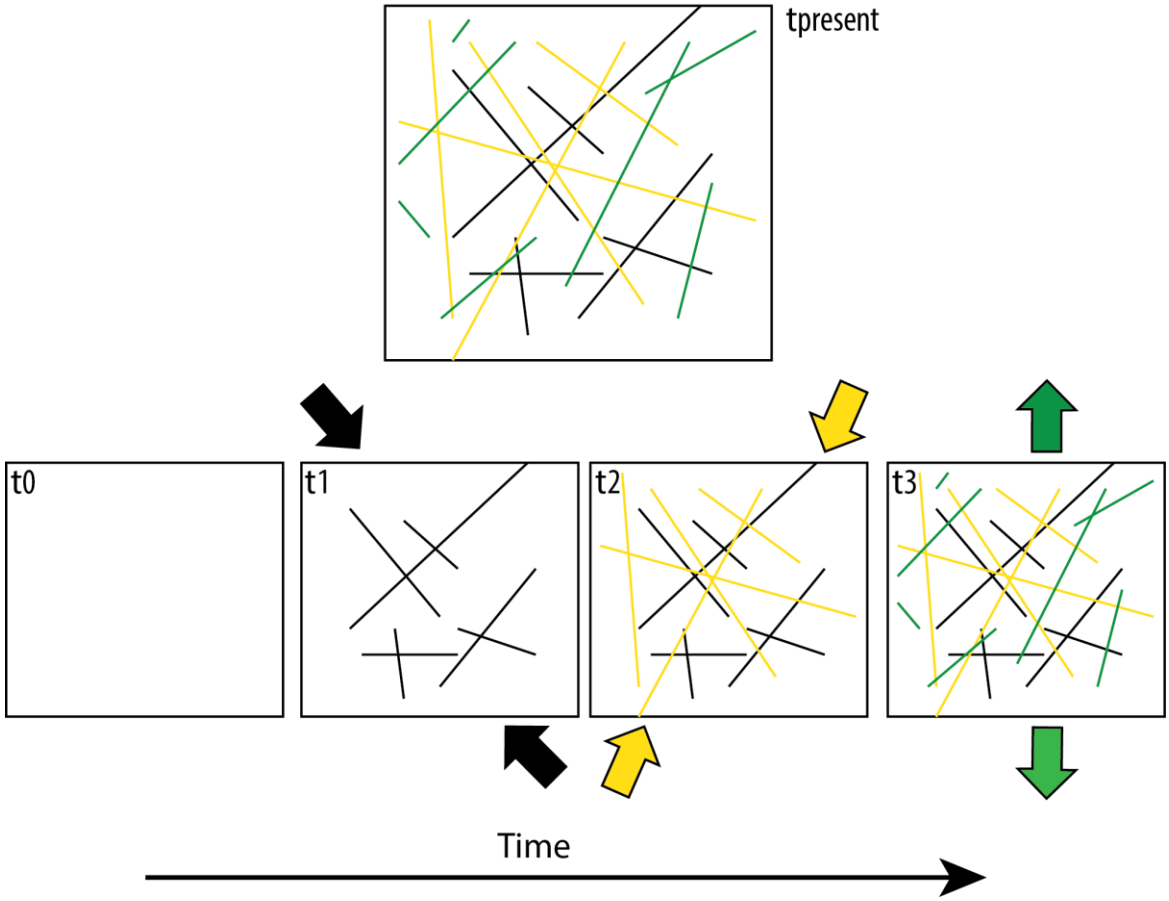

Fig. 1-1: Conceptual approach to sort out the complex , finite strain pattern within an old and multiply deformed terrane. Structural criteria are used to separate the fractures of the present-day configuration into internally consistent sets derived from "n" distinct deformation episodes. As time progresses, the basement becomes progressively saturated with fractures and the need of newly-formed fractures decreases as mechanical reactivation becomes more important.

The goal of this thesis is to better understand the tectonic evolution of the Åna-Sira Anorthosite within the conceptual framework presented above. This was accomplished by initial fieldwork, which allowed for detailed structural geological information to be systematically collected from several key localities within the Åna-Sira Anorthosite. By investigating fault architecture and fracture systems in the field, I could better understand the background mechanical properties of the basement. Following fieldwork, other tools have been used to implement a multiscalar, multidisciplinary approach to the study area to understand its geological evolution in space and through time. Remote sensing was used to investigate the main lineament trends at the regional and local scale, and fault rocks and gouges collected in the field were used for petrological analysis and radiometric dating. The adopted workflow is illustrated in Fig. 1-2.

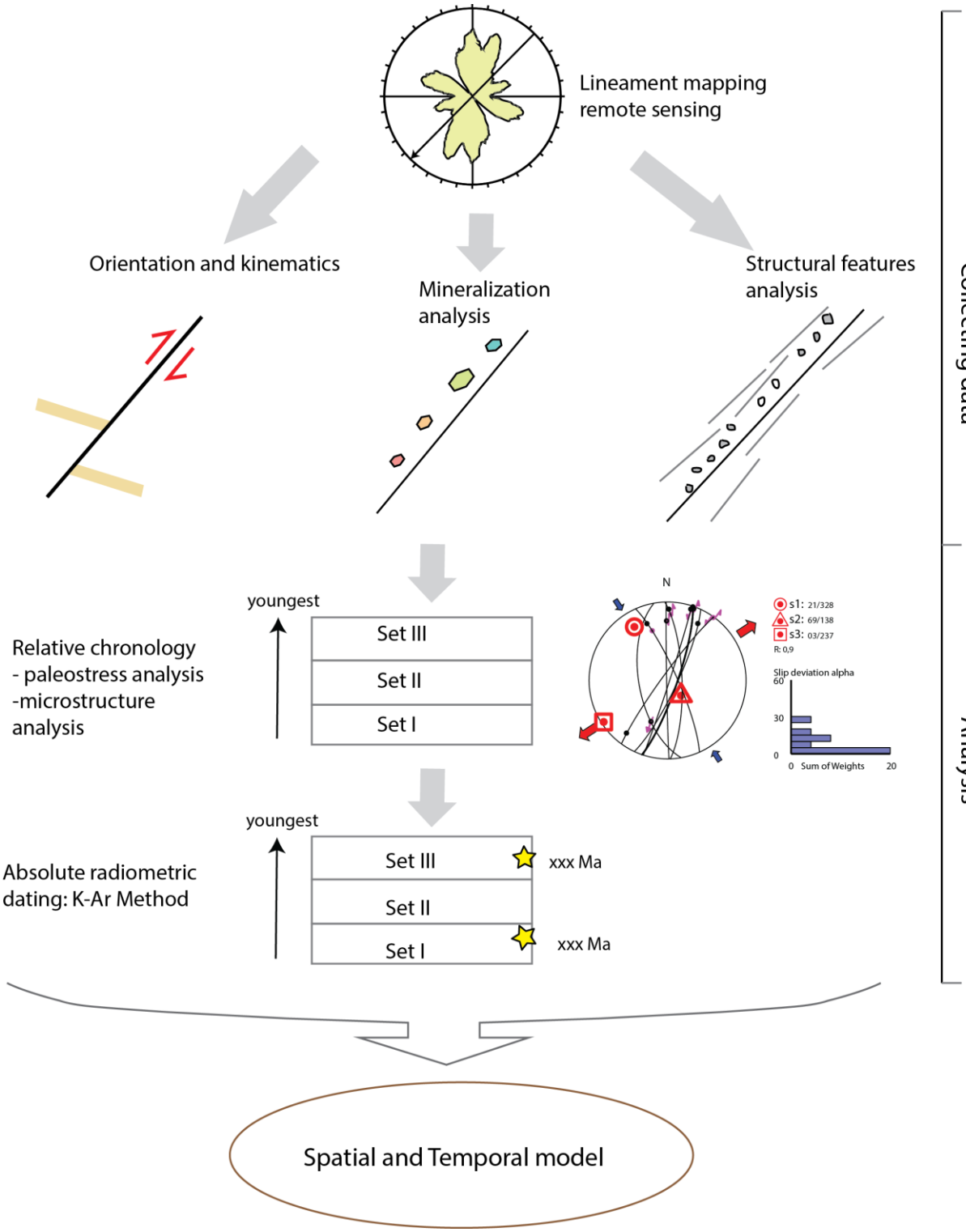

Fig. 1-2: Work flow implemented in the course of the study. The importance of fieldwork to any further analysis cannot be overemphasized.

1.1 Brittle deformation

Brittle faulting accommodates momentous deformation and brittle structures are among the most common features of the Earth's upper crust. They are found in a great number everywhere and have an impact often with dramatic consequences regarding seismogenesis, slope and rock mass stability, water transmissivity, mineral deposit and oil reservoir occurrence and characteristics. They exert a strong control on the topography and morphology of a landscape where features such as valleys, rivers, lakes and fjords are commonly strongly affected by tectonic boundaries.

Fractures, faults and veins – the main subjects of this study – are all products of brittle deformation. Brittle deformation reflects pressure-sensitive deformation in the upper crust, and develops in areas where stress builds up and eventually exceeds the strength of local rock mass resulting in mechanical failure. There are several parameters such as the temperature, rock textural and compositional anisotropy, confining pressure, pore fluid pressure and strain rate that affect how a material responds to the stress it is exposed to in the brittle realm (Fossen, 2010). Complex brittle deformation patterns result from- and may help constrain multiple events of deformation. By studying and analyzing the geometry, kinematics, mineralogy and the mechanical behavior of these features, it is possible to build up an understanding of the brittle deformation history that affected the area of study (e.g. Viola et al., 2009; Viola et al., 2012; Awdal et al., 2013; Scheiber et al., 2016). Brittle features are generally scale-invariant when their characteristics are taken into account and, therefore, can be studied at multiple scales, for example through remote sensing imagery (Gabrielsen et al., 2002; Scheiber et al., 2015), field work and microscopic analysis. Recent analytical developments in the K-Ar radiometric dating of illite formed authigenically in brittle fault rocks (Viola et al., 2013; Scheiber et al., 2016) have permitted to resolve the details of long and complex brittle structural evolutions in an absolute time framework. The K-Ar technique on illite separated from fault gouge has also been used with a couple of samples in this study and the implementation of the method in the workflow adopted in this thesis is illustrated in Fig. 1-2.

Faults

Faults and their geometric, kinematic, and dynamic characteristics are fundamental to our understanding of upper crustal tectonic histories. Furthermore, faults play a key role for the understanding of the migration mechanisms and paths of fluids in rocks and fluid-rock interaction processes, which may result in a modification of the mechanical and chemical properties of the rock at the time of deformation. This gives a unique opportunity to scientists

to study the environmental and stress conditions at the time of deformation. However, once formed, faults are very sensitive to variations in the stress field. The stress needed to cause slip on a preexisting weak plane is generally lower than that necessary to create a new fault plane at an optimal orientation, and faults are therefore often reactivated (Angelier, 1994; Viola et al., 2013). By exploiting already established weak planes in the rock, faults might thus accommodate multiple reactivation events. Brittle deformation histories can therefore be challenging to understand due to multiple overprinting relationships. In older rocks, indeed such as the c. 930 Ma old (Schärer et al., 1996) Rogaland Anorthosite Complex, this is very important to bear in mind. Careful multiscalar structural analysis is therefore necessary to obtain reliable models of the brittle deformation history. In addition to structural characterization of the faults, Ar-Ar and K-Ar dating have successfully been used to date synkinematic mica/illite reflecting the timing of brittle faulting (Eide et al., 1997; Viola et al., 2013; Torgersen et al., 2014; Viola et al., 2016). With this as background, a carefully chosen fault in the study area, the Helleren Fault Zone, was mapped in detail and dated by the K/Ar-method. It is a regionally important structure and, in addition, it is exposed at a Norwegian historical site. The Helleren Fault Zone represents, moreover, the only structure from the post-Caledonian extensional phase dated thus far in southwestern Norway.

The thesis is organized in such way that it starts from regional scale observations with the results from remote sensing analysis and progressively zooms into field evidence, microstructures and radiometric dating, ending up in a discussion that proposes a possible structural evolutionary model of the area.

2 Geological setting

The study area is situated in the Rogaland Anorthosite Province (RAP) and crops out in the southwestern part of Norway along the coast of the counties of Rogaland and Vest-Agder. The province is a part of the Proterozoic basement, specifically the Sveconorwegian orogen where it intruded c. 930 Ma ago (Schärer et al., 1996; Bingen et al., 2008b) during the collapse of the orogenic belt. Classically, the Sveconorwegian orogenic belt is considered as a part of the Grenville Orogen and a part of the supercontinent Rodinia c. 1 Ga ago (Montalbano et al., 2016). The RAP complex consists of anorthositic intrusions together with associated noritic, monzonoritic and mangeritic intrusions (Pasteels and Michot, 1975; Karlsen, 1997) and was affected by several tectonic episodes including the opening of the Iapetus Ocean and the Caledonian orogeny (Bingen et al., 1998a; Boven et al., 2001; Montalbano et al., 2016) as well as later rifting events in the Mesozoic (Tvedt et al., 2013).

2.1 The Sveconorwegian Orogen

The Sveconorwegian Orogen is situated in southern part of Fennoscandia. The orogeny extended between 1140 and 900 Ma ago, when imbrication of terranes formed the orogenic accretionary prism prior to its tearing down by late orogenic collapse (Bingen et al., 2008a). The orogen is built up by four different terranes or domains derived from different tectonic, magmatic and metamorphic events predating the Sveconorwegian orogeny. These domains are the Telemarkia, Idefjorden, the Eastern Segment and Bamble and Kongsberg Terranes, which are separated by crustal scale, generally N-S trending shear zones (Fig. 2-1; (Möller et al., 2007; Bingen et al., 2008b; Viola et al., 2011).

Four different tectonic phases (between 1140-900 Ma) accommodated the main phases of the development of the Sveconorwegian orogen causing episodes of high-grade metamorphism, exhumation and deformation, which changed the framework of the segments and formed an orogenic prism formed by their progressive imbrication (Bingen et al., 2008b). Between 970 and 900 Ma gravitational collapse of the belt and related magmatism occurred, with magmatism increasing towards the western part of the orogen, in an overall extensional regime. The Rogaland Anorthosite Province is a part of the Telemarkia Terrane in the western part of the orogeny and the regional drop of pressure during this extensional phase made it possible to generate an upwelling of hot lithospheric mantle close to the base of the crust and bring hot viscous crust and large plutons up to a shallow crustal level. The Rogaland Anorthosite Province represents the final voluminous pulse of plutonism at 930-920 Ma, which was followed by regional cooling. $^{40}Ar/^{39}Ar$ dating of hornblende implies regional cooling of the

Sveconorwegian orogen between 930-855 Ma (Bingen et al., 1998a; Bingen et al., 2006).

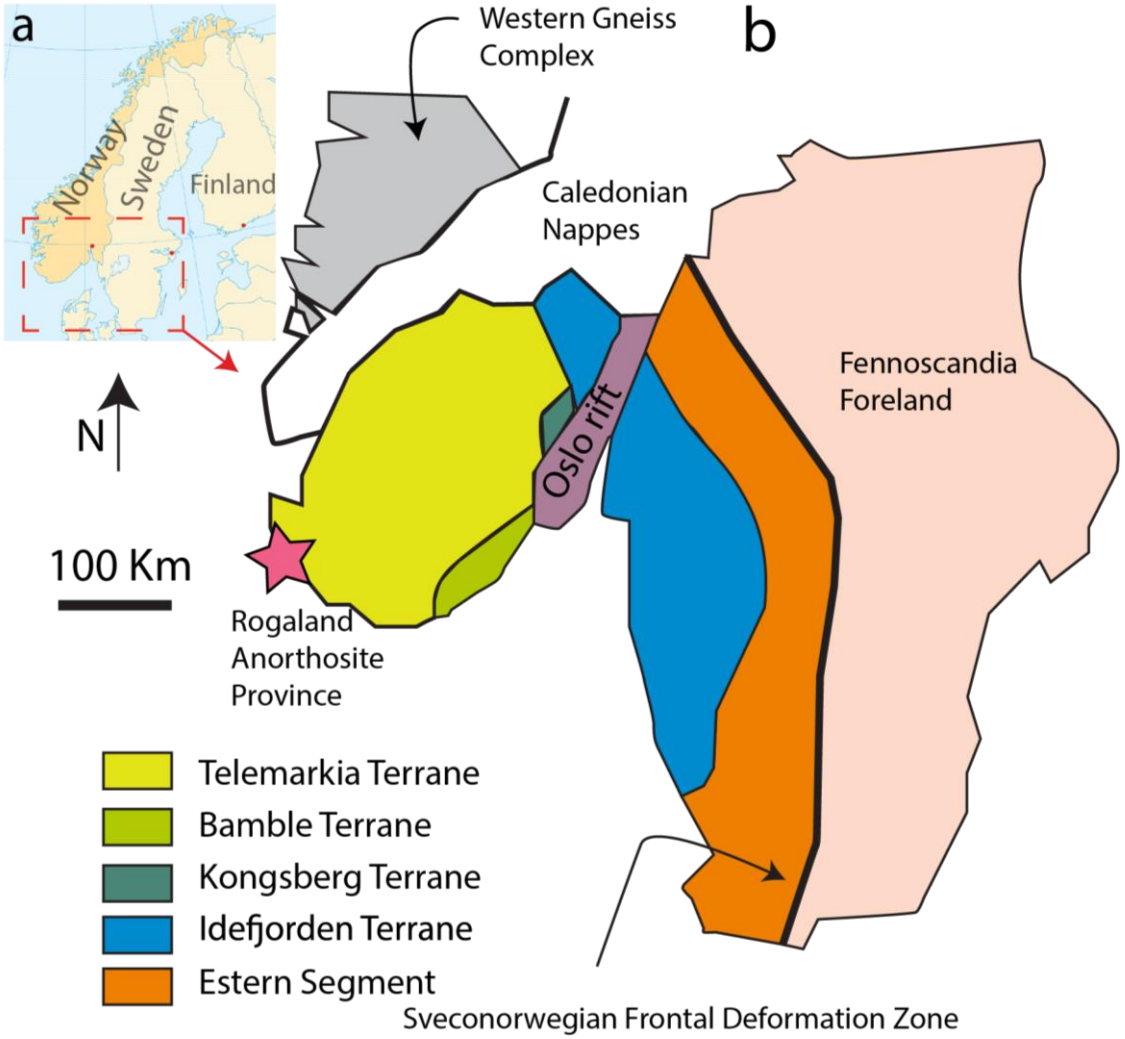

Fig. 2-1: Simplified map of the Sveconorwegian Orogen in southern Norway and Sweden illustrating the different domains and the major deformation zones (figure modified after Bingen et al. (2008b)

2.2 Rogaland Anorthosite Province

The Rogaland Anorthosite Province (RAP) has been of great geological interest for decades owing to its very large Fe-Ti ore deposits (Krause et al., 1985; Schärer et al., 1996; Karlsen, 1997). The RAP consists of four major anorthosite plutons: (1) the Egersund-Ogna, (2) Helleren, (3) Håland and (4) Åna-Sira massifs (ÅS; Fig. 2-2; (Vander Auwera et al., 2011), with the Åna-Sira massif being the most relevant for this thesis. The Bjerkreim-Sokndal layered intrusion (BKSK), the Tellenes ore body and the Egersund dike swarm are also located in this province (Schärer et al., 1996). The Rogaland anorthosite was emplaced as a huge diapir, soon after the regional imbrication of Sveconorwegian orogeny constituent terranes (Barnichon et al., 1999). Barnichon et al. (1999) describe the formation of anorthosite with a model that follows a classical petrological model in which accumulation of plagioclase takes place in a deep-seated magma chamber at the crust-mantle boundary; there, masses of plagioclase

separate and rise though the lower crust up to the final level of emplacement at mid-crustal depths. The deepest stage of anorthosite crystallization occurred at c. 45 km depth and the final emplacement level is generally constrained to c. 15-29 km (Bolle et al., 2010). The last, upward transfer of the anorthosite magma was followed by sinking of the high density BKSK into the low-density anorthosite. At that time, deformation of the Rogaland anorthosite province became steered by gravitational tectonism with diapiric emplacement of the anorthosite and the gravity driven subsidence of the BKSK. The emplacement of the jotunitic dykes (nortite and the Fe-Ti ore body therein) took place at a later stage, as shown by the fact that they cross both the anorthosite and the BKSK (Bolle et al., 2010; Vander Auwera et al., 2011).

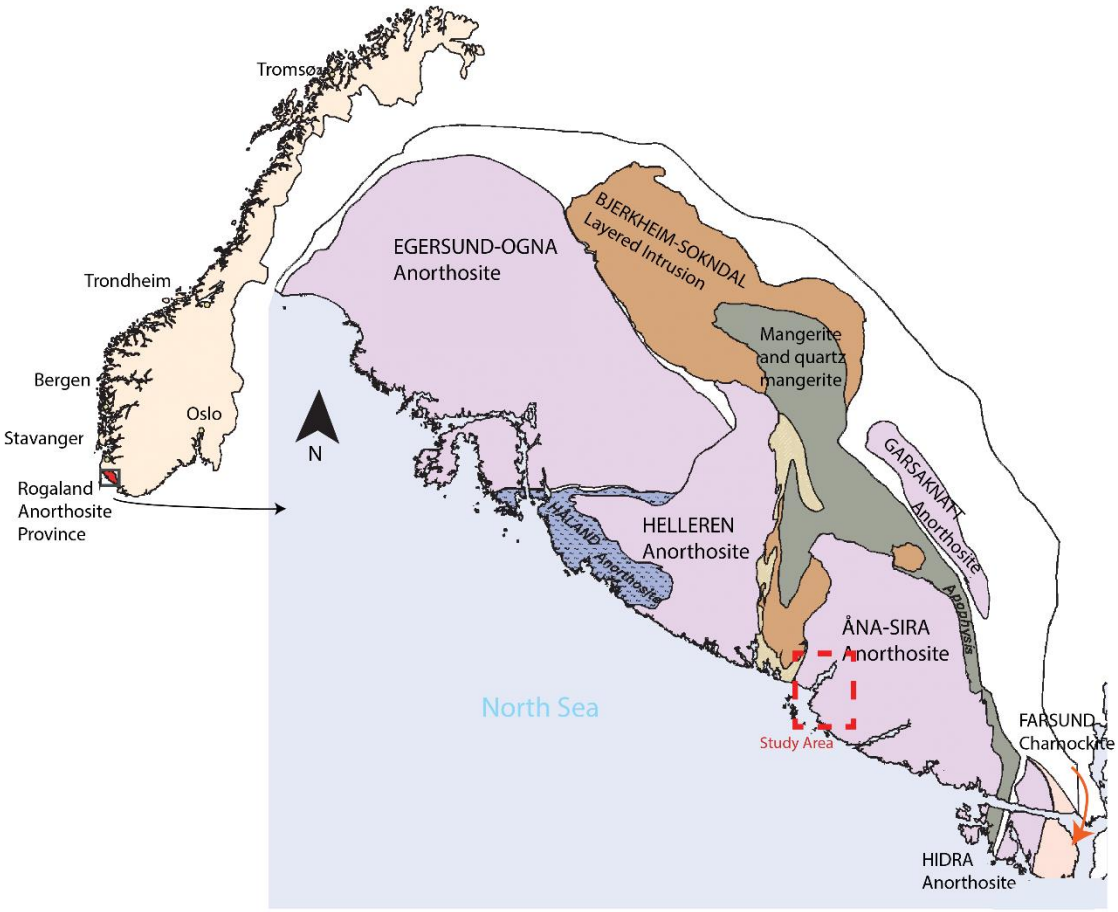

Fig. 2-2: Rogaland Anorthosite Province, with the study area shown by the dashed red frame (modified from Marker et al. (2003)).

2.2.1 Åna Sira Anorthosite

The Åna Sira Anorthosite massif (ÅS) is located in the southernmost part of the Rogaland Anorthosite Province (Fig. 2-2) and is one of the latest intruded massifs. It consists of anorthosite and norite with generally 90-100% plagioclase (An_{40-50}) and 0-10% orthopyroxene

(Karlsen, 1997). The complex can be lithologically subdivided into a series of anorthositic-leuconoritic suits, followed by a noritic series and finally by a mangeritic series that was later cut by the Egersund dike swarm (Krause et al., 1985). The anorthosite consists mainly of plagioclase and is texturally homogenous, coarse grained, with inequigranular crystals characterized by subhedral shapes. The crystallization temperature for the anorthosite was c.1250°-1100° C. After emplacement followed a relatively fast phase of regional cooling as recorded by U-Pb titanite ages, which yielded a weighted average of 918 Ma, that is c. 10 Ma after the initial anorthosite emplacement (Bingen and Van Breemen, 1998; Bingen et al., 1998a). At the same time (c. 920 Ma), intruded the norites and mangerites connected to the Fe-Ti ore deposit (Schärer et al., 1996). Further cooling proceeded much more slowly and $^{40}Ar/^{39}Ar$ ages from hornblende constrain a cooling episode at c. 870 Ma (Bingen et al., 1998a). The ÅS was subsequently affected by dike intrusion marking a change from ductile to brittle regime. The exact timing for the switch of the deformational regime remains ambiguous. Brittle deformation is pervasive throughout the massif with networks of fractures and locally cataclasites and fault breccias. Numerous dikes of mangerite, Fe-Ti-norite intrusions and the younger Egersund dike swarm are cutting through the massif (Karlsen, 1997).

The Tellenes ore body is one of the Fe-Ti-norite intrusions that are hosted by the ÅSM and is of great economic importance in the area. Due to this valuable deposit, very many studies have been carried out in the area. Studies done by Krause et al. (1985) and later by Karlsen (1997 and ref. therein) suggest a close relationship between the intrusion of the ore body and the local brittle evolution.

2.3 Post Sveconorwegian evolution

Following the Sveconorwegian orogeny, the Fennoscandian Shield was affected by regional extension as Rodina started to break up (rifting began at c. 850 Ma, but final break-up occurred between c. 615 and 570 Ma;(Li et al., 2008). Several sedimentary basins developed (e.g. Hedmark basin and Lake Vättern basin) during this extensional phase and there were periods with low regional temperatures and glaciations of Baltica, such as the Varanger Ice Age (653±7 Ma; (Bingen et al., 1998a)). In the Cambrian, marine transgression covered the area, as documented by marine deposits in the stratigraphic record of the preserved sedimentary basins such as Hedmark basin in Southern Norway and Lake Vättern basin in Sweden (Vidal and Moczydłowska, 1995; Bingen et al., 1998a).

Well documented basins from the Neoproterozoic reveal well-constrained record of the sedimentation and rifting during the period. In addition, Neoproterozoic rift-related magmatic

suites in western Baltica have a geochemical signature that implies a transition between continental rifting and seafloor spreading, which eventually led to the opening of the Iapetus Ocean (Bingen et al., 1998b). One of these suites is the Egersund dike swarm, located in the Rogaland Anorthosite Province and in the study area of this thesis. The doleritic dike swarm has an intrusive age of 616 ± 3 Ma and a geochemistry related to the continental rifting episode prior the opening of Iapetus Ocean (Bingen et al., 1998b; Montalbano et al., 2016). There are 11 main dikes, which are oriented N110°-120° with a steep to vertical dip. Recent studies by Montalbano et al. (2016) reveal an accurate history of dyke emplacements, constrained by magnetic fabric orientation, to propose a strike-slip sinistral sense of shear leading to oblique extensional rifting in an overall NNE-SSW stress regime. The dikes make an important time marker for the brittle evolution of the area and imply an important feature regarding this extensional phase (Bingen et al., 1998b).

Caledonian evolution and later rifting phases. High petroleum exploration and production activity on the continental shelf in the North Sea has provided great knowledge of the tectonic history in Southern Norway (Fig. 2-3). Fieldwork, radiometric dating and seismic imaging have helped to constrain the numerous deformation episodes that have affected the area since the Early Neoproterozoic by establishing the steering conceptual framework (e.g. (Bryhni and Sturt, 1985; Sørensen et al., 1992; Eide et al., 1997; Braathen, 1999; Fossen and Dunlap, 1999; Smethurst, 2000; Valle et al., 2002; Gabrielsen et al., 2010; Scheiber et al., 2016; Viola et al., 2016)).Prior to the Caledonian orogeny, arc-related intrusive magmatism and accretion events of Ordovician age resulted from the convergence between Laurentia and Baltica (Bryhni and Sturt, 1985; Fossen, 1992). A Late Ordovician transpressional brittle faulting event, directly dated by Scheiber et al. (2016) to 450 Ma, reflects the accretionary phase prior collision.

During the Silurian-Early Devonian an overall NW-SE convergence between Baltica and Laurentia created the Caledonian Orogen peaking at c. 425 (Bryhni and Sturt, 1985; Scheiber et al., 2016). During Early Devonian times, the over-thickened orogenic pile of the Caledonides started to collapse and accommodated crustal-scale extensional shear zones causing thinning of the crust and uplift of the orogenic roots. The rapid cooling caused a progressive change in the extensional deformation style from ductile to brittle in a short period of time followed by a later slower cooling (Fossen, 2000).

E-W brittle-extensional deformation continued during the Permo-Triassic and was characterized by faults trending NE-SW and doleritic dikes striking N-S to NNW-SSE, also related to the Oslo rift farther east (Færseth et al., 1976; Fossen and Dunlap, 1999; Smethurst, 2000; Valle et al., 2002). Further, brittle extension and re-activations of pre-existing structures reflects a major phase of extension in the Jurassic, causing crustal thinning and development of grabens in the North Sea (Smethurst, 2000; Viola et al., 2016). Large fault systems such as Lærdal-Gjende Fault System and Nordfjord-Sogn Detachment Zone, stayed active or were reactivated throughout the Carboniferous-Permian and Mesozoic (Fig. 2-3) (Eide et al., 1997; Andersen et al., 1999; Larsen et al., 2003). The Cretaceous transgression caused changes in the cooling rates due to sedimentary burial with highest reheating in coastal areas: the rifting slowed down into the Cretaceous, but faults were still active most likely through to the Cenozoic.

Today, the southern part of the Caledonian orogen is exposed north of the Rogaland Anorthosite Province along the west coast of Norway separated from the pre-Cambrian basement by a mechanically weak décollement zone of Cambrian phyllites (Bryhni and Sturt, 1985; Fossen and Rykkelid, 1992).

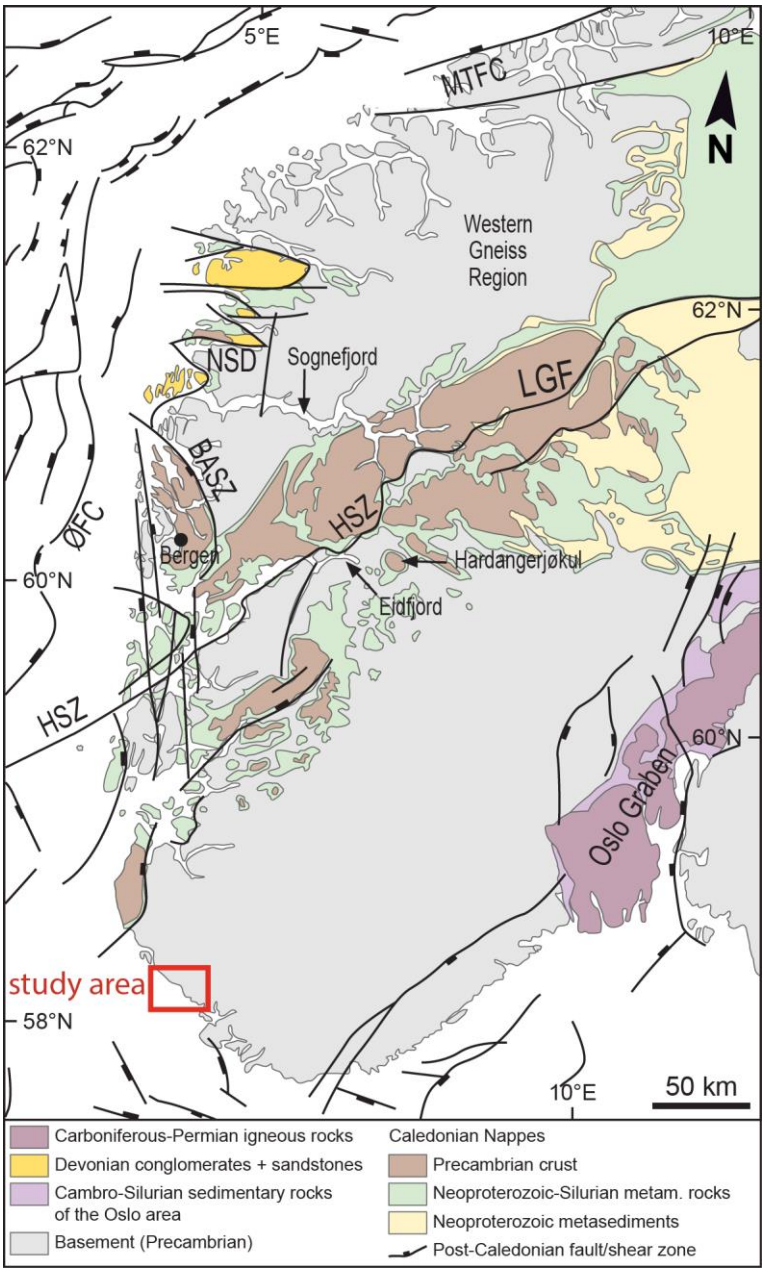

Fig. 2-3: Simplified geological map of Southern Norway, showing the study area and the major, regional fault systems. BASZ: Bergen Arc Shear Zone; HSZ: Hardangerfjord Shear Zone; LGF: Lærdal-Gjende Fault Complex; MTFC: Møre-Trøndelag Fault Complex; NSD: Nordfjord-Sogn Detachment Zone; ØFC: Øygarden Fault Complex (modified from Ksienzyk et al. (2014)).

3 Methods

3.1 Remote sensing

3.1.1 Explanation of concept

Remote sensing is a powerful tool to derive information about the surface morphology and constrain geological surface structures. The first remote sensing technique to be applied in Earth Sciences was aerial photography and as the technology improved high resolution satellite imagery was adopted to investigate geological features at a much improved resolution (Scheiber et al., 2015). Over the last decades, altitude has become one of the most successfully remote-sensed data products. These digital elevation models (DEM) have improved rapidly from kilometers down to a only a few meters' spatial resolution (Smith and Pain, 2009). DEM's contain detailed information about the elevation of the ground and give a three-dimensional model of the surface (Rød, 2015). They allow large areas to be mapped without having to cover them by foot.

High spatial resolution data-sets such as Light Detection and Ranging (LiDAR) have revolutionized the production of digital elevation models. This method uses a laser scanner that sends out a laser pulse and measures the distance from the target by the travel time of the pulse. The pulse detects all objects on its way before it meets the ground. By removing the first incoming signals, the last pulse gives a detailed digital elevation model (DEM) with a ground resolution up to 1 m by creating a point cloud (Rød, 2015). Hillshade/relief shading is a common method to visualize landforms with DEMs. This method can be used to map quaternary deposits, geographic features, man-made structures such as roads, railroads, mines and also bedrock. It is a great tool to investigate surface expression of bedding, foliation, faults, fractures and fractures zones (Scheiber et al., 2015).

Remote sensing is thus exploited to analyze the regional patterns visible in the bedrock, and is thus particularly suited to investigate the effects of brittle deformation (e.g., Wise et al., 1985; Gabrielsen et al., 2002; Raharimahefa and Kusky, 2009; Viola et al., 2012; Awdal et al., 2013). In this study, both DEM 10 and LiDAR were used to analyze the lineaments present in the study area. LiDAR-data was only available in areas in relation to Titania AS, an ilmenite mine in the study area. ArcGIS was used to generate the lineaments as features classes using the DEMs and the obtained data was later exported to MARD (Munro and Blenkinsop, 2012), which is a software generating rose diagrams. The advantage of using this software is that each frequency of each azimuth is evaluated in the context of those in the immediate proximity to it.

This means that the frequency of each azimuth and those of azimuths within a pre-defined range (the aperture, defined by the operator) on either side of it are systematically summed and averaged. The resultant average of each azimuth is then plotted in the final rose diagram. In other rose diagram software's, the aperture is often predefined as 10° bins starting from azimuth 0°, in which the frequencies represent the sum of all the azimuths within that bin and not the moving average of the surrounding azimuths. This pre- defined feature might lead to the loss of important data because of the distribution of data within the bins is unknown.

The DEM has a resolution of 10 m and was first published in 2013 with a standard deviation of ± 2-3 m. Three DEM-raster files were downloaded from "Kartverket" (Kartverket, 2013) and mosaiced together in ArcGIS. Further, three new hillshaded images were generated with three different illumination azimuths, 045, 180 and 315. The chosen areas were mapped at the scale of 1:125 000 and 1:40 000, whereby three lineaments maps were generated for each scale and each lithology. In total, eighteen lineaments maps were produced and later exported to generate rose diagrams discussed in this thesis (Table 4-1).

LiDAR-data was used for a 31 km^2 area within and around the pit. The LiDAR- data that was used was scanned from an aircraft and later processed in ArcGIS. The point cloud was gridded using only "last returns" excluding vegetation, to a DEM with a resolution of 1 m using standard binning interpolation in ArcGIS. Three hillshaded images were generated with three different illumination azimuths at 045°, 180° and 315°. The area was mapped at two scales, 1:20 000 and 1:8000, whereby lineament maps were generated for both scales and the three illumination azimuths creating a total of six lineament maps for the Tellenes area.

3.2 Field Techniques

Fieldwork was an important part of this study to better understand and constrain the geometry and deformation mechanisms of the studied rock and the kinematic behavior to interpret the brittle deformation history in the area. Approximately four weeks were spent in the field to collect structural observations, to map outcrops in detail and collect samples for further petrologic, structural and geochronological analyses (Fig. 3-1).

The first field season was used to get to know the area and gather preliminary structural information. Three areas of special interest were found. The first one was a new roadcut close to Bjånes, which exposed fresh anorthosite outcrops and allowed detailed analyses on a brittly strongly overprinted c. 1000 m long section. The second was the Titania AS open pit, where

total exposure was fundamental to elucidate some structural relationships. Thirdly, the Helleren historic site turned out to be a key locality to understand the evolution of the area.

During the second field season, most of the time was spent in Titania AS and at Helleren. In addition, some areas were visited again to improve first season observations and collect more data.

Field mapping was carried out digitally on a Toughbook provided by the Geological Survey of Norway (NGU). There is a built-in GPS in the Toughbook, which communicates with the ESRI ArcGIS software. To register field observation points I used the software Sigma.

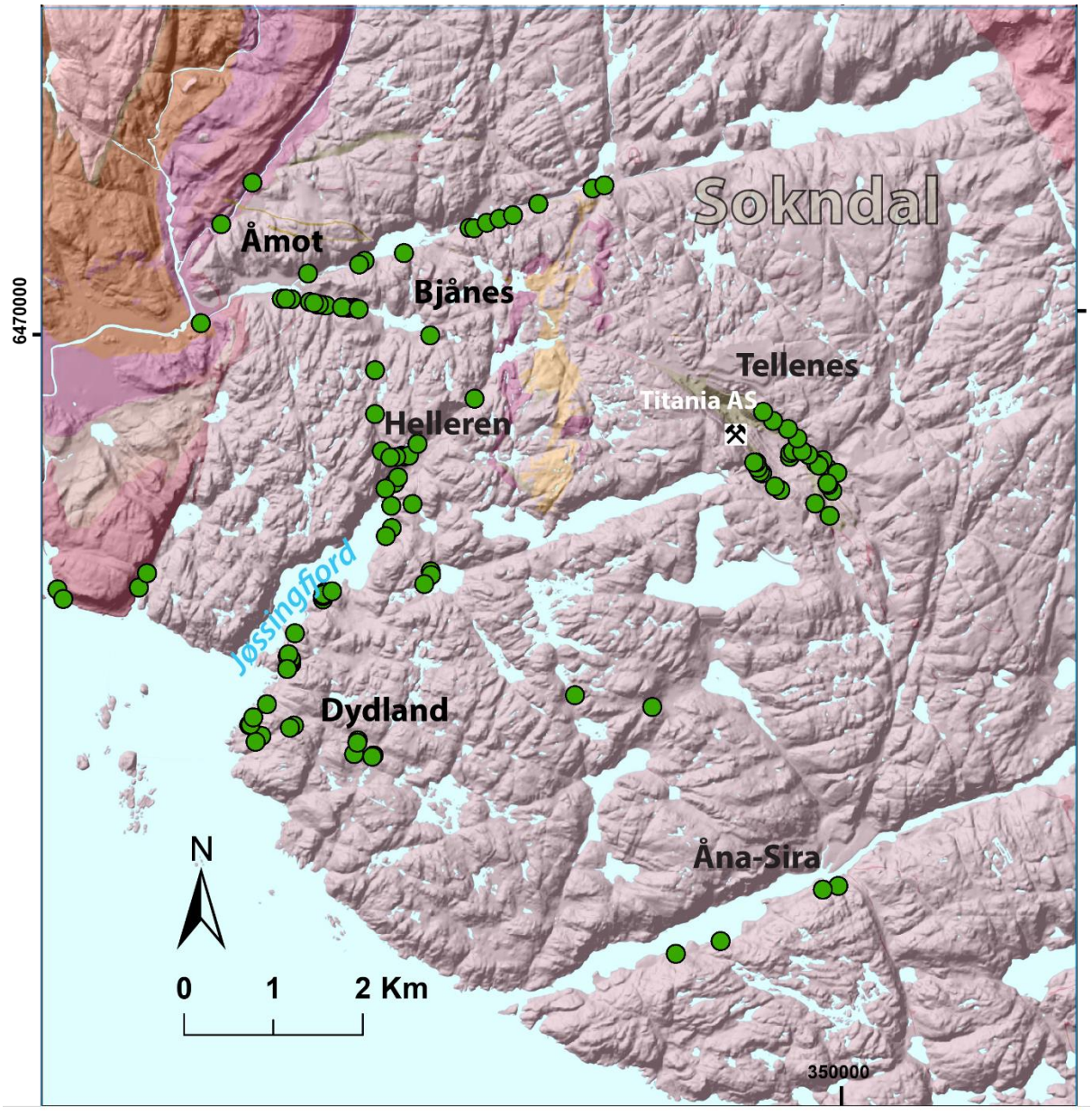

Fig. 3-1: Field localities (green circles) studied in the area covered by the MSc project.

With Sigma, the user can register observation points, field notes, connect photos to field observation points, make sketches and register structural observations. Sigma for ArcGIS is developed by the British Geological Survey, BGS.

Digital mapping offers great possibilities and permits to generate accurate maps. The mapper can bring digitalized and geo-referenced maps to the field and visualize data from different sources at the outcrop, upload and use data from other mappers in the same area, have access to all types of softwares such as stereonet, and all types of literature.

3.3 Thin Section Preparation and microscopy analysis

Samples were mainly from fault zones within the study area and were cut with a diamond saw at the NGU laboratory. The preferred area for making a thin section was marked together with the arrows indicating the orientation of the sample in the field. Due to the general lack of striations on fault surfaces (a preservation issue that might be related to weathering since exposure), the samples were orientated with regards to foliation and fault geometry. The arrows were placed on the back side of the planned thin section. Hereafter, the rock slices were cut into rectangles and handed in to the thin section laboratory at NTNU, where the rocks were prepared into 30 μm thick thin sections. The thin sections were polished to ensure good results also when using the scanning electron microscope (SEM). Standard petrographic polarization microscopy was used to analyze the sections, to take microphotographs and to identify key domains to further study at the SEM.

3.4 Scanning Electron Microscope - SEM

The SEM was used to characterize the mineral assemblage in thin section and to closely study some of the veins that crosscut the anorthosite, which are some of the most common structures observed both in the field and in thin section. Pervasive sericitization is common in all studied sections, especially those from the Helleren Fault Zone and the high magnification possible at the SEM made it possible to better see textures and microstructures of the very fine grained secondary mineralizations. Mineral analysis was carried out by a 1450 Variable Pressure (VP) SEM manufactured by LEO Electron Microscopy Ltd equipped with energy dispersive X-ray spectrometer (EDS) at the electron microscope laboratory at NGU. The SEM was operated at a beam current of 70.0 μA, at 15 kV accelerating voltage, spot size of 0.513

micron, fill target of 2.600 A, EHT Target of 10.00 kV and a 15 mm working distance. The chemical composition analysis was determined by the INCA software from Oxford whereby non-normalized element proportions were automatically calculated. The advantage of using an electron microscope is the high magnification and the ability to take high resolution images to effectively illustrate the details of the thin sections. In addition, results from the electron microscope are helpful when using the microprobe to have better control on the different minerals in the section that are to be analyzed. Results from some of the SEM/EDS analyses are presented in Chapter 4.3.

3.5 K-Ar-dating

3.5.1 Description of the method

When a rock in the brittle regime exceeds its yield point and is exposed to differential stress over time, strain localizes through the development of a fault zone containing cataclastic rocks and gouge. The fault gouge is essentially made of fine grained crushed host rock, but it also contains minerals formed syn-kinematically in-situ, i.e. authigenic (Torgersen et al., 2014). Among these newly grown minerals is illite, a clay mineral forming at generally low temperatures that contains potassium in its crystal structure. K is fundamental to the utilization of illite as a "clock" to date the time of its formation and, so, the time of the last increment of brittle deformation recorded by the fault rock. K-Ar- dating is a radiometric dating method used in geochronology whereby the method is based on radioactive decay of potassium (^{40}K) into argon (^{40}Ar) with a

Fig. 3-2: Sample locations for three gouges dated by the K/Ar-method, marked with yellow stars.

half-life 1.25 Ga. Potassium is a common element in the Earth crust and is present in many minerals, such as clays and micas (Clauer and Chaudhuri, 2012).

The radiogenic daughter product of potassium is argon. It has been demonstrated that it can be retained in the illite crystal structure for millions of years, thus making illite suitable for radiometric dating by K-Ar and Ar-Ar (Torgersen et al., 2014; Ksienzyk et al., 2016).

Brittle fault rocks may have a high content of clays and the method offers therefore the potential to constrain the absolute timing of brittle faulting. To produce meaningful fault ages, the age of authigenic synkinematic illites in fault rocks need to be obtained. This can be challenging because of the contamination of the dated illite by other inherited K-bearing mineral components, partial or full resetting of the radiogenic system by volume diffusion, post-faulting alteration and variations in crystal nucleation and growth mechanisms. As for all isotropic dating, the method is based on a closed systems which assumes no re-equilibration of the system since the minerals formed. Carefully preparation and mineral characterization are therefore nessesarry to use the method in a systematic way and get a proper age (Torgersen et al., 2014).

Gouge-bearing brittle faults are rarely exposed in western Norway due to formation of valleys and fjords during the last ice age (Mangerud et al., 2011). Luckily, well exposed outcrops were available in the study area, because of construction work and mining. Three samples of gouge from three different locations in the field area were analyzed for absolute dating (Fig. 3-2). The sample preparation and later analysis in the laboratory was carried out by Andrew Todd at the CSIRO laboratories in Perth, Australia, and later by Roelant van der Lelji at NGU. To minimize bias of artificial grain-size reduction and avoid contamination of coarser-grained material in the finer size fractions, the samples were gently disintegrated by repeated freezing and thawing. Four grain size fractions were dated per sample. Grain size fraction 2-6 μm and <2 μm were separated in distilled water, whereas fractions <0.4 μm and <0.1 μm were obtained by high speed centrifuging. The K-Ar dating technique follows methods described in details elsewhere (Dalrymple and Lanphere, 1969; Appendix A) and the concentration of Ar in the sample was measured by conventional mass spectrometry.

3.5.2 X-Ray Diffraction (XRD) Analysis

The exact mineral assemblages in the three gouge samples were determined by X-ray Diffraction (XRD) analysis. X-Ray diffraction determines the physical and chemical characteristics of minerals. XRD analysis utilizes the interaction between electrons and X-rays

and the interference from the unique atomic arrangement of a material (Will, 2006). The preparation and analysis of sample GVI_14 and TSC_44 were done by Jasmin Schönenberger at NGU, whereas OFR_3 was done at CSIRO in Perth. Major elements were determined by X-ray spectrometry at the laboratory at NGU and prepared by side-loading. The mineral quantification was done using Rietveld modelling and the TOPAS 5.0 software. For sample OFR_3 mineral quantification was carried out using the commercial package SIROQUANT from Sietronics PTY Ltd with results normalized to 100%.

3.6 Paleostress analysis – inversion of fault-slip data

To be able to understand the brittle deformation history in the study area, we need to investigate how the stress field has evolved and changed during the geological evolution. This investigation can be done by paleostress analysis. By registering the dip and dip azimuth, pitch of the slickenside striations and the sense of motion of a fault plane in field, a complete fault-slip datum is created also known as the kinematic description of a brittle fault (Sæter, 2006; Mattila and Viola, 2014). Fault-slip datum gives an idea of how the stress performed on the rock generating specific fault planes.

The observed kinematic data can be inverted into a single reduced stress tensor by using a paleostress algorithm. The stress tensor contains four unknown parameters; the three principal stress axes ($\sigma_1, \sigma_2, \sigma_3$) and the stress ratio $R = ((\sigma_2 - \sigma_3) / (\sigma_1 - \sigma_3))$ (Mattila and Viola, 2014). To solve a paleostress inversion algorithm, at least four fault-slip datum are required to unravel the four unknown parameters and therefore the stress tensor. However, in practice more than four faults are required to get a reliable result from the stress inversion (Celerier, 1988; Fossen, 2010).

In highly faulted and fractured rocks, such as Åna-Sira anorthosite, it is necessary to identify fault subsets according to their mechanical characteristics. These subsets are associated with different stress tensors that reveal different stress fields through time. To separate these fault sets, field structural observations, kinematic data, mineralization and chronology need to be constrained to produce reliable datasets.

Regardless of which paleostress algorithms that are used, they are all based on some common assumptions. The faults slip independently and randomly of each other, the volume of rock has to be large compared to the dimensions of the fault whereby stress is distributed homogenously, the rock needs to give rheologically linear response to the applied stress, the

rock volume is homogeneous and isotropic and slip direction is parallel to the shear direction on the fault plane (Mattila and Viola, 2014).

All the different paleostress algorithms search for the best theoretical stress tensor to fit the data from the field. This is achieved by analysing statistically the sum of the misfit angle, α, for all faults. This angle is defined as the acute angle between the theoretical maximal shear effect vector and the measured slip vector in field. α is calculated for each individual fault plane (Delvaux and Sperner, 2003). In this project, the software 'WinTensor' is used to perform stress invention (Delvaux and Sperner, 2003). The software calculates the best fitting stress tensor for a given fault-slip data set. The advantage of using this software is the function called 'rotational optimisation", in which rotates the stress tensor until the best oriented stress tenor is obtained with respect to the fault-slip data set and the misfit angle α. Chapter 4.5 constrains the results from paleostress analysis from the study area.

All additional stereonet plots in this thesis are projected with lower hemisphere projection (Grohmann and Campanha, 2010).

4 Results

In this chapter, five sub-chapters are presented, each elaborating on the results from a different part of the study. Remote sensing results are discussed at the beginning of the chapter and are used to identify regional lineament patterns. This is followed by the description of the structural analysis carried out during the project, the detailed study of the Helleren Fault Zone, the discussion of the K/Ar dating results and the palaeostress analysis of the brittle structural data.

4.1 Remote sensing and lineament analysis

Goals of lineament mapping in study area

Lineament mapping from DEM's has been carried out both at a regional and more local scale in the study area. This technique is used to identify regional and local patterns of the main fracture sets in the Åna-Sira Anorthosite (ÅS) and use those data in combination with field observation and multiscalar structural analysis to unravel the tectonic evolution of the area. The Bjerkreim-Sokndal layered intrusion (BKSK) and the nearby Sveconorwegian basement are used as reference time markers to see if the fracture patterns vary between the different rock types during deformation episodes pre- or postdating the emplacement of the ÅS. High resolution DEMs (LiDAR) were available only for a relatively small area close to the Titania AS open pit mine and allowed a local detailed lineament map.

4.1.1 Regional mapping

4.1.1.1 Technical details

The study area is affected by a large-scale lineament system, as can be established from the analysis of DEM's. An area of 34 x 30 km^2 was mapped (Fig. 4-1b); it contains three main rock units, the ÅS, the BKSK and the Sveconorwegian basement. The three different domains were analyzed by remote sensing individually and the covered area is shown in Fig. 4-1. Three new hillshaded images were generated with three different illumination azimuths, 045, 180 and 315 respectively (Fig. 4-1c-e). The chosen areas were mapped at scale 1:125 000 and 1:40 000, thus making it possible for three lineaments maps to be produced for each scale and each lithology. In total, eighteen lineaments maps were generated and later use to populate rose diagrams (Table 4-1). To minimize bias and to increase the reproducibility of the study some operating guidelines were followed, as suggested by Scheiber et al. (2015):

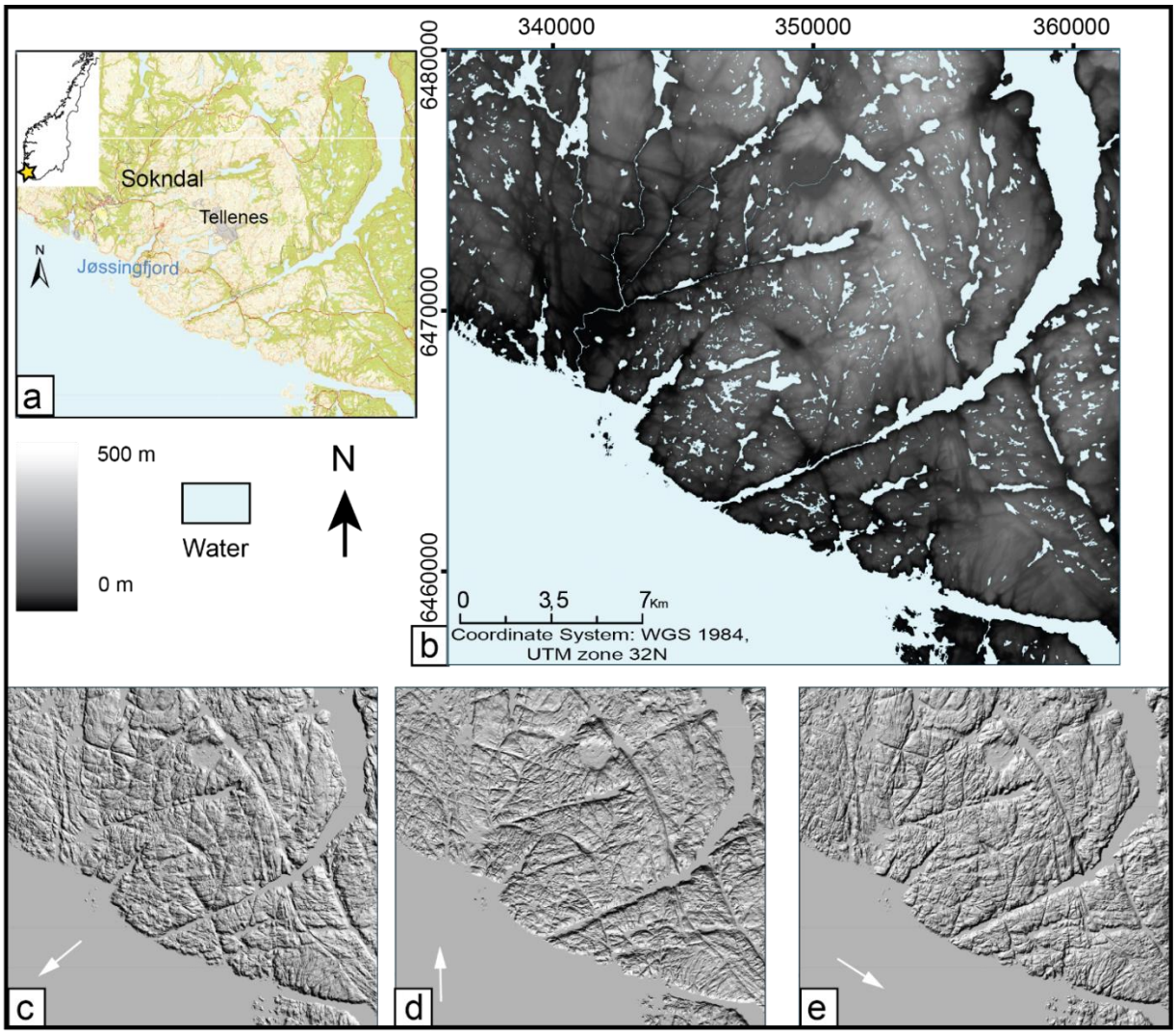

Fig. 4-1: The area analyzed for lineament mapping. The DEM is illuminated from azimuth (c) 045, (d) 180 and (e) 315, as indicated by the small white arrows.

Scale: what is the most appropriate scale

By using the 1:125 000 scale, possible large-scale patterns are better recognized and this scale is thus appropriate to gain an idea of the main fracture sets dissecting the study area at the regional scale. However, the area was also mapped at the 1:40 000 scale aiming at more details of the regional lineaments and aiming at a critical comparison with the results obtained from the maps mapped at the 1:125 000 scale. Because of the limitation of the 10 m DEM, smaller scales than 1: 40 000 would make the elevation model blurry and difficult to read. The smaller the scale, the more lineaments are mapped. Generally, the larger scale enhances some more distinctively existing spatial trends, but the smaller scale highlighted one more distinct pattern oriented NW-SE that did not emerge at the 1:125 000 scale (Table 4-1).

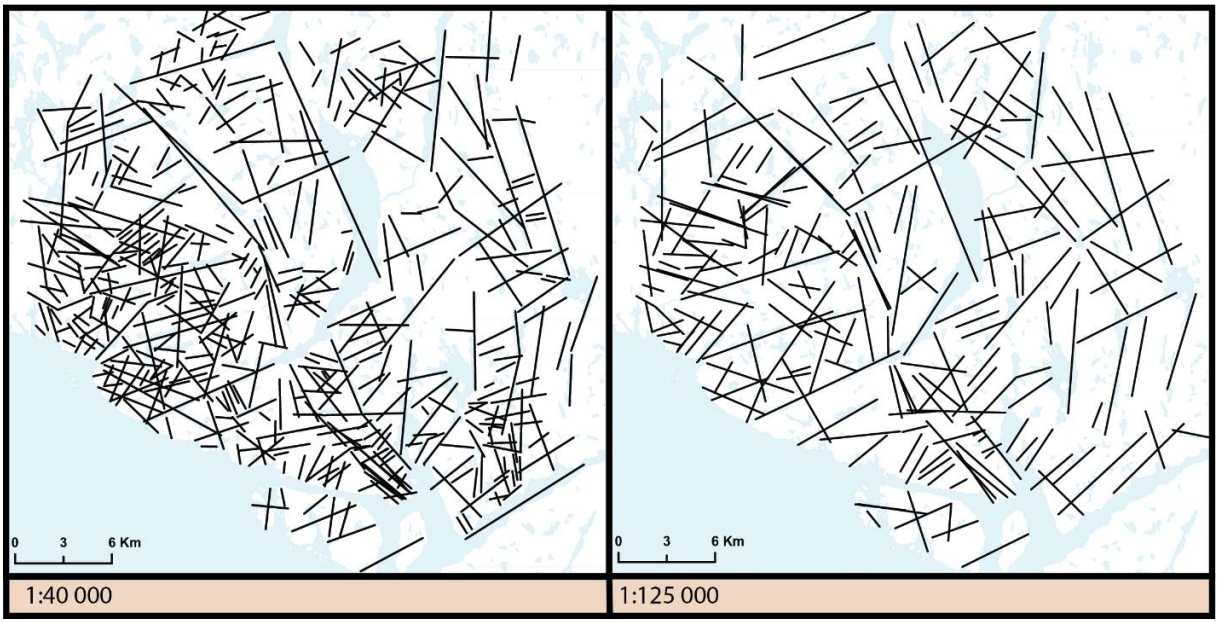

Fig. 4-2: The effect of different scales. Lineaments are picked longer at the largest scale whereas for the smaller scale they become shorter, more fragmented and more patterns are recognized. Both are mapped with illumination azimuth 315° on the DEM.

Illumination azimuth: what direction to use and why?

To prevent overlooking of some structural trends or artificial enhancement of others, lineament mapping was carried out at three different illumination azimuths, including parallel and perpendicular to the dominant and most obvious fracture trends. The dominant fracture trends in the anorthosite are oriented WNW-ESE, N-S and WSW-ENE; illumination azimuths were therefore chosen to be 045, 180 and 315, with 315 being the most commonly used orientation in general (Scheiber et al., 2015). Illumination from 180° seems to be the most reliable, because lineaments perpendicular to 180° are not distinct for any scale or rock type. For illumination azimuth 045° and 315°, perpendicular lineaments are more easily detected than other trends, thus biasing the result of the remote sensing picking. The quality of the results from rose diagrams generated by mapping with illumination sources at 045° and 315° can therefore be reduced.

4.1.1.2 Regional lineament systems

A great number of lineaments has been characterized by regional mapping, which made it possible to identify different systems based on their orientation and geological characteristics (Fig. 4-3). The names of the main structural trends are after Karlsen (1997), except one modification introduced in this MSc thesis, which changed the name of N-S trending lineaments to Bjånes lineament system, named after the location where these were observed and best

characterized in field

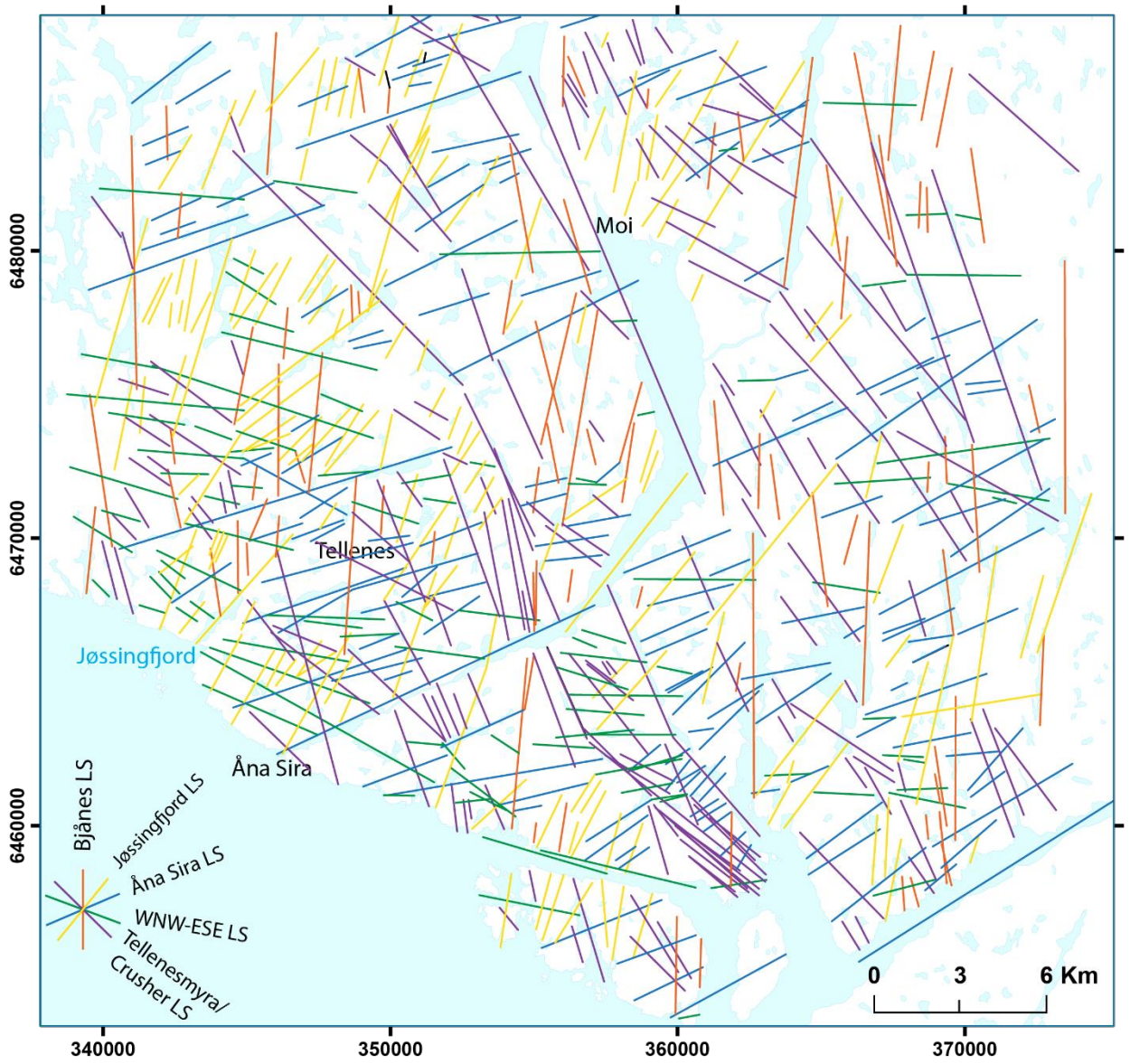

Fig. 4-3: Lineaments at a regional level mapped at the 1: 40 000 scale and divided into five different lineament systems. Colors refer to the graphic key shown in the bottom left corner of the map. The trends highlighted by remote sensing and ground-truthed by fieldwork were named according to the work by Karlsen (1997).

4.1.1.3 Comparing lineaments in the different lithological domains

By looking at the rose diagrams (Table 4-1) developed for each scale and each illumination azimuth, distinct patterns can be recognized. In the layered intrusion (BKSK), a N-S trend is very strong and obvious, regardless of the illumination azimuth (Table 4-1 m-r). This lineament-trend follows the geometry of the layered intrusion and reflects the magmatic structure of the body (Bolle and Duchesne, 2007). When considering jointly the ÅS and the

BKSK, the rose diagrams exhibit a similar pattern for each illumination azimuth, except for the 180° azimuth at the 1:125 000 scale. The two magmatic bodies are temporally related as they are dated to approximately intruded at the same time (c. 930 Ma) and both are cut by the 10 Ma later intrusion of noritic-mangeritic dikes (Bolle et al., 2010) and therefore have been exposed to the same deformation events. This is enhanced by strong N(NE)-S(SW) and ENE-WSW lineament trends in both ÅS and BKSK. When comparing the basement with the ÅS and BKSK, a NNW-SSE-trend is more distinct in the basement than in the two other lithological domains. Fractures and faults oriented NNW-SSE might therefore be due to an event that pre-dates the anorthosite and is thus only recorded in the host basement. This might be related to the development of the basement regional foliation and metamorphism during the Sveconorwegian or to the emplacement of the anorthosite plutons (Bingen et al., 2008b).

Table 4-1: Eighteen rose diagrams generated from regional lineament mapping. For scale 1:125 000 aperture=19°, weighting factor = 0,9 and maximum radial axis are set to 1,0. For scale 1:40 000, aperture = 13°, weighting factor = 0,9 and maximum radial axis are set to 1,6. The axial radial value is slightly different for the two scales, to make it easier to see the trends in each scale. For scale 1:40 000, the aperture is reduced to 13° to prevent the data to be too generalized i.e. too smooth (Munro and Blenkinsop, 2012). This effect is due to more observations at lower scales than higher scales.

Scale	1:125 000			1:40 000		
	045	180	315	045	180	315
Basement	a 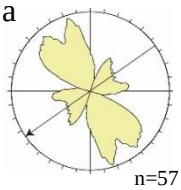 n=57	b 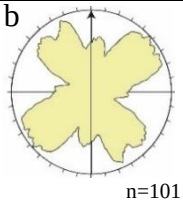 n=101	c 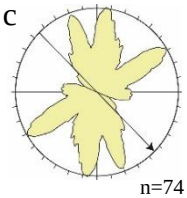 n=74	d 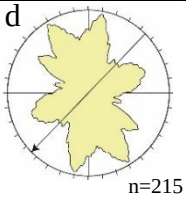 n=215	e 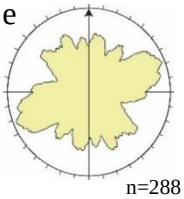 n=288	f 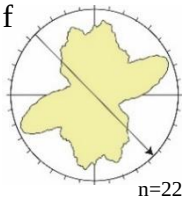 n=22
Åna-Sira Anorthosite (ÅS)	g 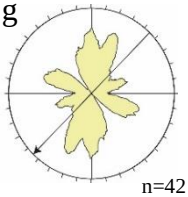 n=42	h 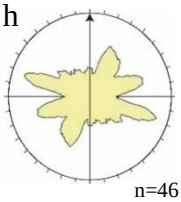 n=46	i 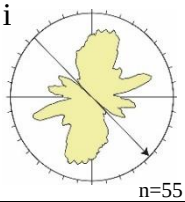 n=55	j 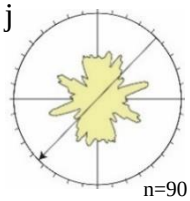 n=90	k 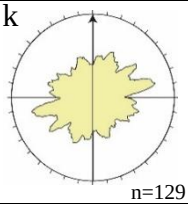 n=129	l 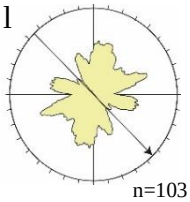 n=103
Layered Intrusion	m 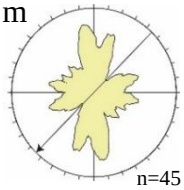 n=45	n 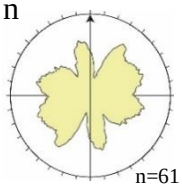 n=61	o 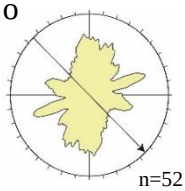 n=52	p 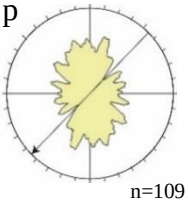 n=109	q 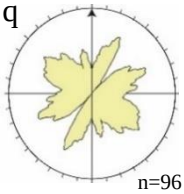 n=96	r 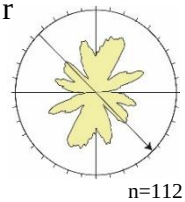 n=112

1. N-S to NNE-SSW Bjånes lineament system

The distinct N-S trending lineaments appear to be strongly represented in all the rock types present in the study area apart from the basement at the 1:125000 scale and illuminated from 045°, which contains more obvious NNW-SSE lineaments (Table 4-1a). These lineaments are long and distinct widely distributed over the whole ÅS. At the north- western part of the Tellenes ore-body these lineaments are very distinct and close to Bjånes these features are observed in the field as faults with lateral movement. The BKSK and the basement have distinct N-S patterns that are likely associated with magmatic layering and foliation of the basement and do not reflect regional fracture systems.

2. ENE-WSW Åna-Sira lineament system

The lineaments of this system stand out in ÅS as forming a significant trend in the rose diagrams regardless of scale or illumination azimuth (Table 4-1 g-l). The same system is also present in the basement and BKSK. These lineaments are pervasive over large areas and can be up to 12 km long. They are named after the lineament running through Åna-Sira. This system can be identified and traced in the entire Åna-Sira Anorthosite (ÅS) Complex, where it defines one of the most distinct lineament sets in the body. Major lineaments in this system are the Tellenesvatn, Åna-Sira and Åmot (Fig. 4-4). The Åna-Sira lineament exhibits an interesting contact to the layered intrusion, possibly indicating a sinstral strike-slip displacement or a normal fault if the lineament is dipping gently towards NW or a thrust if the lineament is dipping towards SE (Fig. 4-4). Anyhow, the lineament can be associated with a fault.

3. NE-SW Jøssingfjord lineament system

This system is best seen with a 180° illumination azimuth (Table 4-1), which is also the preferred azimuth for the general remote sensing analysis of the area. The Jøssingfjord lineament system is best developed near the coast and the Jøssingfjord lineament is the major feature of this system. These lineaments are generally short (max. 4 km) compared to other sets, but are very distinct. The Helleren Fault Zone is part of this lineament system, and the last brittle deformation increment accommodated along it was dated by illite K-Ar to 405 ± 10 Ma.

4. WNW-ESE lineament system

This is a strongly developed system, which is well-defined in all the rose diagrams for the ÅS complex. The system is particularly well developed near the coast with the longest lineaments extending up to c. 7 km (Fig. 4-4). They are also parallel to the Egersund dike

swarm, which require an evaluation of the possible genetic relationships between the dykes and the brittle lineaments.

5. NNW-SSE "Crusher" lineament system

This system is most dominant in the basement (Table 4-1), but occurs in the other lithologies as well. The fracture system is recognizable at all scales and illumination azimuths. This system contains short lineaments, which are difficult to separate from the Tellenesmyra lineament system at a regional scale.

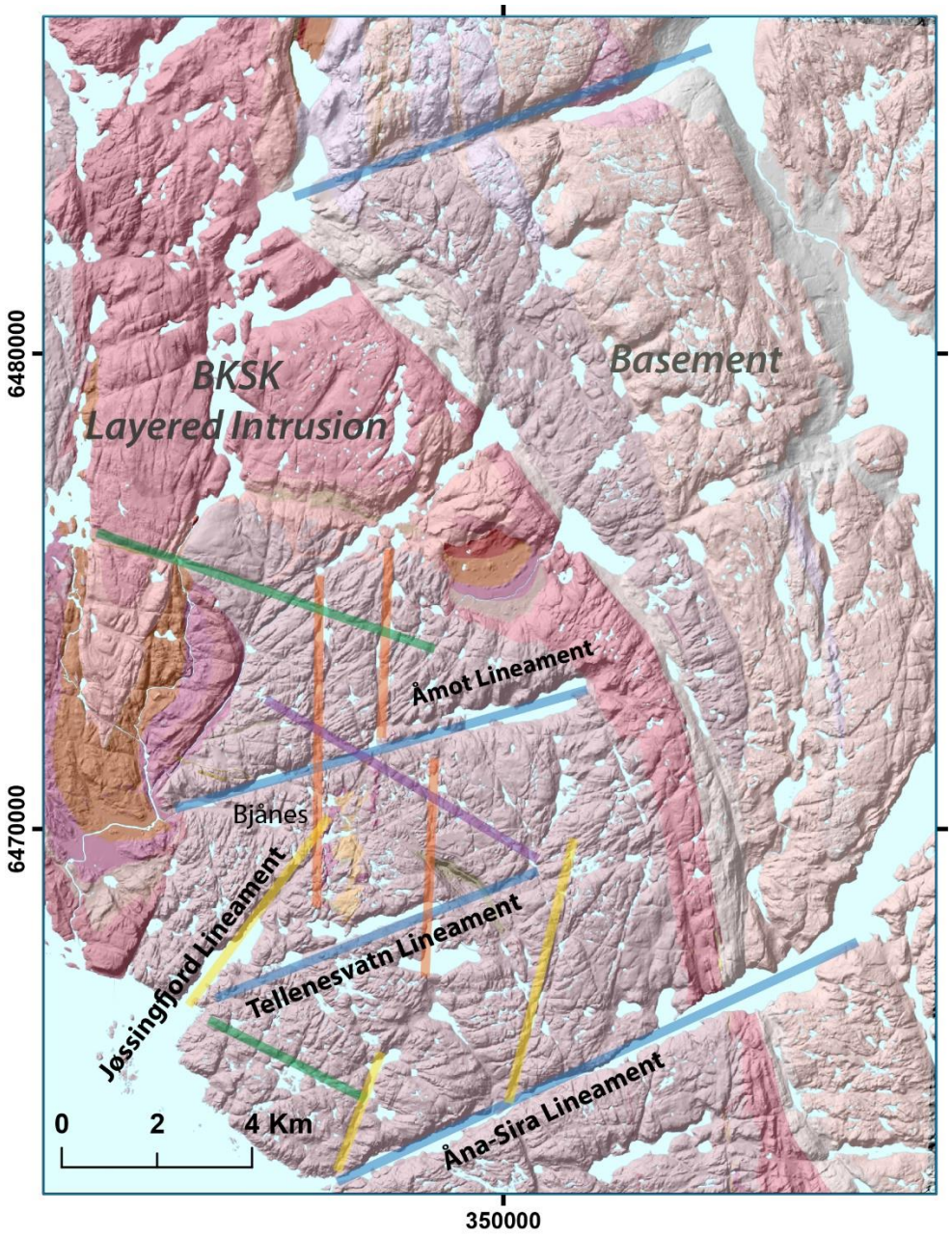

Fig. 4-4: Major lineaments in Åna-Sira anorthosite. Notice the lateral displacement of ÅS and BKSK along Åna-Sira Lineament.

6. NW-SE Tellenesmyra lineament system

This is the dominant fracture system at the 1:40 000 (Table 4-1) scale except when the illumination azimuth is parallel to the fracture system, i.e., illumination azimuth 315°. Lineaments are most distinct and extensive near the coast, where they can be up to 8 km long, whereas they become shorter close to Tellenes. The elongation direction of the Tellenes ore body is parallel to this lineament system.

4.1.2 Analysis of lineaments in the Titania AS open pit by LiDAR-data

The economic importance of the world's greatest ilmenite deposit located just above the Jøssingfjord, made it possible to interpret an even more detailed DEM of some parts of the study area. Therefore, a specific lineament study by using LiDAR data from the area around the pit, called Tellenes, was carried out to generate a detailed lineament map and to see whether the results derived from the high-resolution dataset compare well with those derived from the regional DEM interpretation. Geologically, the orebody is situated in a norite body within the Åna-Sira Anorthosite.

A 31 km^2 area within and around the pit was mapped. Three hillshaded images were generated in ArcGIS with three different illumination azimuths of 045°, 180° and 315°. The area was mapped at two scales, 1:20 000 and 1:8000, and lineament maps were generated for both scales and the three illumination azimuths (Fig. 4-5), thus creating a total of six lineament maps (Table 4-2). The advantage of using the 1:20 000 scale is the possibility to enhance the main lineament trends and give a better understanding of the fracture patterns at the larger scale. The 1:8000 scale is used as the smallest scale because details of the bedrock structures are shown clearly enough, such that smaller scales were not necessary.

Illumination azimuths were chosen to be the same as for the regional lineaments maps, because the ore body is situated in the ÅS and therefore shares the same dominant fracture trends. This gives also an opportunity to better compare the two different DEMs.

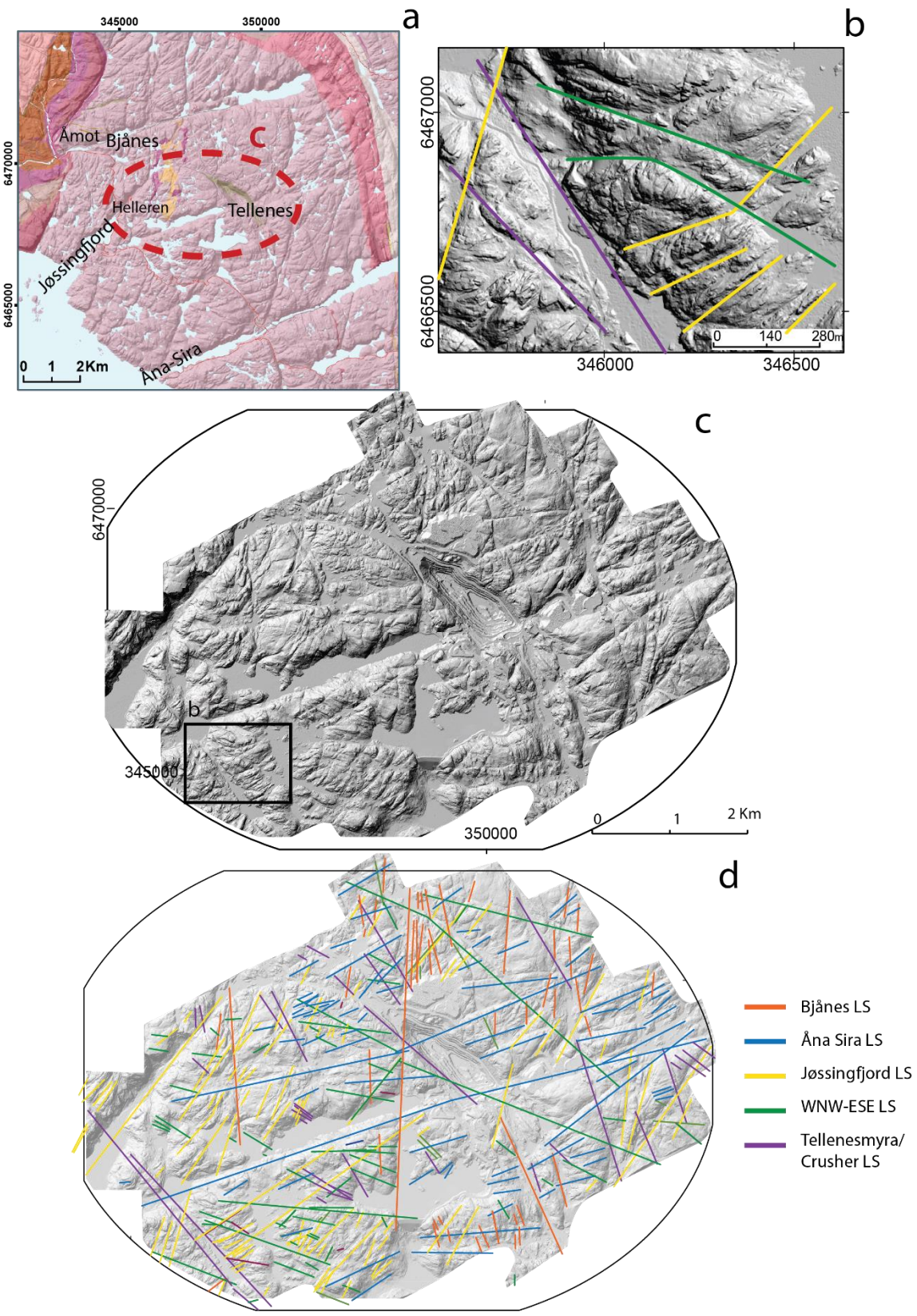

Fig. 4-5: (a) Geological base map highlighting the study area covered by the LiDAR-data (Marker, 2013). (b) Detail of the three mapped lineament sets down to scale 1:8000. (c) Hillshaded DEM with illumination azimuth 315°. (d) Lineaments divided into the lineament systems (LS) mapped at 1:8000 scale.

Table 4-2: Rose diagrams of lineaments mapped in the area around Titania AS ilmenite mine. Lineaments are mapped at two scales, 1:20 000 and 1:8000 and with three different illumination azimuths (045°,180° and 315°) creating six maps that were used to create six rose diagrams. Parameters for the rose diagrams in the MARD software (Munro and Blenkinsop, (2012) were set to aperture=9°, weighting factor=0,9 and maximum radial axis = 1,6. Remarkable is the strong NE-SW trend that appears in all diagrams.

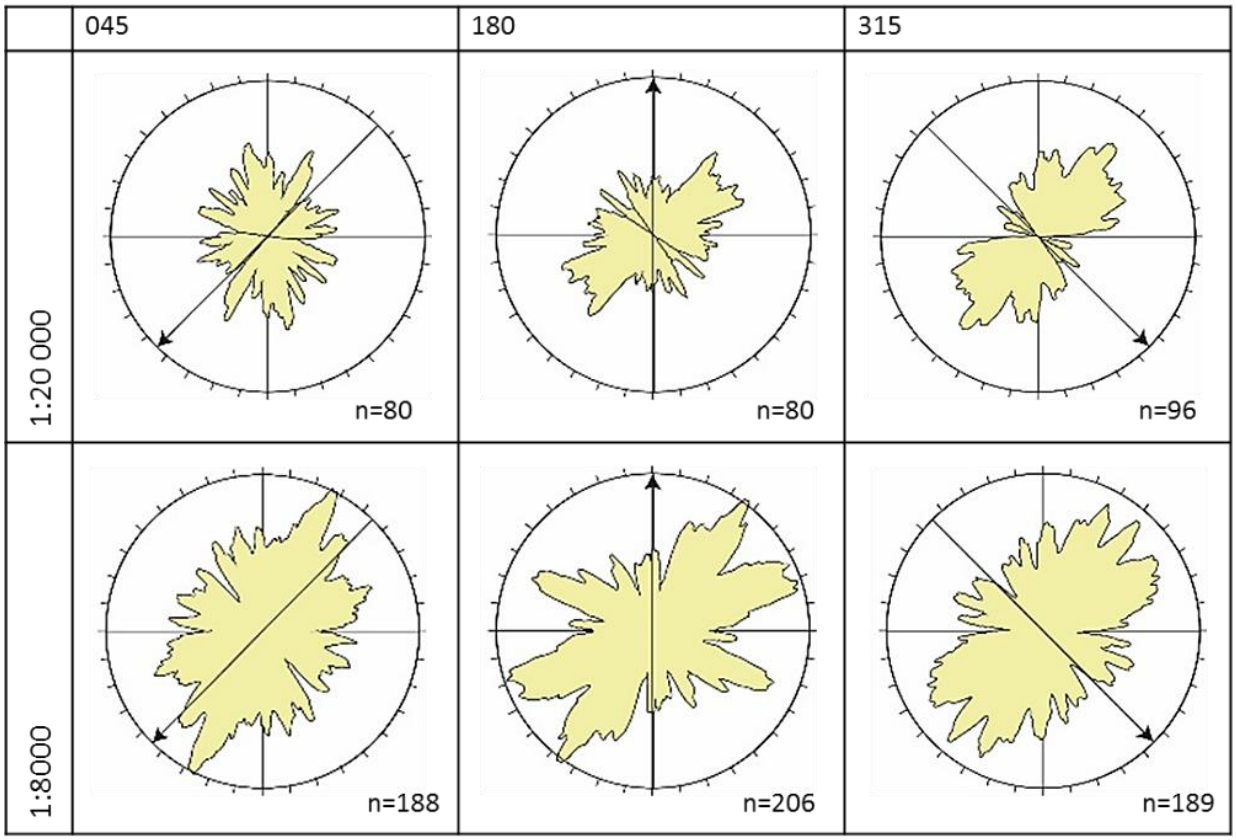

Comparing the rose diagrams

The six rose diagrams (Table 4-2) created from the Tellenes area share the same shape of the rose diagrams mapped in the ÅS and the BKSK. However, there are some interesting differences. The six rose diagrams form Tellenes have a very distinct NE-SW trend regardless of illumination azimuth and scale, which is not so clear in the ÅS in Table 4-1. This orientation reflects essentially the Jøssingfjord lineament system, which contains the Helleren fault zone (HFZ). The N-S trend is not as dominant in Tellenes as it is at the regional scale, the WNW-ESE trend is dominant locally and regionally with 180° as the most reliable illumination azimuth. The main trends can be classified according to the same classification used for the regional scale:

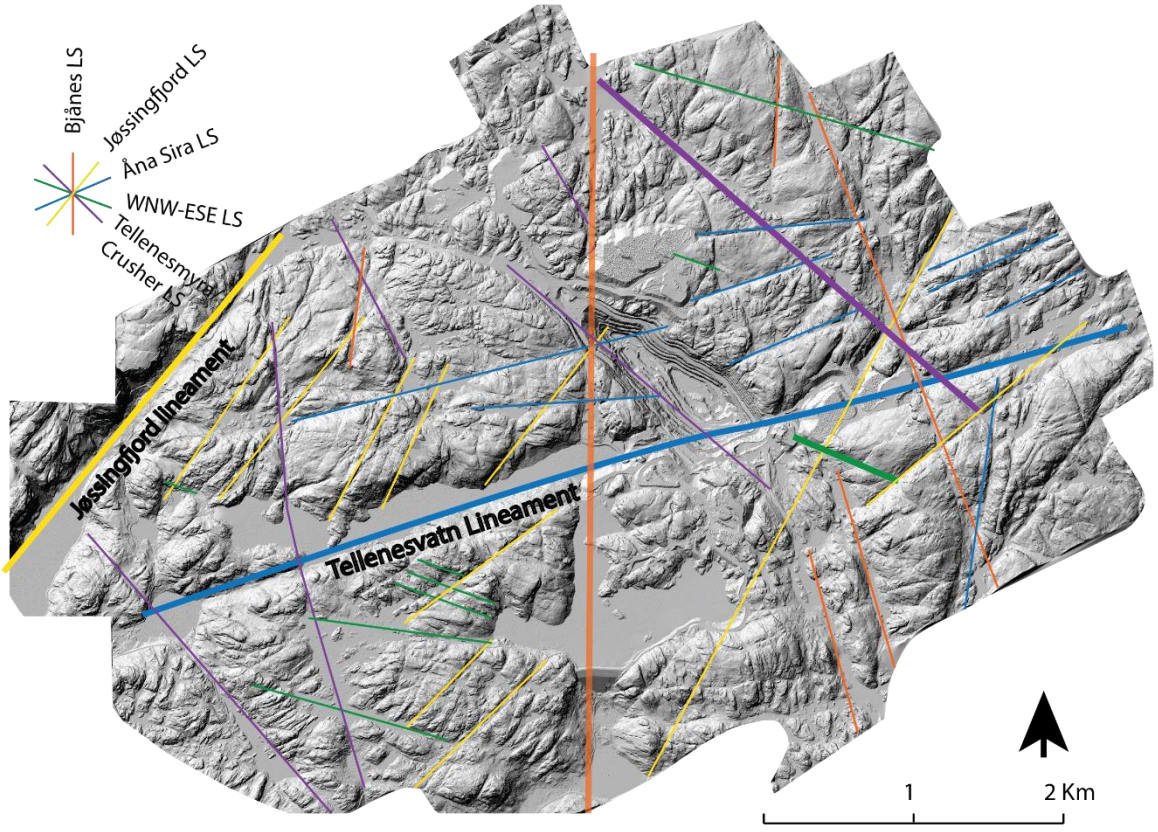

Fig. 4-6: Main lineaments in the area near Tellenes Ore body.

1. N-S Bjånes lineament system

There is one major lineament possibly belonging to this set that crosses the whole DEM-image (Fig. 4-5). Krause et al. (1985) mapped this lineament and interpreted it as a fault dipping 70° towards the west. This fits my observations along the roadcut close to Bjånes (see section 4.2.1) that indicate the same steep attitude associated with brittle faults decorated by complex fault rock associations. In addition, these lineaments occur commonly together, with only low spacing separating them (c. 60-100 m) and pervasive alteration of the host rock.

2. ENE-WSW Åna-Sira lineament system

This set contains very distinct lineaments. Three major lineaments crosscut the pit. The Tellenesvatn lineament is the most distinct, with a length up to 8 km. In the field, lineaments belonging to this set are characterized by well-defined damage zones defined also by bleached anorthosite and increased fracture density.

3. NE-SW Jøssingfjord lineament system

One distinct lineament of this system is seen in the southeastern part of the pit. The Jøssingfjord is also seen in the LiDAR-image in the southwestern corner (Fig. 4-5). The Jøssingfjord lineament system can be difficult to distinguish from the Åna-Sira lineament system in the rose diagrams (Table 4-2), but at the 1:8000 scale with illumination azimuth 180° the two lineament systems have distinct peaks and in Fig. 4-6 these two systems are clearly distinguishable.

4. WNW-ESE lineament system

This is a less developed system in the Tellenes area, but some larger scale lineaments are mapped. These lineaments are parallel to the Egersund dike swarm and the bold green line in Fig. 4-6 indicates the orientation of one of these dikes crossing the pit. The southern part is also affected by lineaments that geometrically can be assigned to this WNW-ESE trend.

5. NNW-SSE "Crusher" lineament system and NW-SE Tellenesmyra lineament system

This system is not indicated by any distinct peaks in the rose diagrams, but the detailed analysis of the lineament map (Fig. 4-5d) demonstrates that this system has some extensive lineaments running parallel to the ore body. Since we know that the norite, which contains the Tellenes Fe-Ti deposit, was emplaced at 920 Ma, i.e. about 10 Ma later than the anorthosite (Schärer et al., 1996), we might conclude that this lineament system is one of the oldest in the area.

4.2 Mapped structures in the study area

This section describes important fault zones in the study area. Three main areas were studied in detail in field; these are indicated on the map as Bjånes roadcut, Tellenes Fe-Ti ore deposit and Helleren (Fig. 4-7). In addition, structural observations were collected in other subareas within the study area. The fault zones have undergone different deformation phases; however, all have a dominant brittle component characterized by clay rich gouge and brecciated fault rocks. Observations made in the field can be conveniently related to the structural trends that were mapped through remote sensing.

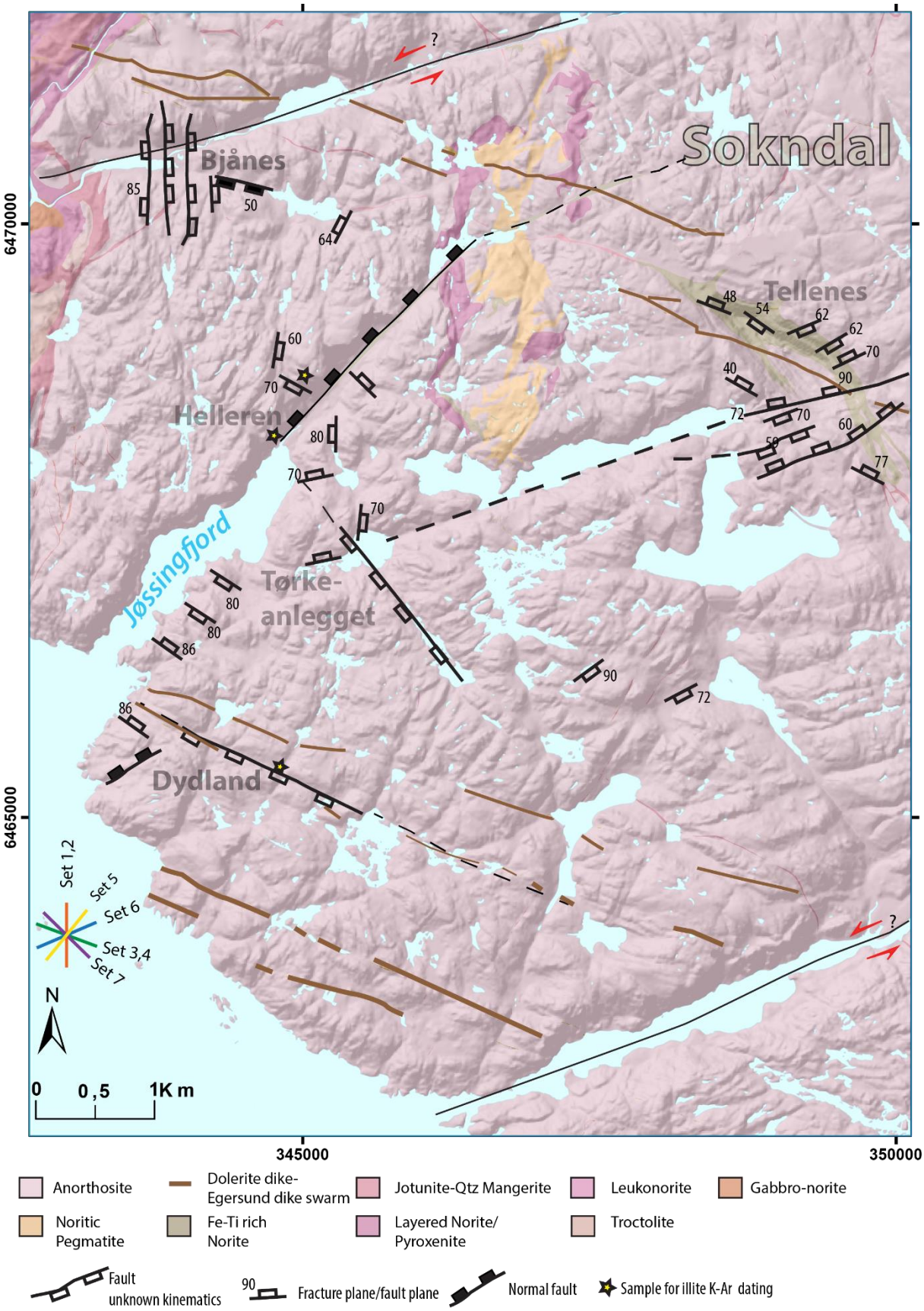

Fig. 4-7: Structural map of the study area mapped in this study. Lithologies were not mapped in this study and are taken from NGU national data base and Marker (2013).

4.2.1 Bjånes road cut

The Bjånes road cut is c. 1km long and is crops out along the southern side of Rv44, close to Bjånes in Hauge i Dalane (Fig. 4-8). The easily accessible road cut is entirely within anorthosite and contains several fault zones that were mapped and studied systematically and are described below. Fault zones vary from a few cm up to 5 m in thickness.

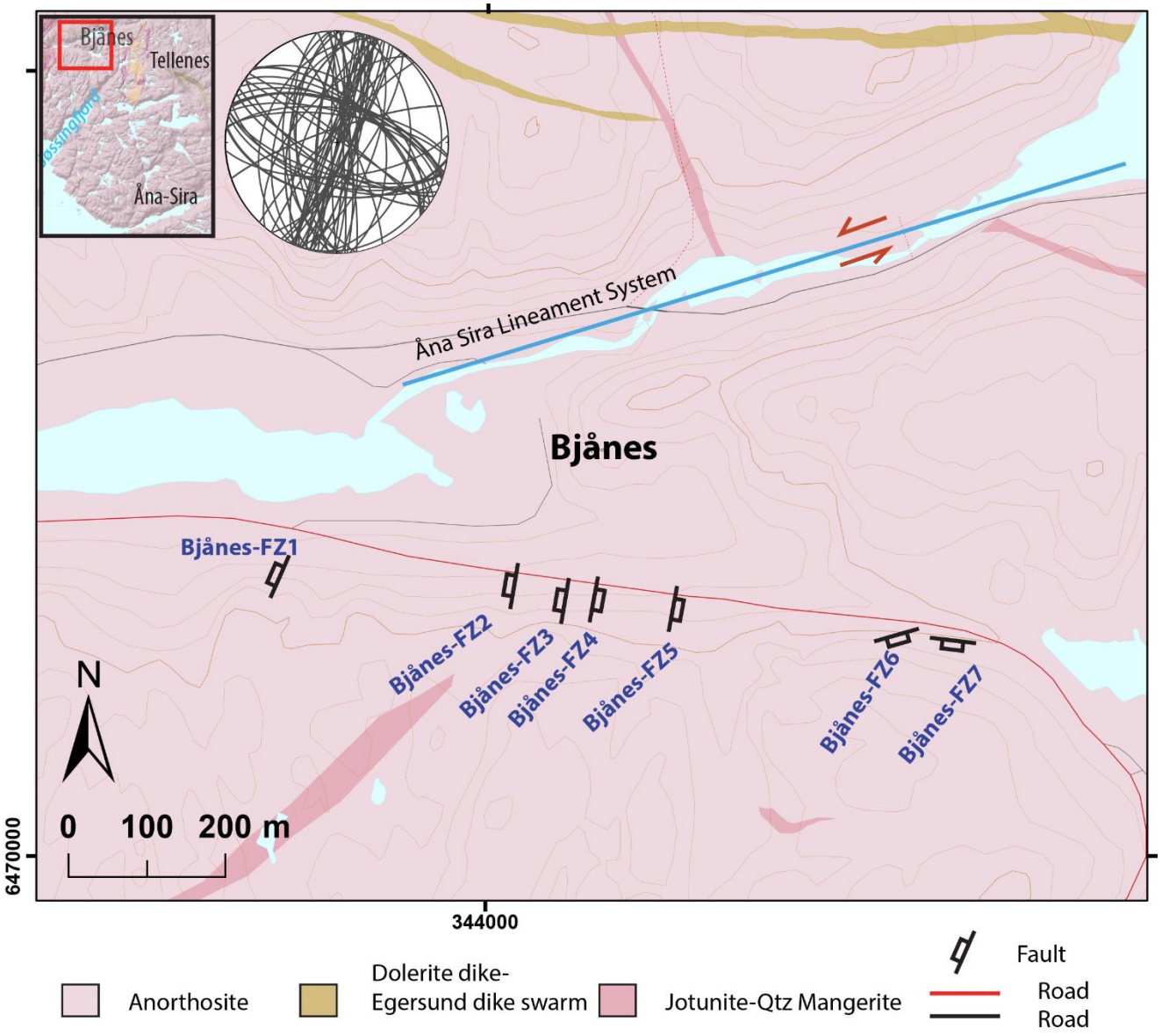

Fig. 4-8: Bjånes road cut with the seven steep dipping fault zones (FZ) that are described in this sub-section. The stereonet plot show all measurements from Bjånes.

4.2.1.1 Bjånes Fault Zone 1 (BFZ1)

Fault zone 1 is exposed in the western part of the road cut. It is a c. 2 m thick sub vertical fault that strikes N-S perpendicular to the road with a steep dip that varies between E and W. Two discrete zones of high strain localization, defined by gouge and brecciated rock fragments, define the margins of the fault and enclose a more massive center (Fig. 4-10a). The margins are characterized by the presence of alternating thin levels of white clay and bleached crushed host rock, whereas the core is pervasively fractured and infilled by multiple generations of mineral phases such as sulfides, coarse grained quartz (Qtz) and K-feldspars (Kfsp) in lenses interspersed with the bleached anorthosite (Fig. 4-10c). The high content of Qtz and Kfsp within the fault core suggests high fluid circulation along the fault zone during an overall dilatant brittle deformation episode. Frictional sliding and cataclasitic flow are suggested as the dominant deformation processes within this fault but a weak foliation defined by the alignment of Hbl, Bt and Ilm/Mag are observed locally within the fault core. One example is the eastern flank of the fault core that has large elongated clasts of felsic rock trapped in a darker mafic matrix (Fig. 4-10 b&d), indicative of a ductile component with viscous deformation at mineral level (Fig. 4-10b). Because the foliated lenses are reworked in the brittle fault, they are presumably part of an earlier tectonic phase.

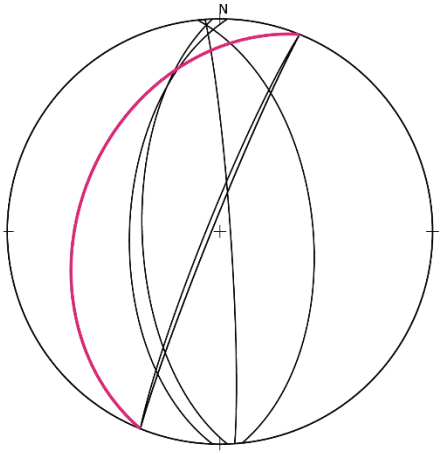

Fig. 4-9: Fault plane measurements, together with measurement of foliation marked with red.

Thin section analysis of the fault zone shows alternating layers of fine and coarser grained bands consisting of Hbl, Bt, Ilm/Mag and Qtz and Kfsp, respectively (Fig. 4-10e, f). Sample AFE_2 document the transition between coarse and fine-grained minerals (Fig. 4-10f). The fine-grained layer consists of Ilm/Mag, Bt, Ep, Hbl, Qtz and Pl while the coarser layer consists of Pl with sericitization interrupted by some coarse grained Hbl and Bt (Fig. 4-10f). The fine-grained layer might be recrystallized cataclasite. Sample AFE_3 consists mainly of very coarse-grained Qtz and Pl. Qtz shows microstructures indicative of a weak dynamic recrystallization by bulging suggesting temperatures once around ~250°C. Quartz shows undulose extinction and elongated subgrains that pass laterally into domains of small new grains formed by bulging and localized subgrain rotation recrystallization. Fluid inclusions follow the grain boundaries of the new subgrains (Fig. 4-10e). Pl and Kfps are pervasively sericitized along the grain boundaries but

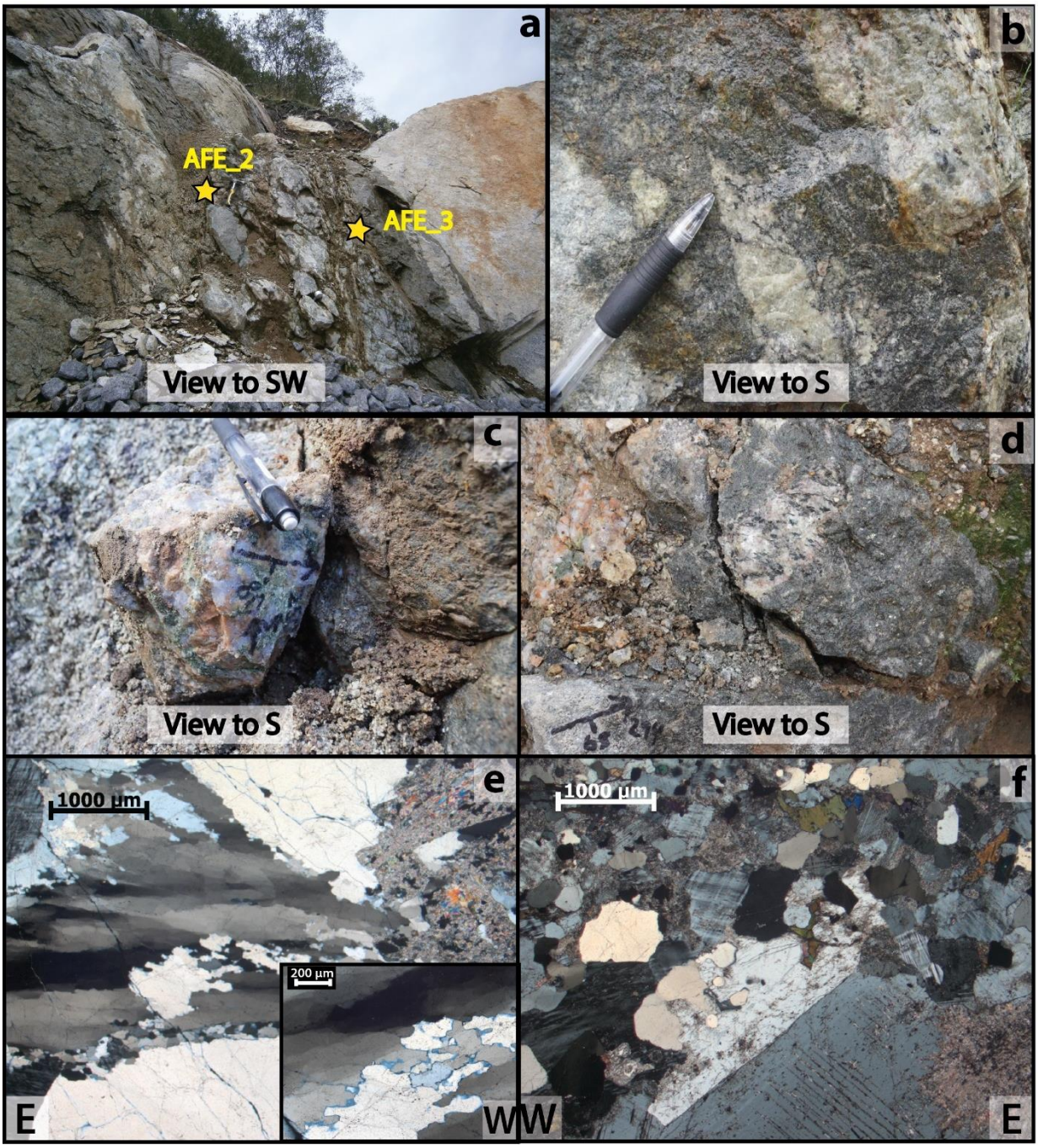

Fig. 4-10: (a) The exposure of Fault Zone 1 with zones of ultra cataclastic rock and gouge on the margins to the host rock. Rock samples for thin section analysis are marked. (b) Elongated felsic clasts with a weak foliation, no clear evidence of frictional deformation. (c) Sample AFE_3, Kfls and Qtz interspersed with bleached anorthosite. (d) A foliated felsic clast within a mafic matrix and sample AFE_2 in bottom right corner. (e) Sample AFE_3 in thin section shows quartz microstructures that are indicative of a weak dynamic recrystallization predominantly bulging. Upper right corner show high sericitization of Pl. (f) Sample AFE_2 in thin section documents a transition from fine grained Pl (upper part) to coarser grained domains (down part). Seritization of Pl is most pervasive in coarser grains. Grain size reduction in the upper part of the image might be in relation to frictional sliding and recrystallization.

also within the grains (Fig. 4-10e; upper right corner). The recognized style of deformation indicates that the fault deformed under various environmental conditions, experiencing both viscous(ductile) and frictional (brittle) deformation. The bleached anorthosite and the various mineral associations within the core suggest important hydrothermalism.

4.2.1.2 Bjånes Fault Zone 2 (BFZ2)

Fault Zone 2 is exposed in the western part of the road cut, where it is exposed as a c. 4 m thick vertical fault that strikes roughly N-S, perpendicularly to the road. The fault dip is sub-vertical (Fig. 4-11 a). The fault is characterized by a highly fractured fault core defined also by c. 10 cm thick bands of gouge on both edges of the core arranged parallel to the fault zone. The gouge zones have a sharp contact to the host rock and are characterized by clay minerals with brecciated fragments of the host rock. The core is formed at the expense of coarse-grained anorthosite but the high density of fractures causes grain size reduction and increases the alteration of the rock, which is expressed by the bleached color of the faulted volume (Fig. 4-11a,b). In addition, thin strands of clay oriented parallel to the fault are distributed within the fault core. Striations on Ep-Chl coated planes were measured and suggest strike-slip faulting (Fig. 4-11c). One set of pervasive fractures, parallel to the road, are observed on the western flank of the fault. Sample, AFE_21 (Fig. 4-11d), is from the fault core (Fig. 4-11e-h) and documents a cataclastic texture developed at the expense of the host anorthosite. Thin section analysis shows that cataclastic deformation initiated by frictional cataclastic flow, as indicated by abundant micro faults, multiple generations of veins and microcracks. Diffuse veins though the thin section overprint the cataclastic texture and attest to repeated fluid flow events.

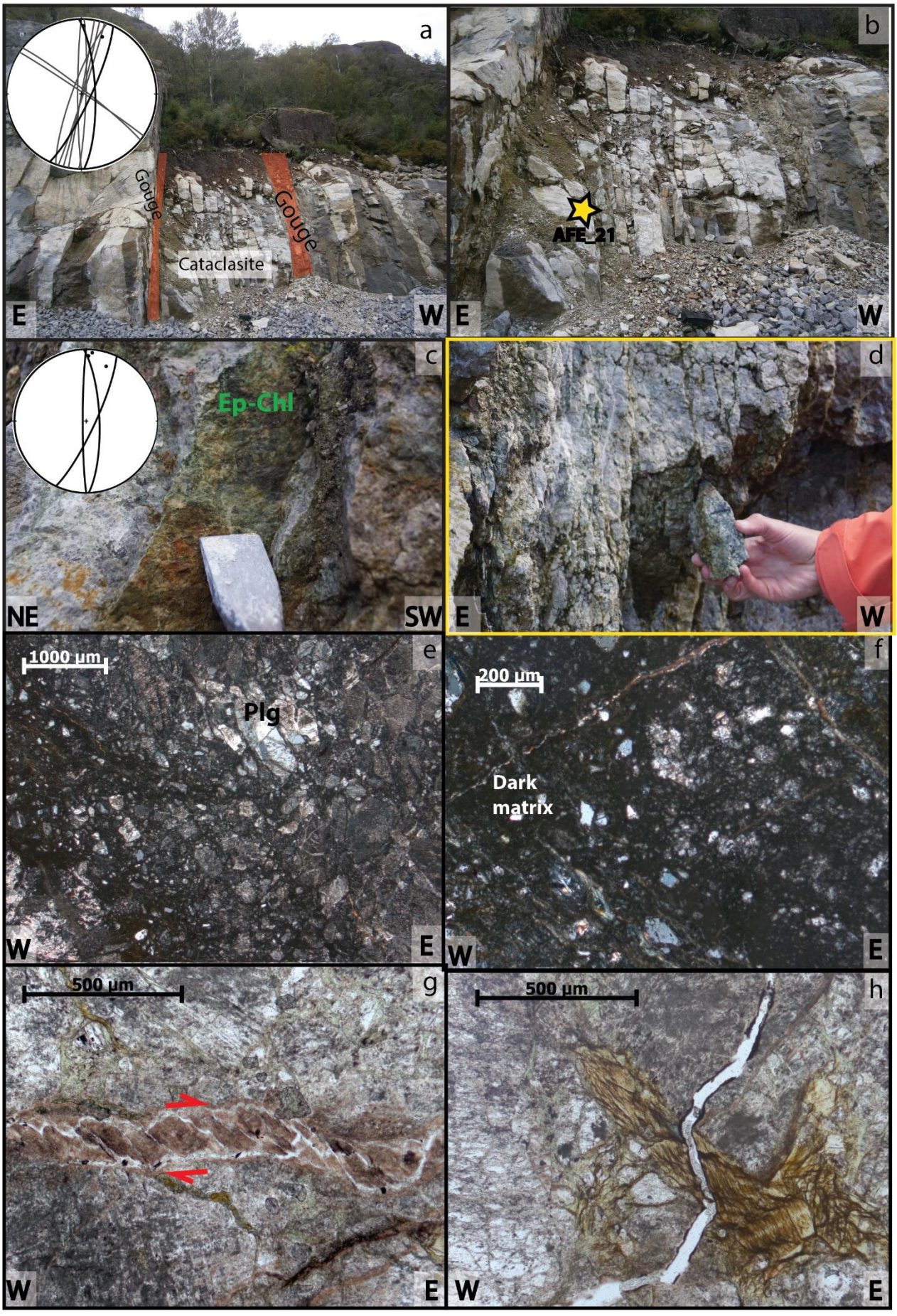
a
Gouge
Gouge
Cataclasite
E
W
b
AFE_21
E
W
c
Ep-Chl
NE
SW
d
E
W
e
1000 µm
Plg
W
E
f
200 µm
Dark
matrix
W
E
g
500 µm
W
E
h
500 µm
W
E

Fig. 4-11: Bjånes Fault Zone 2. a) Fault outcrop characterized by a highly fractured core sandwiched by gouge seams along the edges of the core. The stereonet indicates two distinct sets of fractures. (b) Fractures and microfaults, which only locally produce matrix-dominated cataclasites at the margins of the fault. (c) Ep-Chl coated plane with striations, suggesting a strike-slip faulting component. (d) Sample AFE_21 from the highly fractured fault core. Note the small clasts of crushed host rock. (e) Cataclasitic texture with a very fine grained dark matrix and clasts of brecciated anorthosite. (f) Closer look at the cataclasitic texture and veins cutting this texture. (g) Micro faults within a domino structure formed at the expense of a large Kfls, suggesting a dextral sense of shear. (h) Unfilled vein cross cut the cataclasitic texture.

4.2.1.3 Bjånes Fault Zone 3 (BFZ3)

Moving further east along the road cut (Fig. 4-8), a c. 0.6-0.5 m thick fault zone cuts the outcrop with a c. N-S strike and with a steep dip up to 80° (Fig. 4-12a). The fault has a sharp contact to the host rock with a weak alteration halo surrounding it. At the edges of the fault, the fracture density increases and Ep-Hem-Kln-veins envelope numerous lenses of anorthosite (Fig. 4-12f). This resulted in high alteration of the core expressed by a diffuse lighter color of the anorthosite and a bleached halo at the contact to the dark purple host rock. The eastern fault boundary contains a higher-strain cataclastic texture with locally rotated, white undeformed clay- rich clasts dispersed in a brown-black matrix (Fig. 4-12b, c, d). The clasts are elongated and transposed parallel to the fault and can be characterized as forming a foliated ultracataclasite to gouge. Locally, this texture is disrupted by a texturally more mature gouge (Fig. 4-12 f). This gouge also envelopes fresh anorthosite blocks, generating a boudinage-resembling structure (Fig. 4-12e). A weak striation measured on this fault plane suggest a strike-slip kinematics (Fig. 4-12f). The westernmost fault boundary is less deformed containing only a 1 cm thick gouge rich zone reflecting a higher strain localization on the eastern margin.

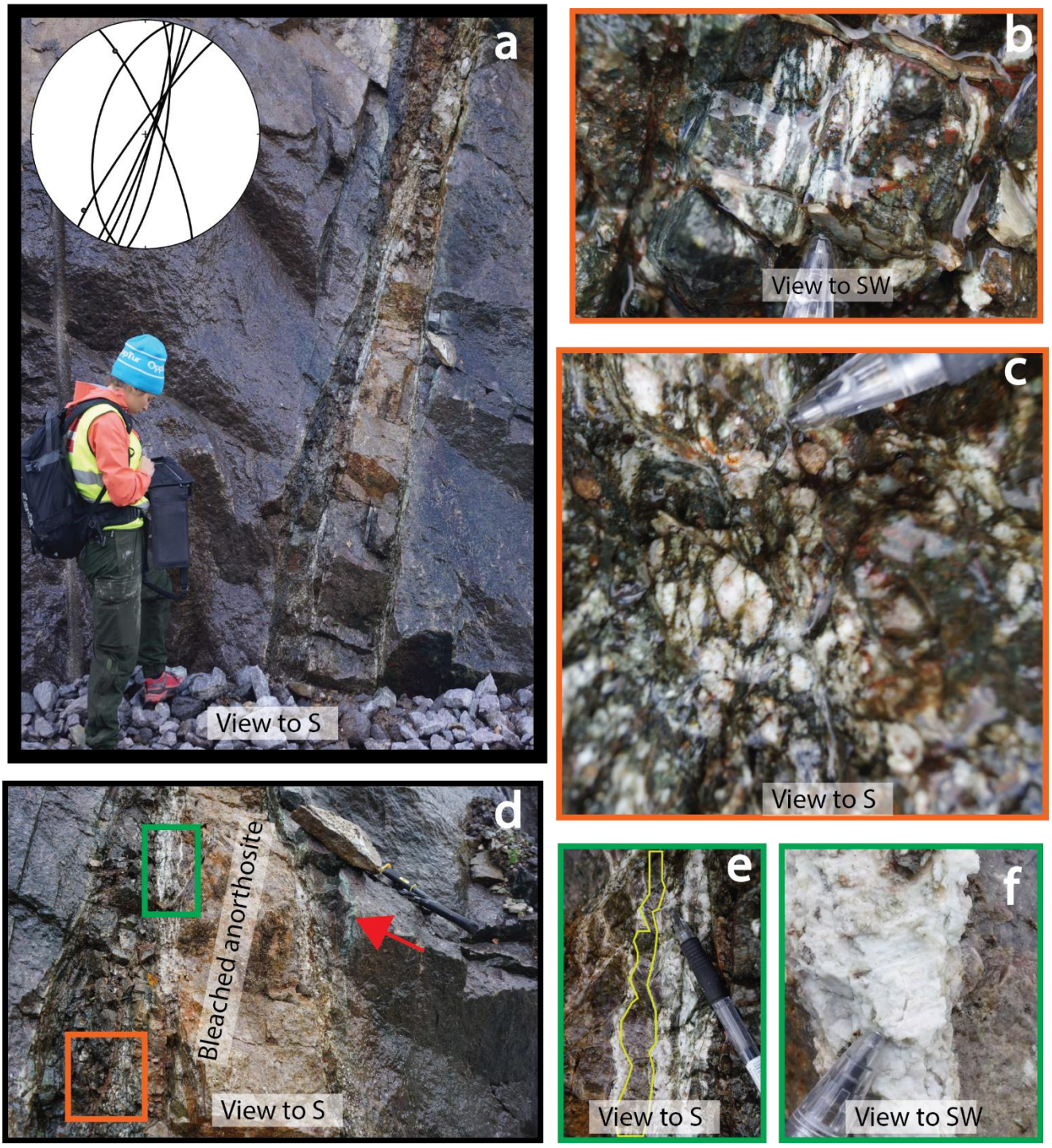

Fig. 4-12: Bjånes Fault Zone 4. (a) Overview of the fault core and stereonet plotting the measured fault planes. The fault has a bleached halo, c. 5 cm wide in thickness. (b) White colored elongated clasts in a dark matrix. (c) Rigid body rotation of white clasts in a dark matrix and some deformation bands. (d) Location of (b), (c), (e) and (f) showing the fault with a bleached anorthositic core, two zones with gouge on the borders and the location of the weakly foliated anorthosite in (b) and (c). (e) Veins filled with clay and some Ep enveloping a lens of still fresh anorthosite (outlined by the yellow lines) reminiscent of a weak boudinage structure. (f) Striation on mature gouge plane indicating strike-slip kinematics.

4.2.1.4 Bjånes Fault Zone 4 (BFZ4)

C. 40 cm farther east from last fault zone is exposed another discrete fault zone. It is a c. 20 cm thick zone trending N-S with a sub vertical dip (Fig. 4-13a & f). The anorthosite has a dull white color along the contact to the fault and the alignment of mafic minerals defines a local weak foliation in the host rock close to the fault (Fig. 4-13a-b). The core contains evidence of pervasive fluid flow as indicated by some greenish, metasomatic and secondary minerals arranged within sub vertical layers and Hem and Kln-rich bands of gouge at the edges of the fault core (Fig. 4-13c). Strain is concentrated at the edges of the fault, as indicated by the gouge bands and the high fracture density that locally generates s a pervasive sub vertical fracture cleavage (Fig. 4-13a). Thin section analysis of sample AFE_6 shows that the green-mineral layers are formed mainly by Ep and some Ms (Fig. 4-1d-e). The coarsest grained Ep is inside the vein while the matrix is fine grained Ms and Ep. This zone differs from the other faults from the same system by the green core. This suggests high interaction between circulating fluids and the rock, resulting in a new mineral phase in the core of the fault.

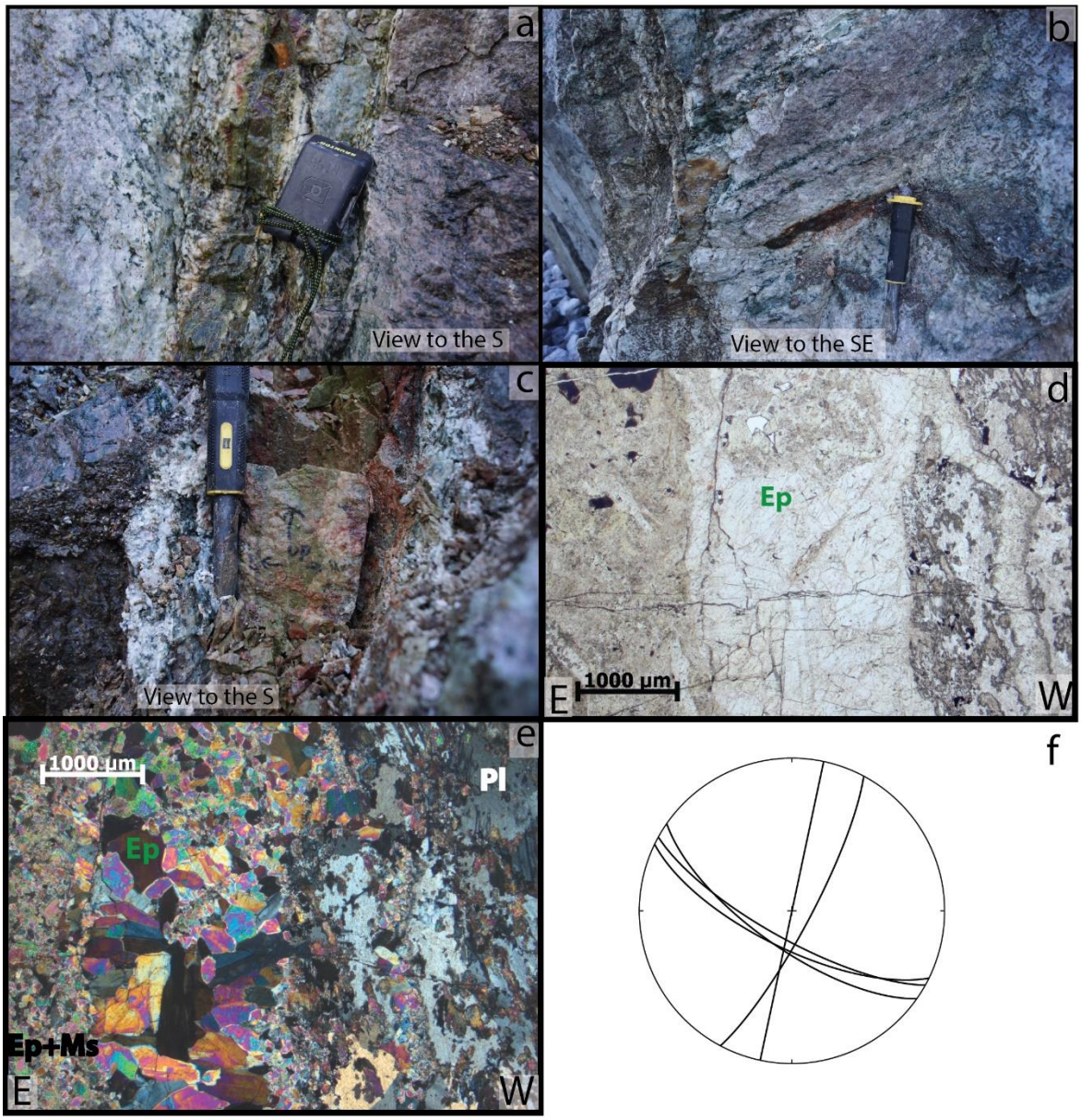

Fig. 4-13: Bjånes Fault Zone 5. (a) Fault core with a bleached halo at the margins. Note the foliated anorthosite to the right. (b) Foliation bands in the immediate surrounding host rock. The mafic minerals define the bands and the host rock varies in color. (c) Sample AFE_6. (d) Green vein in (a) and (c) seen in a thin section, filled by Ep surrounded by finer grained Ep and Ms, PPL (e) Coarse-grained Ep in the vein surrounded by fine grained Ep and Ms. (f) Fault plane trending NNE-SSW with a fracture set parallel to the road (WNW-ESE).

4.2.1.5 Bjånes Fault Zone 5 (BFZ 5)

Fault zone 5 is exposed at the eastern part of the road cut. It is a 40 cm wide cataclastic fault core with a sharp contact to the anorthosite to the east whereas the western contact is a continuous damage zone with high fracture density for 1 m, before reaching the massive anorthosite. The fault dips c. 60° towards ESE and contain more clasts of crushed rock than the steeper faults seen along the road cut. Alteration and deformation have induced a bleached color in the anorthosite affected by the fault. The fault contains bands of gouge interrupted by highly fractured rock where the thickness changes from 40 cm in the upper part to a wider, diffuse fan in the lower part (Fig. 4-14a). The highest amount of strain seems to be localized along the easternmost contact as shown by very significant grain size reduction towards east (Fig. 4-14b). Colors in this zone vary from green to black, red and pink, indicating a mix of different mineral phases created by active faulting and hydrothermal activity (Fig. 4-14b). The cataclastic structure seen in the field is confirmed by microscopy and by diffuse veins filled with Ep (with minor Op) and a cataclastic matrix formed by Ep, Pl, Ms/sericite (Fig. 4-14 c&d).

Sample AFE_8 is very fine grained due to grain size reduction from frictional processes of coarse grained anorthosite documented by micro faults, fractures and several veins (Fig. 4-14c). High alteration caused by saussuritization and sericitization generate a dusty color of the mineral assemble. Cataclastic deformation is dominant towards the east while coarser grained Ep cut by micro faults dominates towards the west. Metasomatic processes overprint the cataclastic texture.

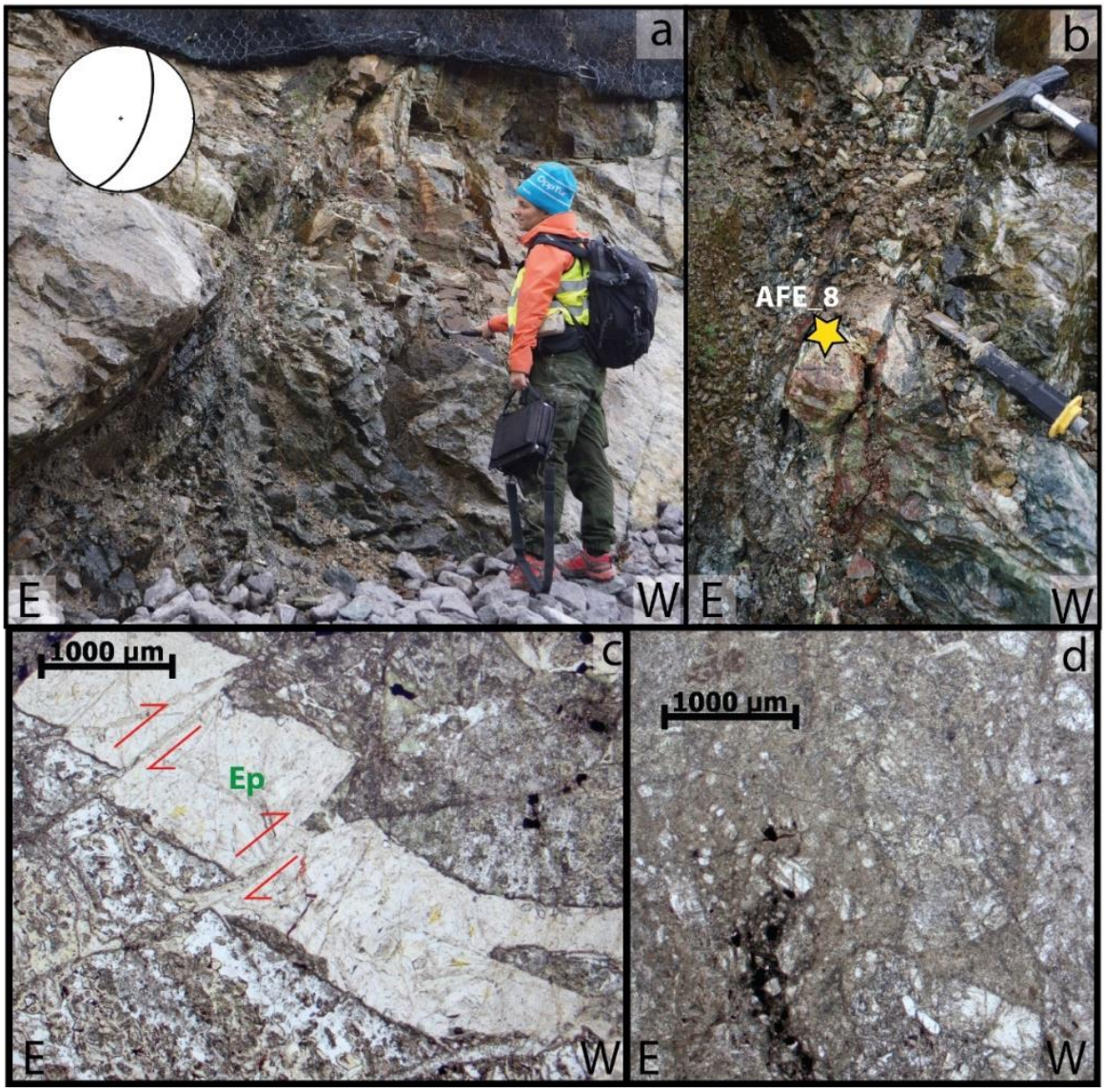

Fig. 4-14: Bjånes Fault Zone 6, Cataclastic fault. (a) Overview of the fault with a high strain zone to the east and an ambiguous contact towards the west to the fresh, undeformed anorthosite. (b) Zooming into the cataclastic fault core. Note the various mineral phases in band parallel to the fault core. (c) Vein filled with Ep investigated in the microscope. Microfaults indicate a dextral sense of shear. (d) Cataclastic deformation dominates towards the east.

4.2.1.6 Bjånes Fault zone 6 (BFZ6)

Along this section of the road cut, the appearance of the anorthosite changes significantly. The color is brighter, there are several fracture sets and there seems to be an enrichment in mafic components in the brittle fault core overprinted by cataclastic deformation. Fault zone 6 stands out from the other fault zones in the area with an E-W trending strike and c.60° dip (Fig. 4-15a). It is exposed over a c. 5 m thick section and it contains a c. 1 m thick core. Similarly oriented fracture sets are observed farther west, but not as discrete fault strands as in this part of the road cut. The fault core is weakly foliated, with the planar anisotropy defined by alignment of Cpx and alteration product in a pale white matrix of altered Pl and pegmatite. The foliation is exclusively localized within the fault core. Lenses of coarser grained massive rock formed by Qtz and Kfsp are disseminated within the foliated core (Fig. 4-15b). The core has a sharp contact to the bleached anorthositic hanging wall (Fig. 4-15a) and a less defined contact to the footwall. The upper most part of the core at the border to the hanging wall is magnetic and a thin vein of magnetic material crosscuts the core associated with a sinistral sense of shear (Fig. 4-15d, e). Striations along the fault plane suggest a dip-slip normal sense of shear (Fig. 4-15a; stereonet).

A closer look at the geological map (Fig. 4-7), shows that there is a thin body of quartz mangerite with the same orientation as the fault, mapped just 800 meters from the fault with only a little lake between them. Farther east, the quartz mangerite forms the continuation of the norite, hosting the Fe-Ti deposit at Tellenes. It is known that the zone of norites, leuconorites and mangerites intruded c. 920 Ma years ago, c. 10 Ma after the anorthosites (Schärer et al., 1996) and intruded along tectonic weaknesses within the anorthosite. Since the foliation is concentrated in the fault core, later deformation might have caused strain localization in the fault core and creating this local foliation. Later brittle deformation overprints the foliation with fractures, crushed rock and the two brittle fault margins envelopes the fault core with striation indicating normal faulting. In the same location, thin (c. 0.5m) pegmatites are observed and seem to follow fractures and other planar anisotropies of the rock.

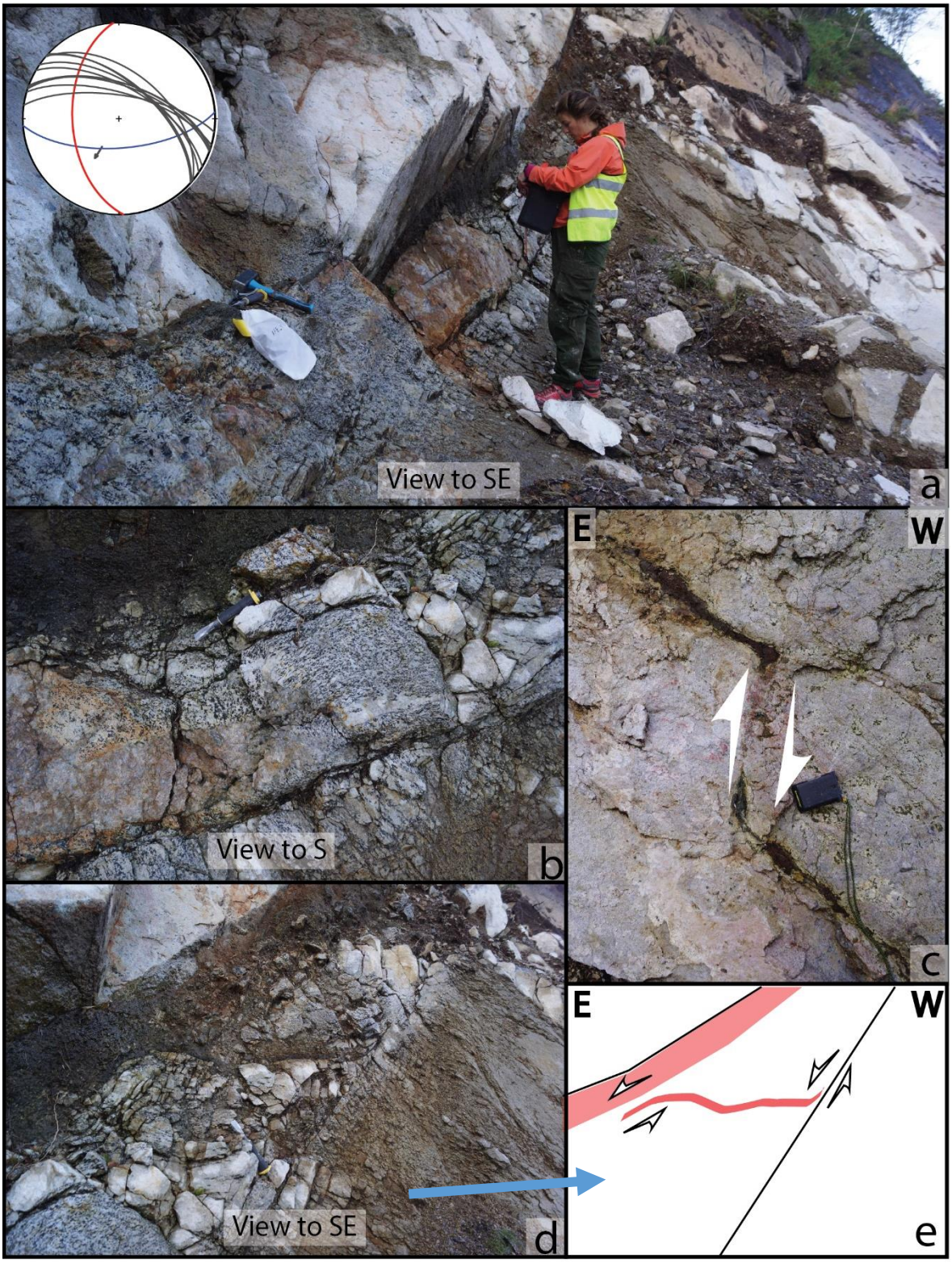

Fig. 4-15: Bjånes Fault Zone 6. (a) E-W trending fault with a stereonet plot of the fault plane (blue line), a pervasive fracture set (black lines) and a magnetic dike (red line). Note the sharp contact to the hanging wall and its bright white dull color. (b) Two pervasive fractures outline the fault core that contain foliated rock interrupted by more massive pegmatite. (c) Displacement of magnetic dike in the anorthosite. (d) A thin magnetic vein indicates a sinistral sense of shear, as illustrated in the cartoon drawn in (e).

4.2.1.7 Bjånes Fault zone 7 (BFZ 7)

At the eastern edge of the road cut is fault zone 7, exposed over a 4 m thick interval and varies between c. 0.2 m to 0.5 m in thickness. The fault is oriented E-W, like FZ 6 and dips c. 50-60° towards the S (Fig. 4-16a). The hanging wall has a bleached aspect and is whitish, whereas the footwall is dark purple. This can indicate a displacement of altered anorthosite over fresher anorthosite, displaced by the fault or differential permeability to the synkinematically infiltrating fluids between footwall and hanging wall. The fault is characterized by grain size reduction in the fault core by cataclastic flow. The core contains alternating thin layers or bands of clay minerals and red-green minerals parallel to the fault (Fig. 4-16b & d). Further, mafic minerals (amphibole/Hbl) elongated perpendicular to the fault zone overprint the alternating layers or bands suggesting rotation due to sliding (Fig. 4-16d). The mafic component varies through the fault core and is more intense where the layers of clay-minerals are less developed (Fig. 4-16f). The preferred orientation of the mafic minerals might be indicative of viscous deformation at some stage during the evolution of the fault. Hem and probably Lmt (laumontite) decorate the fault plane (Fig. 4-16b), Hem occurs also in the fault core, possibly suggesting synkinematic hydrothermal activity (Fig. 4-16e). A high fracture density though the fault core implies a strong brittle control of the fault. In addition, faint striations (Fig. 4-16c) suggest normal faulting. A magnetic dike c. 0.1m thick is cut by the E-W striking fault and is therefore older. FZ 7 shares many characteristics with FZ 6 and might also be related to the quartz-mangerite seen farther east on the geological map.

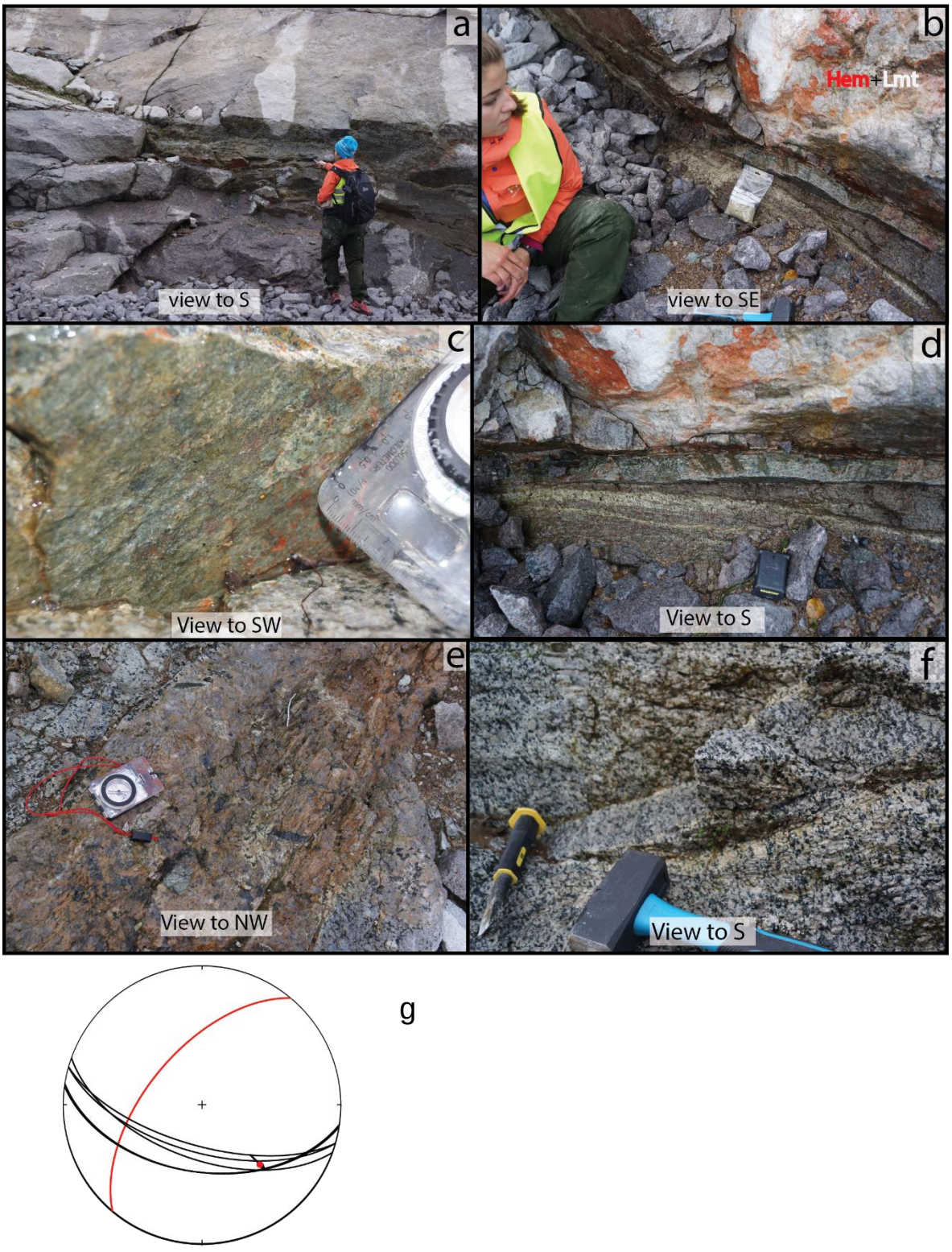

Fig. 4-16: Bjånes Fault zone 7. (a) Overview of the fault with a bleached hanging wall and the dark purple footwall separated by highly fractured fault zone. (b) Farther west than (a), the fault core has a cataclastic texture with gouge and crushed host rock affected by hydrothermal processes (c) Striation with Ep and Hem coating. (d) Fault core with multiple layers with fluid interaction. (e) Pegmatite further west with big clasts of Bt and Fsp. (f) Close look at the fault core and the aligned dark Hbl crystals interrupted by fractures with a bleached halo. (g) Structural measurements of the fault's orientation (black great circles) and the magnetic dike cut by the fault (red great circle).

4.2.2 Titania open pit

The Company “Titania A/S” runs the production of ilmenite from the Tellenes ore deposit. Access to the open pit, had made it possible to study the anorthosite from a lower structural level and to gain a full 3D perspective of many of the fractures sets and deformation zones of the area. Four locations from the open pit will be presented in this chapter (Fig. 4-17); two locations with fault zones characterized by cataclastic deformation, location three exposes the relationship between Egersund Dike Swarm and the anorthosite and finally, location four, expose the crusher fracture system.

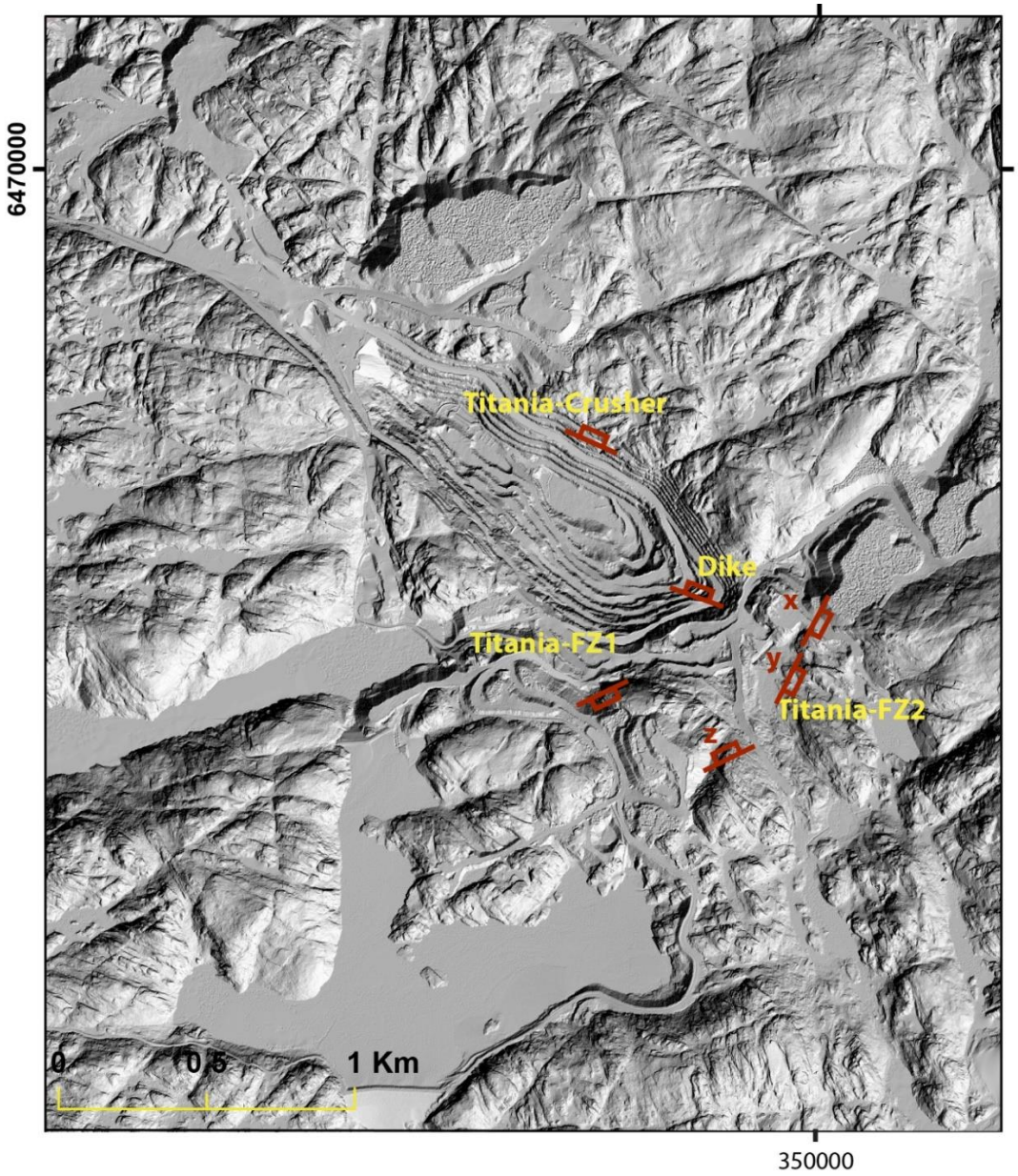

Fig. 4-17: Hillshaded LiDAR data and the locations of four localities that were studied in detail and are described in the text. The stereonet plots all structural observations from the pit.

4.2.2.1 Titania FZ 1 (Åna-Sira lineament system)

The fault is exposed in the southwestern part of the pit; it is 10 m thick but it structurally affects a c. 30 m long outcrop (Fig. 4-18a). The fault strikes NE-SW and dips 60° towards SE. Based on its orientation and field characteristics, the fault is therefore assigned to the Åna-Sira lineament system. A sharp contact on both side of the fault separates the bleached white-greenish-pale pink faulted rock from the dark purple fresh anorthosite. The fault zone is complex and displays evidence of both brittle and ductile deformation. Viscous deformation is only observed locally close to the western margin of the fault and is defined by a weak foliation formed by the alignment of mafic minerals (Fig. 4-18c). This foliation is sub parallel to the fault and bends away from it into the western margin. Brittle deformation is characterized by grain size reduction by cataclasis towards the two zones on the margins of the fault containing gouge. A relatively late phase of brittle deformation is expressed by conjugate fracture sets with white mineral infill indicating a vertical sigma 1 (Fig. 4-18b), together with an increased fracture density within the fault core and the gouge rich zones at the margins. In addition, fractures with mineral infill cut the foliated rock representing a younger brittle deformation phase (Fig. 4-18).

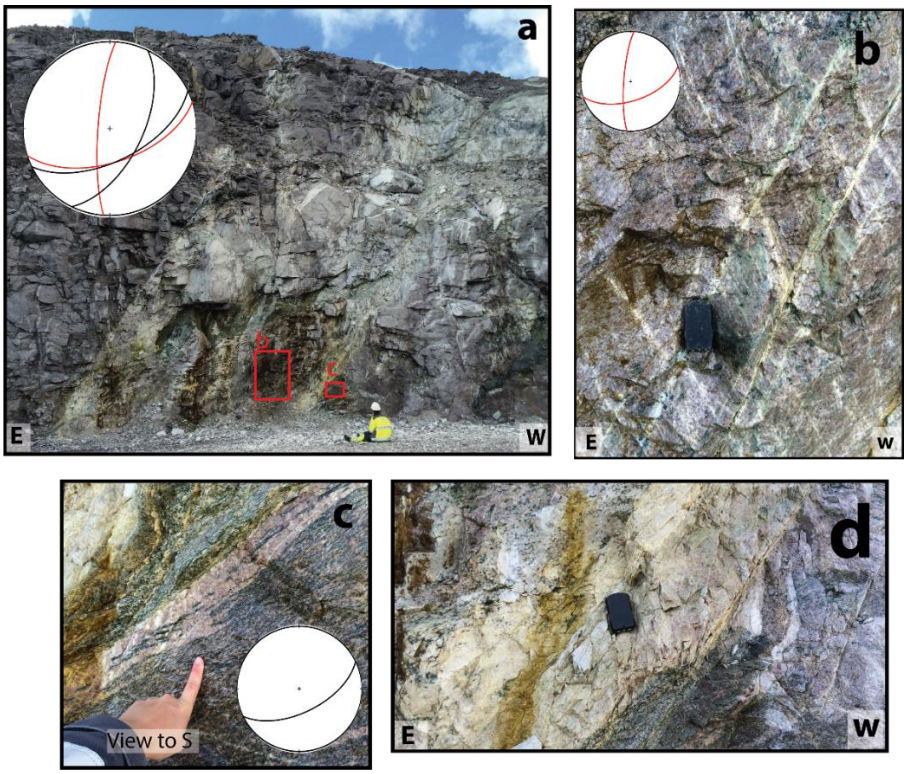

Fig. 4-18: Titania Fault zone 1. (a) overview of the fault zone notice the bleached fault and the sharp contact to purple anorthosite. Stereonet plots the two fault planes and the conjugate fractures (red great circles) (b) Conjugate fractures filled with clay suggesting sigma 1 close to vertical. (c) Local foliation at the western flank characterized with alignment of dark minerals in the purple anorthosite. (d) Bleached anorthosite with thin bands of clay-rich gouge cutting through the foliated mafic minerals in the down-right corner of the picture.

4.2.2.2 Titania FZ 2 (Jøssingfjord lineament system)

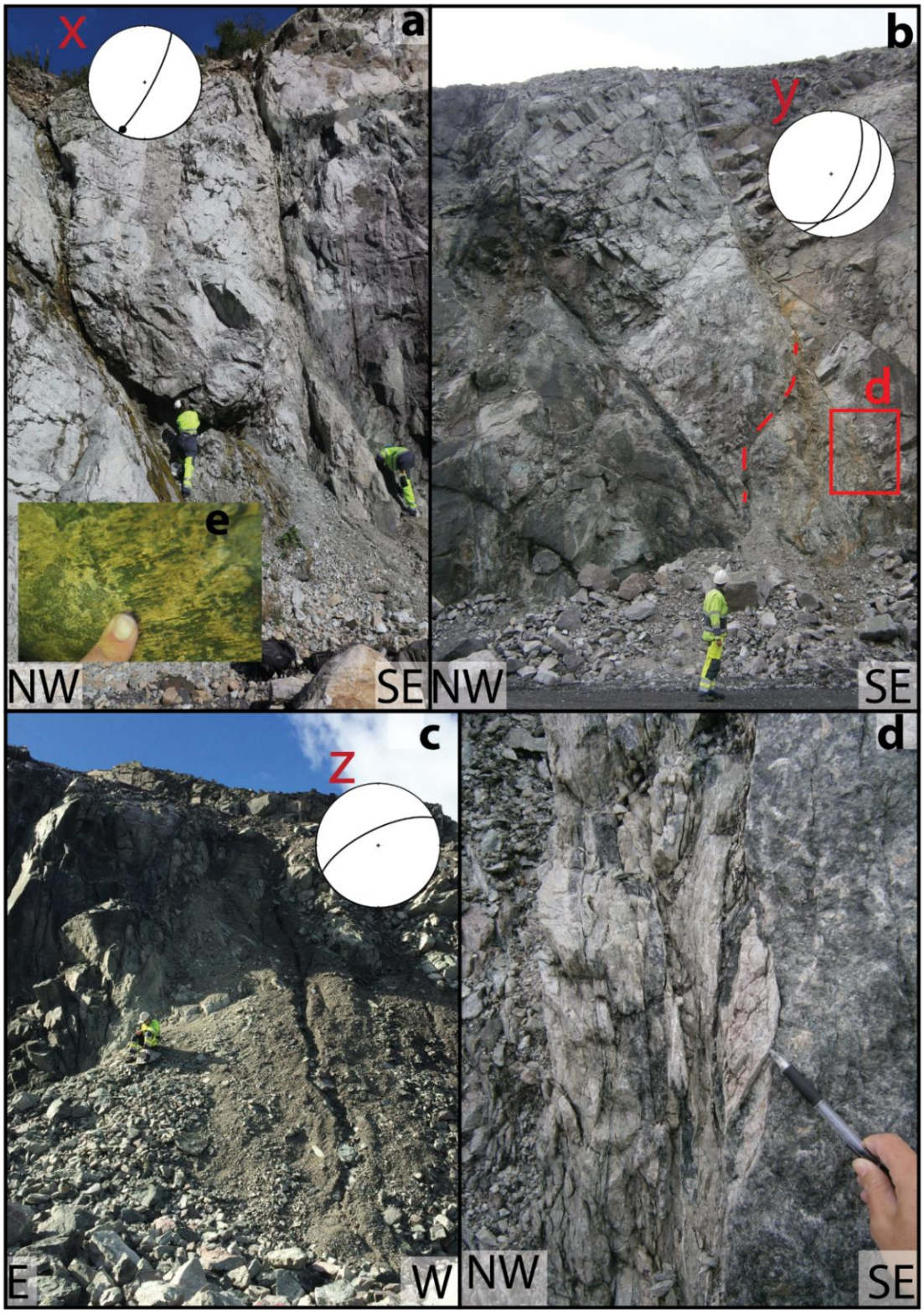

Fig. 4-19:Titania Fault Zone 2. (a) Location x in Fig. 4-17 showing the distinct fault zone with two distinct gouge-rich zones enclosing a fractured anorthositic fault core. Ep-Chl striation in figure (e) suggesting strike slip displacement. (b) Location y share the same characteristics as location x. (c) Location z is covered by sediments but show brittle deformation characterized by highly fractured rock. (d) High fracture density towards the margin of the fault core and a clast with sigmodal shape.

Titania Fault zone 2 is exposed in three locations marked in Fig. 4-17 as x, y and z (Fig. 4-19a, b, c). There are local variations but on average the fault zone is 5 m thick and continuous through the 30 m tall outcrops exposed by quarrying. The fault strikes NNE-SSW and dips c. 60° toward SE or NW. Based on its orientation and overall characteristics, this fault is assigned to the Jøssingfjord lineament system (Fig. 4-6). The fault is associated with significant metasomatism, evidence of fluid ingress, circulation and fluid-rock interaction as expressed by the bleached dull appearance and the presence of different mineral phases of secondary origin. The fault is characterized by two gouge-rich zones that separate a highly fractured fault core from the host rock. Within the core, there are angular blocks of anorthosite, although slip localized mostly along the two gouge rich zones at contact with the host rock. These two gouge-rich zones are c. 0,1m thick (Fig. 4-19 d).

4.2.2.3 Titania Dike (WNW-ESE lineament system)

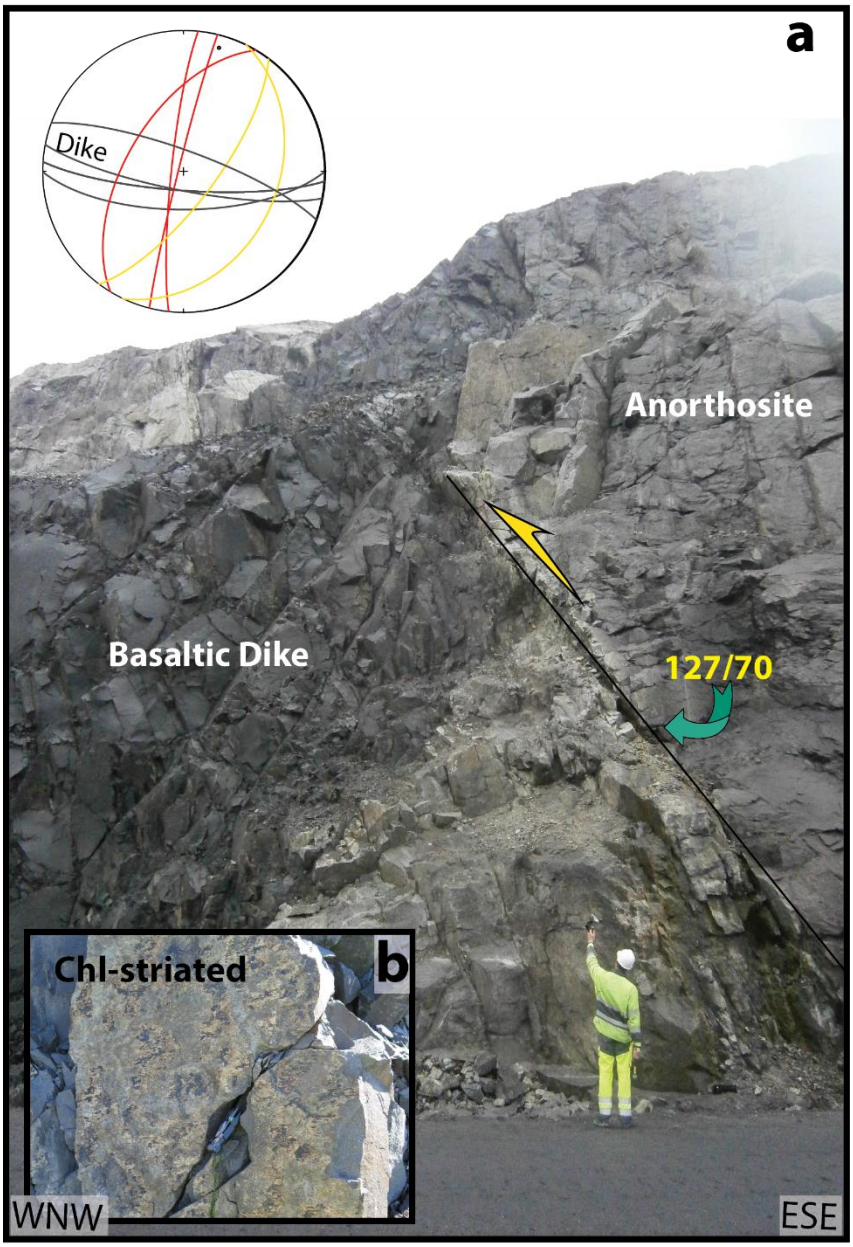

Fig. 4-20: Egersund dikes crosses the pit. (a) Sharp contact between the anorthosite and the dike. The stereonet plots the orientation of the dike together with a pervasive fracture set (red great circles) and the thrust displacing the dyke (yellow great circles). (b) Fracture set in the dike with striated fault planes indicating strike-slip kinematics.

One of the basaltic dike that belongs to Egersund Dike Swarm crosses the entire pit and is exposed in several locations throughout the pit. It dips c. 80° towards NNE and strikes WNW-ESE (Fig. 4-20). The basaltic dike has a sharp contact to the metasomatised anorthosite, it is c. 10 m thick and is easily recognizable throughout the pit. At the site described here, the dike is displaced by a NE-SW striking thrust (yellow great circle in stereo plot Fig. 4-20) that causes c. 4 m top-to-W displacement. The dike is parallel to the WNW-ESE lineament system and the fault is parallel to Jøssingfjord lineament system with the same trend as the Helleren Fault Zone but opposite dip. One fracture set oriented c. 280/85 contains striations indicating strike-slip that are common though the dike and anorthosite. This set is parallel to Bjånes lineament system (Fig. 4-6).

4.2.2.4 Titania Crusher lineament system

A pervasive fracture system associated with a discrete brittle deformation zone goes though the pit causing stability issues. The fractures and fault are oriented NNW-SSE and dip c. 50° towards NE. Striations on Ep-Chl coated planes (Fig. 4-21) suggest an oblique slip but unfortunately no kinematic indicators were observed.

Fig. 4-21: Fractures assigned to the Crusher lineament system oriented NNW-SSE. (a) Plane with Ep-Chl coating, suggesting oblique slip displacement. (b) Photo taken from the western part of the pit looking up to a pervasive crusher fracture plane.

4.2.2.5 Tørkeanlegget Fault Zone -Tellenesmyra lineament system

The Tørkeanlegget fault zone (Fig. 4-22) is c. 15 m thick and is characterized by a complex fault architecture with several gouge zones, cataclasite and brecciated rock zones (Fig. 4-23a). The fault zone accommodated fluid ingress and fill and metasomatic processes bleaching the host anorthosite. Hem and other mineral phases are indicative of hydrothermal processes and metasomatism (Fig. 4-23b, c). Three high strain zones between 0.2 and 0.6 m in thickness contain gouge and are separated by blocks of severely fractured anorthosite (Fig. 4-23a). The gouge changes color from white in the middle to reddish at the margins of the zone (Fig. 4-23d) whereby gouge zone 2 is the most damage zone (Fig. 4-23d &e). Gouge zone 2 and 3 envelope block 2, which is fairly rounded as a lens with fractures bending around the

lens-shaped block (Fig. 4-23e). If the block is rotated, it would indicate a dextral sense of shear, corresponding to thrusting with top to the NE. This fault is parallel to the Tellenesmyra lineament system and, due to the high deformation seen in this zone and the structural complexity, it is reasonable infer a complex structural evolution, with multiple reactivation. In addition, a fracture set oblique to the fault was measured and can also be recognized in the DEM (Fig. 4-23f).

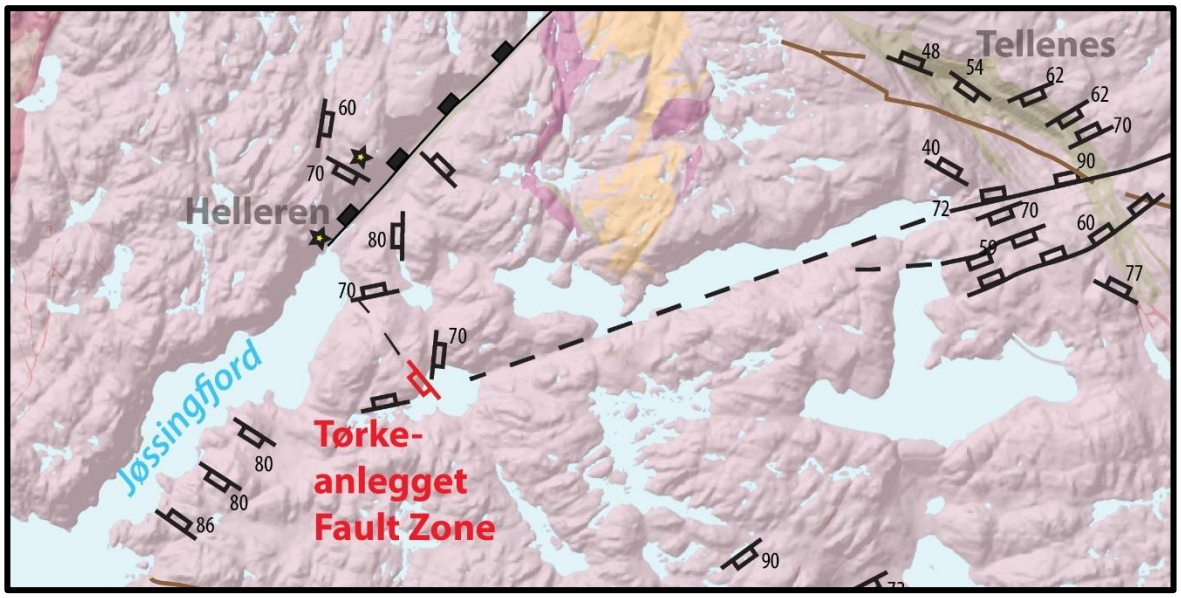

Fig. 4-22: Part of the structural map of the study area (Fig. 4-7) highlighting (red) the location of Tørkeanlegget Fault Zone.

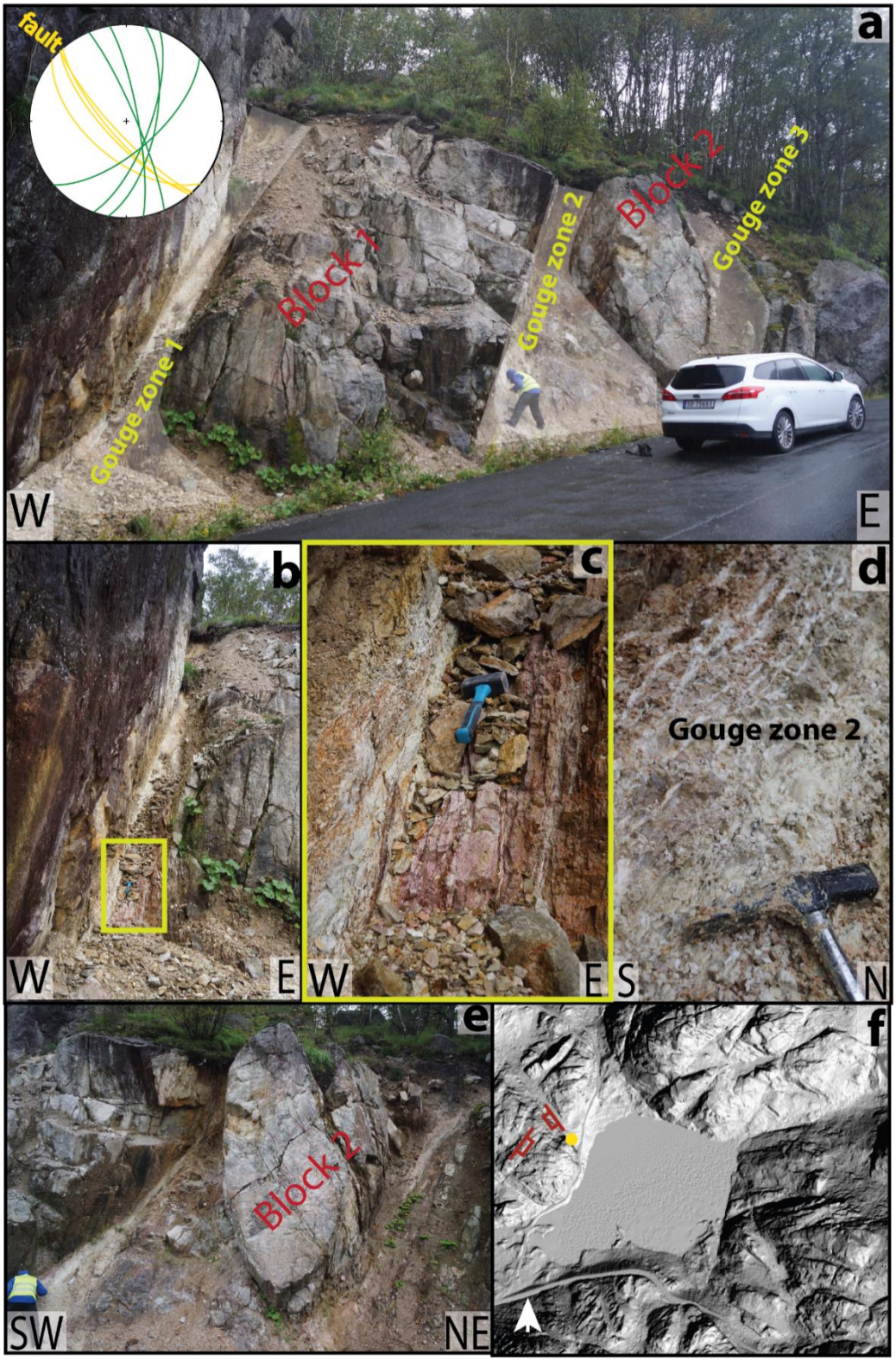

Fig. 4-23: Tørkeanlegget fault zone. (a) Overview of the complex fault. (b) Detail of gouge zone 1 containing a 10 cm thick zone of white gouge. Zooming further in (c) shows that there are several secondary mineral phases that impart the rock a red-pinkish color. (d) Gouge zone 2 changes color from reddish to white-gray moving towards the middle of the gouge zone. (e) Block 2 has a lens shape with fractures enveloping the lens, attesting to the overall anastomosed geometry of the fault zone. (f) The fault appears on the DEM together with a second, distinct fracture set trending NE-SW.

4.2.3 Jøssingfjord Pass fault

Jøssingfjord Pass fault is exposed on the curvy road leading down to the Jøssingfjord (Fig. 4-24a). It is a c. 12 m thick zone of high fracture density within a heavily bleached anorthosite. It is oriented NW-SE and dips c. 65° towards SW (Fig. 4-24b). The transition from fresh anorthosite to the fault is extremely sharp and is defined by clay-rich zones. Several fractures within the fault contain themselves layers of clays together with Ep, Chl, Qtz and Cal (Fig. 4-24d). Haloes around some of the veins are indicative of fluid-rock interaction. The structural trend coincides with Tellenesmyra lineament system and Dydland kaolin mine (Fig. 4-3, Fig. 4-24, Fig. 4-25).

One clay-rich zone c. 5 cm wide was sampled and authigenic illite therein was dated by K-Ar (Fig. 4-24c). The smallest fraction (<1 μm) yielded an age of 184.7 ± 17.6 Ma.

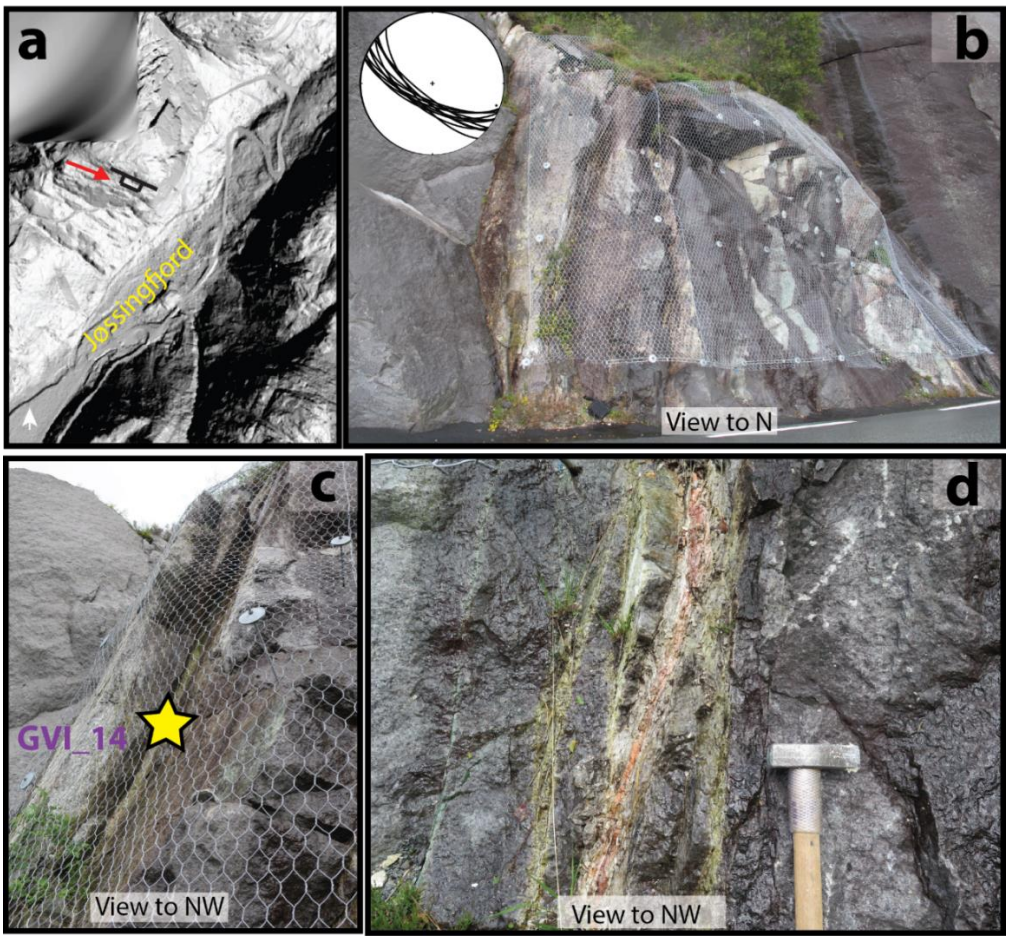

Fig. 4-24: Jøssingfjord Pass Fault. (a) LiDAR data showing the fault location; note the distinct lineament set parallel to the fault. (b) Overview of the fault with a c. 12 m thick fault zone that is clearly preferentially eroded with respect to the fresh anorthosite. (c) C. 5 cm thick clay-rich fault strand sampled for illite K-Ar dating (sample GVI_14). (d) Hem(red), Ep(green), Qtz and clay distribution within one of the fault strands.

4.2.4 Dydland dismissed kaolin quarry

Dydland is an old kaolin mine that was quarried by exploiting a mineralized gully oriented NW-SE (Fig. 4-25c), located in the southern part of the study area. (Fig. 4-7). Heavy alteration causes granular disintegration of the anorthosite in the gully. Hydrothermal fluids and metasomatism have caused the alteration of the fresh anorthosite and the authigenesis of the economically viable kaolin, but the structural patterns of the area have controlled the spatial distribution of alteration and the development of the highly altered gully (Fig. 4-25a & d). Dydland strikes NW-SE and so shares the same orientation of the Jøssingfjord Pass fault. The contact to the host rock is less sharp in the gully compared to Jøssingfjord Pass fault. A clay-rich sample from the gully (Fig. 4-25b) was dated by K-Ar, with the < 0.1 μm finest fraction yielding an age of 170.58 ± 5.86.

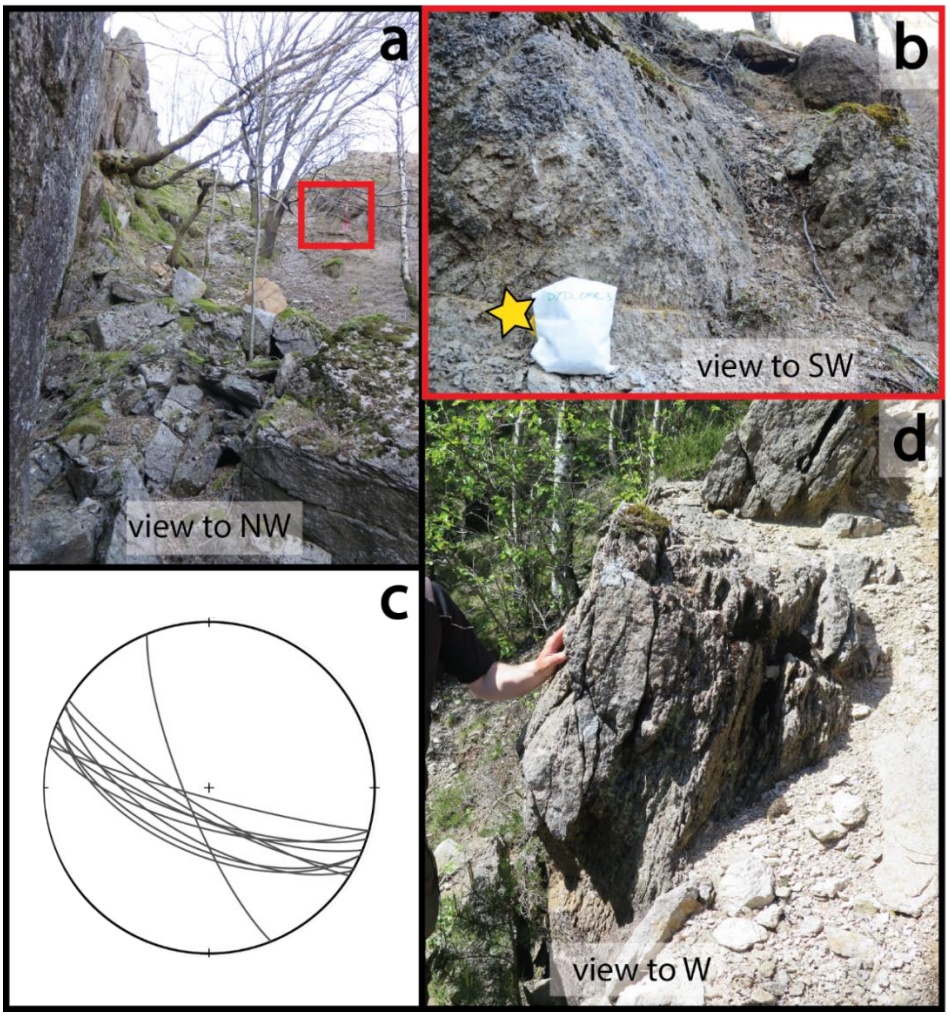

Fig. 4-25: Dydland kaolin gully. (a) Overview of the gully and the location of (b). (b) Clay-rich zone along the contact with the anorthosite. The dated sample, OFR_3, was taken from this zone mark with a yellow star. (c) Stereonet plotting the orientation of the gully. (d) High fracture density in the weathered anorthosite

4.3 The Helleren Fault Zone

The studied segment of the Helleren Fault Zone (HFZ; Fig. 4-26) is located along the western side of the NNE-SSW trending Jøssingfjord,. The outcrop is located at the Helleren historic site, a natural roof and shelter located in the dramatic landscape of the fjord that have been taken advantage of by people for thousands of years (Fig. 4-26, Fig. 4-27).

The HFZ is entirely intra-anorthositic and deforms the 932±3 Ma Åna-Sira Anorthosite massif (ÅS) (Schärer et al., 1996). The massive ÅS structurally consist of thousands brittle fractures and faults. The HFZ is one of the largest recognized deformation structures in the area and, given its peculiar structural features, it was decided to investigate it in detail. The easily accessible studied section is a c. 100 m long fault damage zone, whose thickness varies from 4 m to only a few cm. An overhang outlines the hanging wall of the fault, which provided the geological shelter for the people living at Helleren for hundreds of years (Fig. 4-27C). The main fault plane dips moderately towards the NW (Fig. 4-27G) and two discrete clay-rich slip surfaces, named the upper slip surface (USS) and the lower slip surface (LSS), respectively, mark the boundary between the fault core and the damage zone (Fig. 4-27A). The fault core is characterized by a cataclastic texture with high fracture density and numerous vein sets. Structures such as veins and Riedel fractures in the footwall (Fig. 4-27B), below the LSS, indicate a damage zone in the immediate surroundings of the fault core. The USS is a planar and almost continuous surface that can be followed along the section. The USS is characterized primarily by a c. 5 cm thick zone of gouge and brecciated fragments of the host rock, with subordinate hematite and calcite mineralizations. The LSS is an irregular and undulating plane and steers the overall architecture of the fault core, which is reminiscent of a pinch and swell structure along strike (Fig. 4-26). The LSS changes along strike from a c. 5 cm thick distinct clay rich zone, to a more diffuse and therefore ambiguous contact in the northern part of the HFZ. The fault zone is apparently folded by an open, upright fold with a fold axis trending NW (Fig. 4-26B & D). Farther north, the fault disappears under the slope scree.

Three sections (A, B, C) extending from footwall to hanging wall across the fault zone were studied in detail in the field (Fig. 4-26). The structural observations from the field are presented in a structural log for each of the sections farther down. Here, all the structural features are defined, illustrated and placed in their respective domains. The structural logs are separated into several intervals and described individually. In addition, section A and C were systematically sampled and later analyzed in detail in thin sections (Fig. 4-28, Fig. 4-34) and a sample, TSC44, of gouge close to USS was dated by K-Ar on authigenic, synkinematic illite.

4.3.1 Structural characterization and evolution of the HFZ

Despite the overall brittle character of the HFZ, careful analysis of the HFZ has indicated the presence of an early ductile phase of deformation characterized by a pervasive foliation due to the alignment of mafic minerals within the anorthosite, typical of an SL-tectonite. The foliation within the fault is pervasive in the footwall and only poorly developed in the in current brittle core, whereas it becomes penetrative again in the hanging wall. Some weak evidence of thrust kinematics are found in the foliation (sigmoidal foliation clasts and gently E-dipping SC planes) indicating an overall top-to-the southeast viscous deformation that predates the brittle deformation. Clearly, the observed foliation changes planar attitude in response to the pinch and swell mesoscopic structure of the fault, where the foliation is oriented parallel to the main fault plane in section C (Fig. 4-26B) but rotates towards NE in section B (Fig. 4-26D). This means that the foliation is bent by an open, upright fold with a fold axis oriented NW. The mylonitic foliation localizes later brittle deformation, as shown by the host rock being highly brecciated with a strong fracture cleavage in the immediate proximity to the foliated volume of the Helleren FZ (Fig. 4-35C). NW-SE brittle extension is supported by, striations and slicken sides suggesting top-to-NW displacement and Riedel fractures also suggesting top-to-NW displacement and the radiometric dating of authigenic-synkinematic illite. Veins with secondary mineralization are abundant within the fault core, hanging wall and footwall. Some are parallel to the main fault plane while others clearly crosscut it (Fig. 4-32C&D). Metasomatic processes have caused severe alteration of the anorthosite generating a bleached rock. Veins and fractures are spatially and genetically closely related to this process, having presumably acted as channels for localized fluid ingress and flow (Fig. 4-32B)

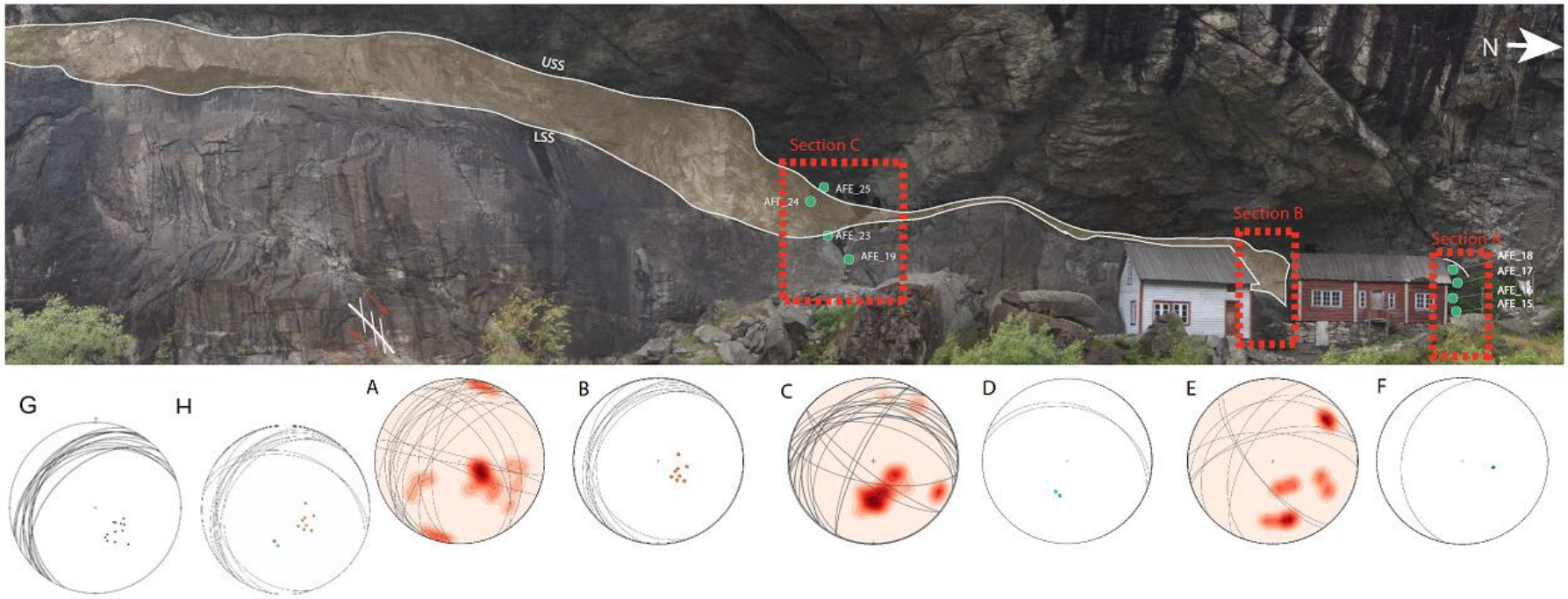

Fig. 4-26: Photo of the outcrop of the Helleren Fault Zone (HFZ). The Upper Slip Surface (USS), the Lower Slip Surface (LSS) and the three section that are carefully studied and sampled in the field are marked on the photo. The stereonets show the structural observation made in field, where (A) is all fractures, veins and fault plane measured in section C. (B) is the foliation measured in the same section. (C) is the measurements for section B,

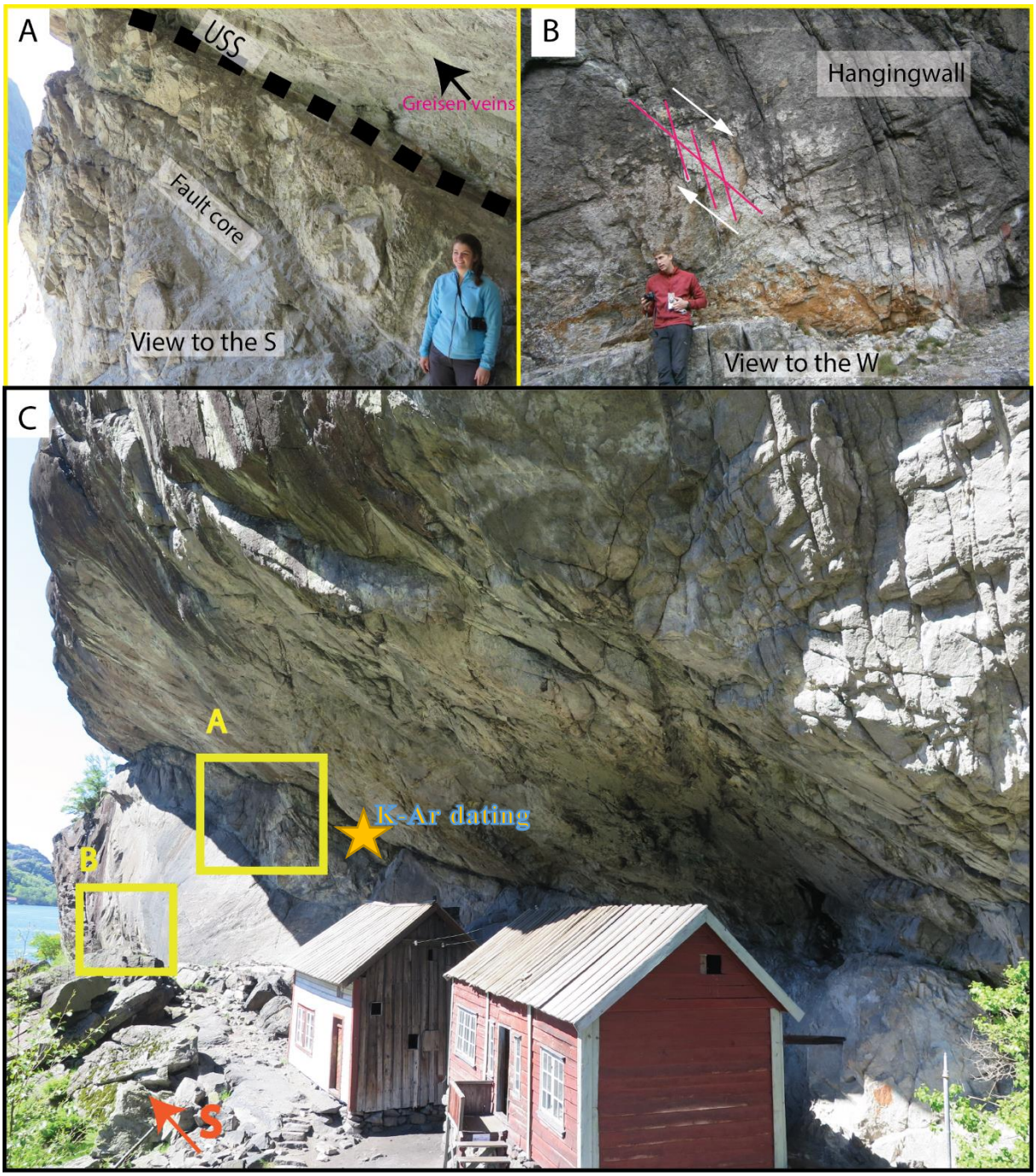

Fig. 4-27: Helleren Fault Zone (HFZ) with a closer look at (A) the fault core. Note the high fracture density in the fault core. (B) The footwall with fractures and Riedel fractures and (C) an overview photo of the fault zone, note the planar hanging wall and the undulating footwall defined by the LSS. The sample used for K-Ar dating is marked with a yellow star.

4.3.2 Section A

Section A is located at the northernmost corner of the red house (Fig. 4-26). Here, the fault core is up to 2.5 m thick and it attains its maximum documented thickness (Fig. 4-28, Fig. 4-29). The section was sampled systematically from the footwall through the fault core into the hanging wall (Fig. 4-28 C & D). Moving north, the fault zone disappears under the slope talus. Section A is described following the conceptual structural subdivisions proposed in the structural log in Fig. 4-29.

Interval 1

In interval 1, the anorthosite has a medium-dark purple color, it is coarse grained with a phaneritic texture and exhibits bands of pervasive foliation defined by alignment of altered mafic minerals such as chlorite (Chl) and ilmenite (Ilm). Sample AFE_15 (Fig. 4-28D) was collected from the base of this interval, in the footwall. The sample is of pure pink to white anorthosite with altered mafic minerals and opaques. At the same structural level, there are veins with secondary epidote (Ep), muscovite (Ms) and chlorite (Chl) with a parallel and crosscutting relationship to the NW dipping main fault plane (Fig. 4-30a), which is here reflecting entirely brittle deformation. The Lower Slip Surface, LSS, is located a few cm above sample AFE_15 and exhibits a diffuse contact to the fault core where there is a slightly change in color from dark to lighter purple and there is an increase in fracture density moving higher up into the core.

Interval 2

Interval 2 has a slightly lighter color and corresponds to the actual fault core. The brittle component of the fault is dominant in this interval and the rock has a fully protocataclastic texture. Discrete fractures with whitish clay infill cut though the core with abundant cataclastic deformation in the immediate surroundings. This fault rock is possibly indicative of a higher amount of strain accommodated along these fractures. Although the brittle component is more dominant in this interval, the foliation is still distinct. Sample AFE_16 is sampled c. 1 m above AFE_15 and is of a whitish anorthosite with a pervasive sub horizontal foliation defined by Chl and opaques (Fig. 4-28D). The coarse grained anorthosite still preserves its primary magmatic texture but pervasive veins filled with secondary minerals such as Ep, Chl, Ms and fluids, have caused alteration of the feldspar.

Interval 3

In interval 3, the color variations are vast between dull white and dull pink. The grain size is reduced and strain intensity increases. As for interval 2, interval 3 is characterized by fractures with clay mineral infill and penetrative cataclastic deformation in the immediate surroundings parallel and oblique to the main fault plane (Fig. 4-28A). A dominant set of fracture planes was measured to be 28/348 with possible Riedel fractures oriented 62/004 that can be used to infer a normal top-to-NW sense of shear associated with the brittle component of deformation (Fig. 4-28A). The interval also contains a zone of viscous deformation characterized by SL-tectonites whose planar fabric is outlined by the alignment of Chl and opaque minerals (Fig. 4-30c). Metasomatic processes have caused the severe overprinting of the fault by the ingress of hydrothermal fluids that changed the mineral composition of the foliation-defining- minerals and the rest of the rock (Fig. 4-30c). Sample AFE_17 (Fig. 4-28 C&D) is collected 1 m above sample AFE_16, close to a cataclastic zone cutting through the core. Veins with secondary mineralization of Ep and Chl are common in this part of the interval.

Interval 4

In this last interval, the rock has a dull pale pink-whitish color and the foliation-defining-minerals have a dark blue to green color. The fracture density is the highest in this part of the section and viscous deformation is overprinted with a clear fracture cleavage parallel to main fault plane (Fig. 4-30b).

The last sample of the section, AFE_18, was sampled c. 40 cm below the USS. Sample AFE_18 is pervasively fractured, it has a distinct foliation but contain no veins. A few cm above sample AFE_18, there is a zone of gouge and brecciated fragments of anorthosite with subordinate Hem and Cal parallel to the USS. A distinct, sharp, thin zone (3 cm thick) of white clay and hematite defines the USS. When looking up at the hanging wall, deformed enclaves of mafic rock and greisen veins decorate the hanging wall of the fault.

Farther north, the hanging wall can be followed and an Ep and Chl striated fault plane was measured and characterized as dip-slip with a top-to-NW normal sense of shear (Fig. 4-39).

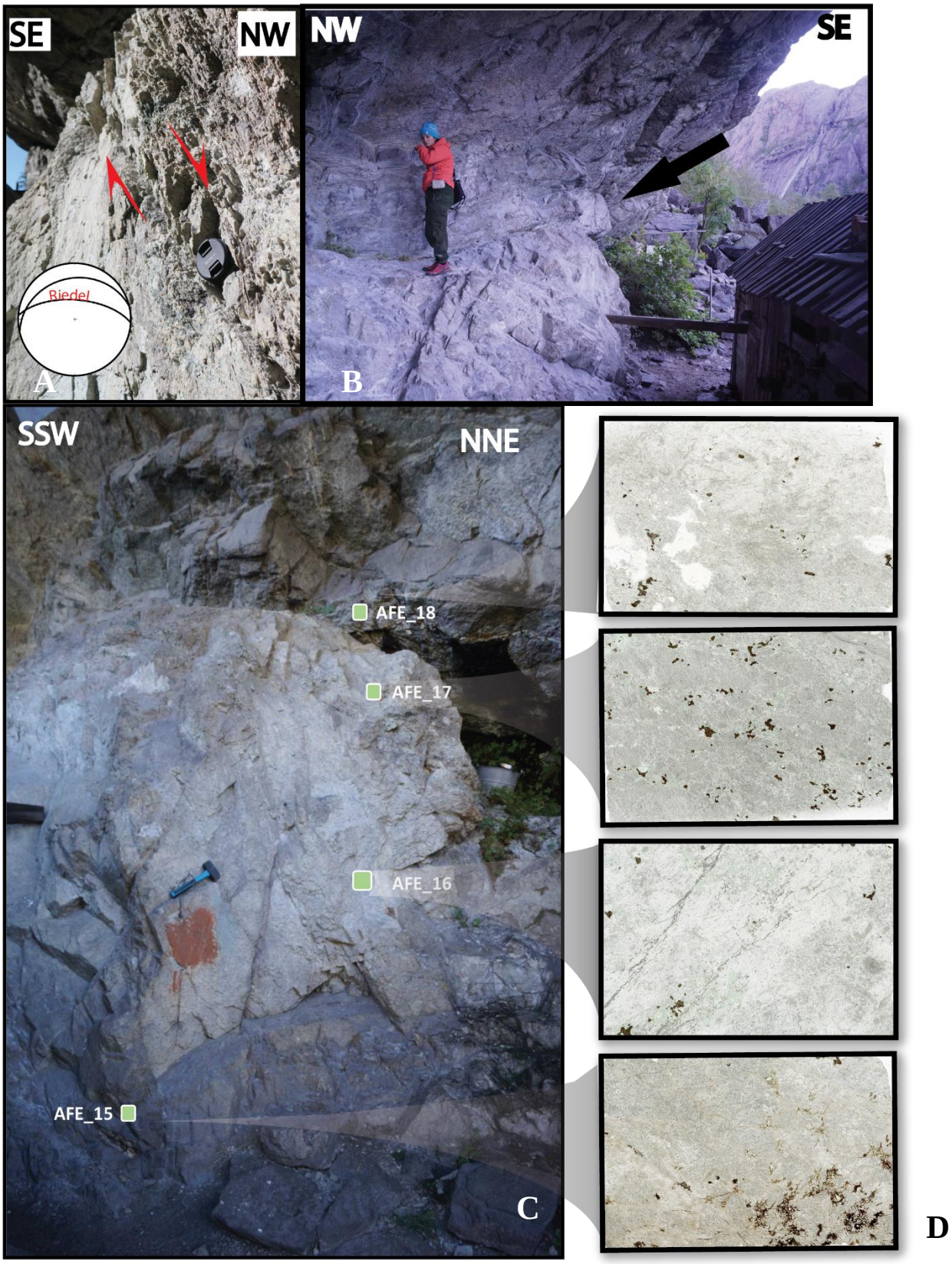

Fig. 4-28: (A) Upper part of the HFZ in section A with a discrete fracture cleavage and a 2 mm zone of white clay infill located just under the scale. This second-order fracture suggests extension with overall top-to-NW kinematics. (B) Overview of the uppermost part of section A. Black arrow indicates sample location for section A. (C) Sample location and (D) scanned images of the thin sections of the four samples with PPL.

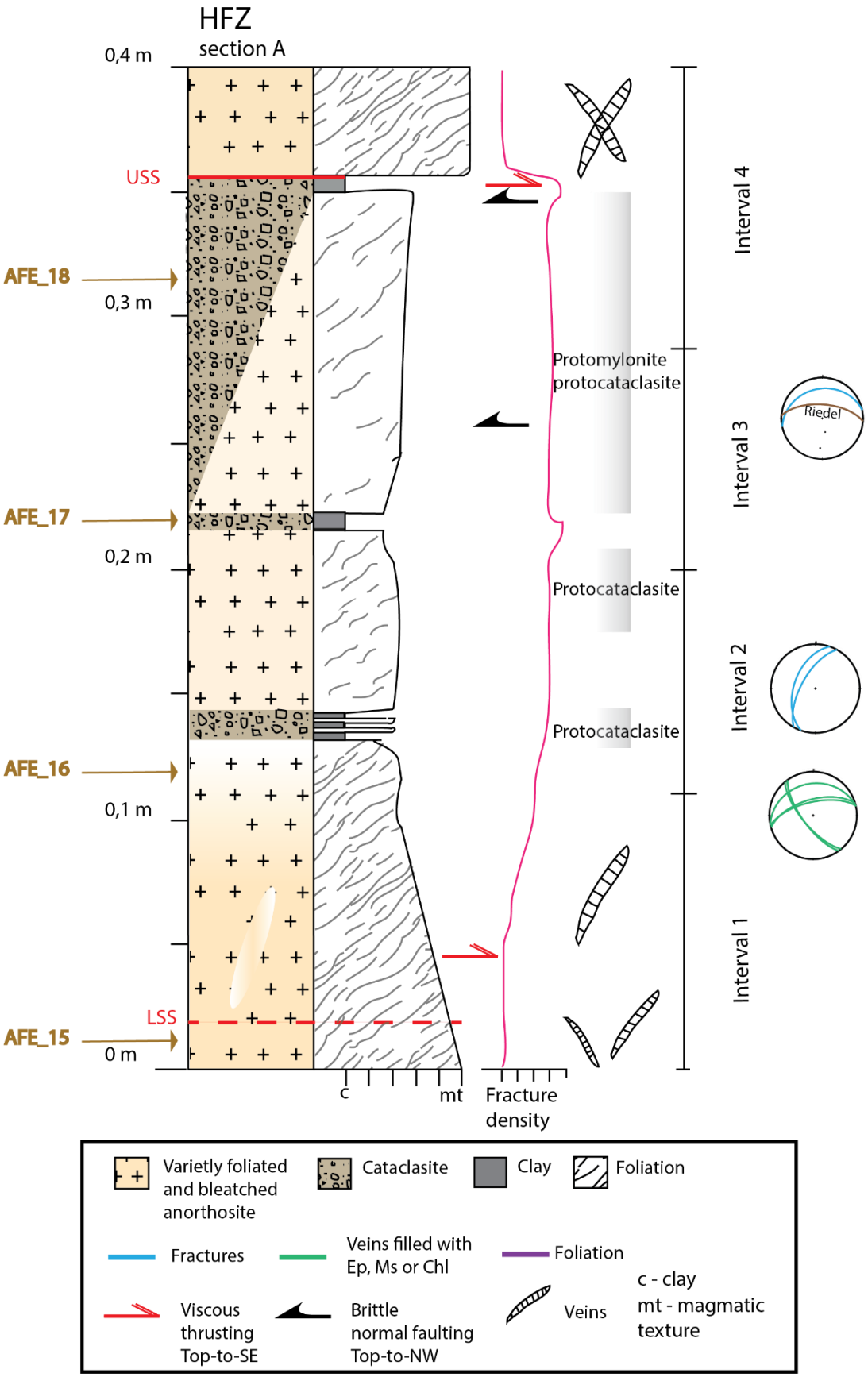

Fig. 4-29: Structural log of section A.

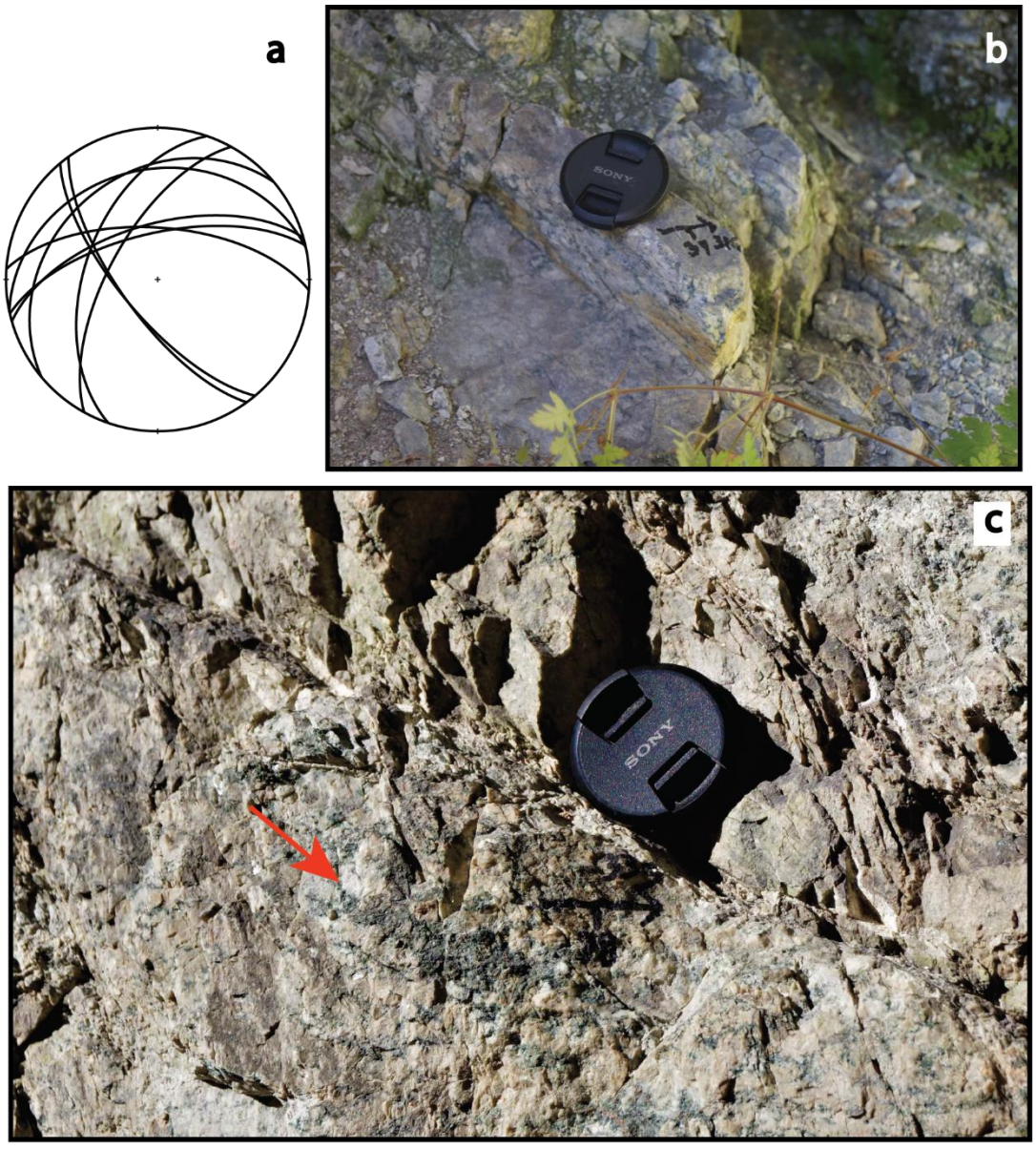

Fig. 4-30: (a) Fracture/ vein measurements for Section A with two main trends striking c. NE-SW and NW-SE. (b) Fracture density in interval 4 with fractures oriented parallel to the fault core. (c) Alignment of Chl-Ilm in interval 3 close to sample AFE_17.

4.3.3 Section B

Between the white and the red house, the HFZ core is well exposed in a 1 m thick zone where the main fault planes dip towards NW (Fig. 4-26). The whole zone was mapped from the footwall across the fault core and into the hanging wall (Fig. 4-31). Section A is described after the intervals marked on the structural log in Fig. 4-33.

Interval 1

Interval 1 has a dark purple color, it is coarse grained and has a phaneritic texture. A weak mylonitic foliation in the footwall dips at c. 34° towards NNE and is characterized by alignment of dark minerals (Fig. 4-32E). Together with the foliation (SL-tectonite), sub vertical fractures are observed throughout the footwall and are invariably decorated by Ep-Qtz veins. This distinct set of fractures dips toward SSW c. 70/190 (Fig. 4-32A). A cross-cutting fracture set with a steep dip towards N, c. 50/015, are filled with Ep and Qtz. Some of these fractures/veins have a white halo of decolored anorthosite, probably due to metasomatism.

Interval 2

Interval 2 starts just below the fault core. The color change from purple to variations between dull pink and dull white, indicating more alteration of the rock in this part of the section. Below the actual fault core, a set of lower angle fractures with a mean orientation 358/46 are bordered by a continuous whitish halo filled with Ep and Qtz (Fig. 4-32B). These veins, seen in Fig. 4-32B (stereonet), are oriented more or less parallel to the foliation measured throughout section B and the USS (Fig. 4-26D). Fractures in the same set have zones with white clay materials. The upper part of interval 2 is strongly controlled by strain localization in thin, distinct, clay-rich planar features. The transition from the footwall to fault core is progressive, and the fracture density increases when approaching the fault core (Fig. 4-31B). The foliation is still recognizable but is clearly overprinted by brittle deformation.

Interval 3

The rock has a white dull color and is fine grained with a cataclastic texture. Interval 3 is fully within the fault core where the rock becomes highly cataclastic and contains a pervasive fracture cleavage (Fig. 4-31B and Fig. 4-32D) with discrete slip planes oriented 46/342. The pervasive cataclasite is associated with discrete and spaced clay zones in the more massive anorthosite. Riedel fractures to the USS, oriented in this section 80/300, cut through low angle planes sub-parallel to the USS (Fig. 4-32C) and infer a normal top-to-NW sense of shear associated with the brittle component of deformation. The mylonitic foliation is apparently absent in the core volumes defined by the highest fracture density but appears again in the hanging wall. The USS has a sharp contact to the hanging wall and is characterized with a c. 2 cm thin zone of gouge and very fine grained brecciated fragments of the host rock (Fig. 4-31B).

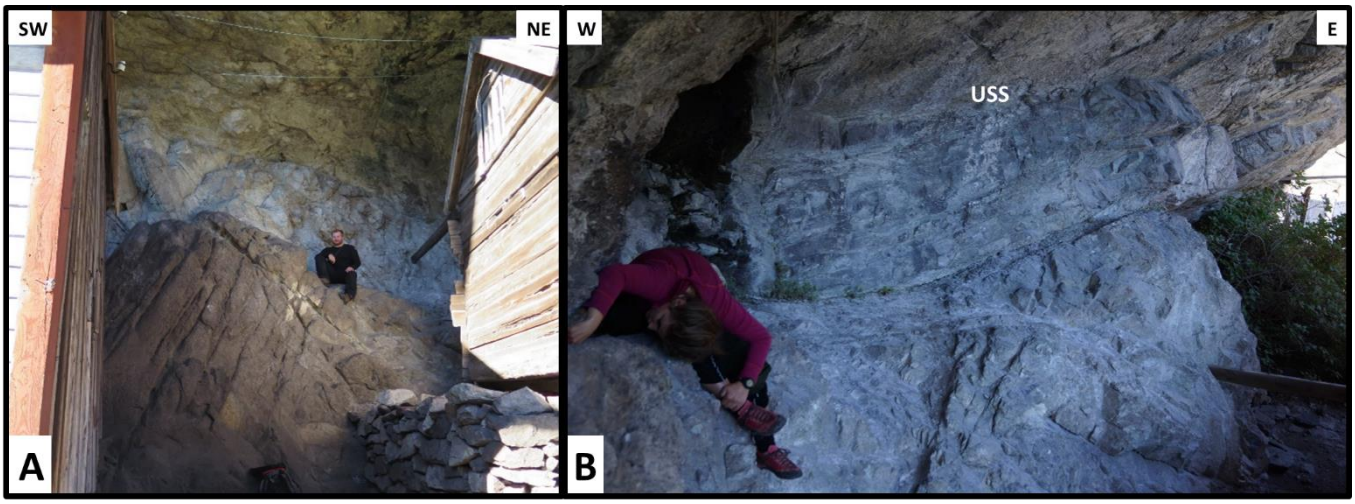

Fig. 4-31: Section B with fault core located just above the person. Note the significant change of color from the reddish-brown footwall to the whitish fault zone. B: Close-up picture of the fault core characterized by a white dull color and a high fracture density parallel to the main fault plane.

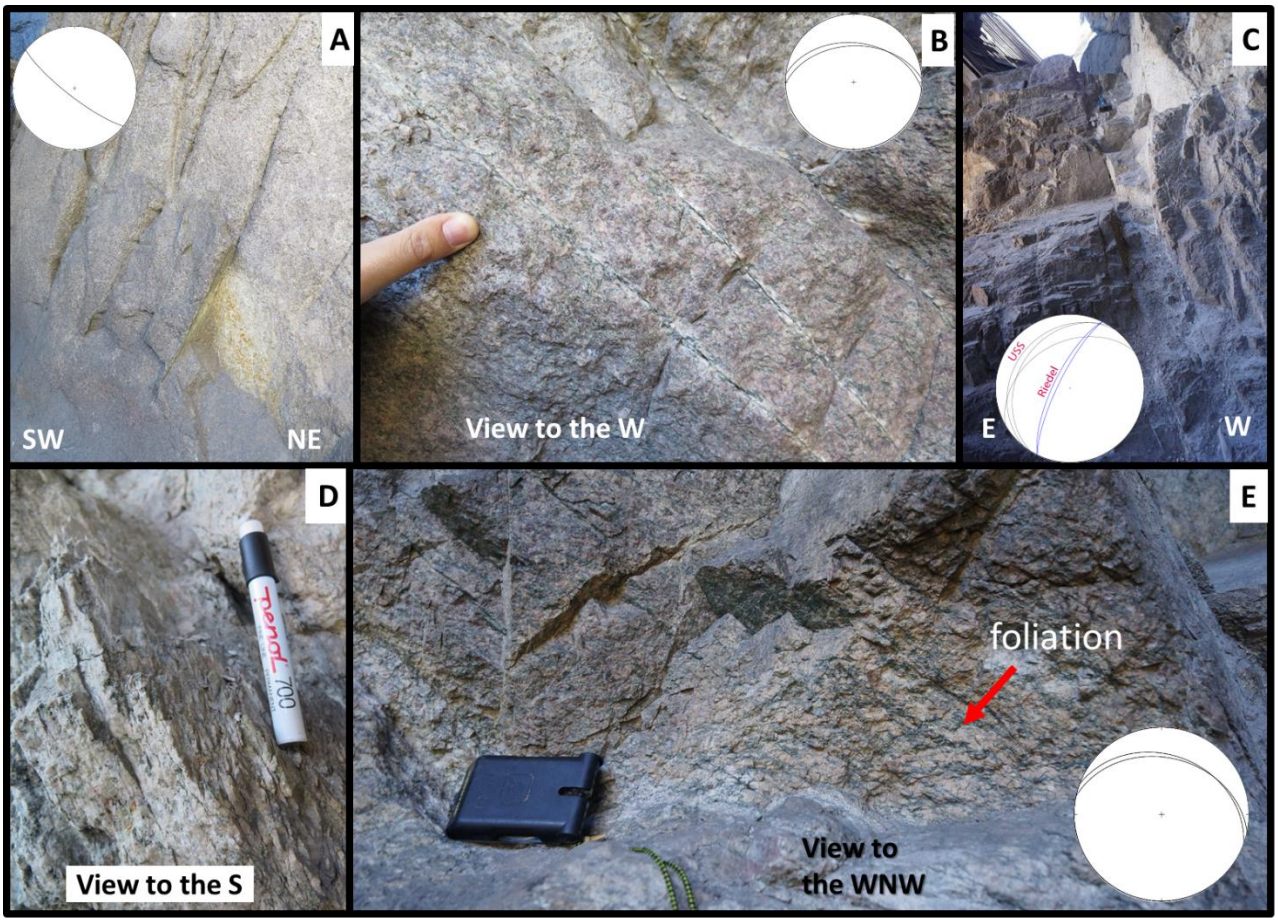

Fig. 4-32: Field characteristics of section B and stereographic projections of the main geometric features. (A) Epidote coated fractures. (B) Low angle veins with a white halo and an epidote rich core. (C) Riedel fractures to USS. (D) Pervasive fracture cleavage. (E) Pervasive foliation in the footwall.

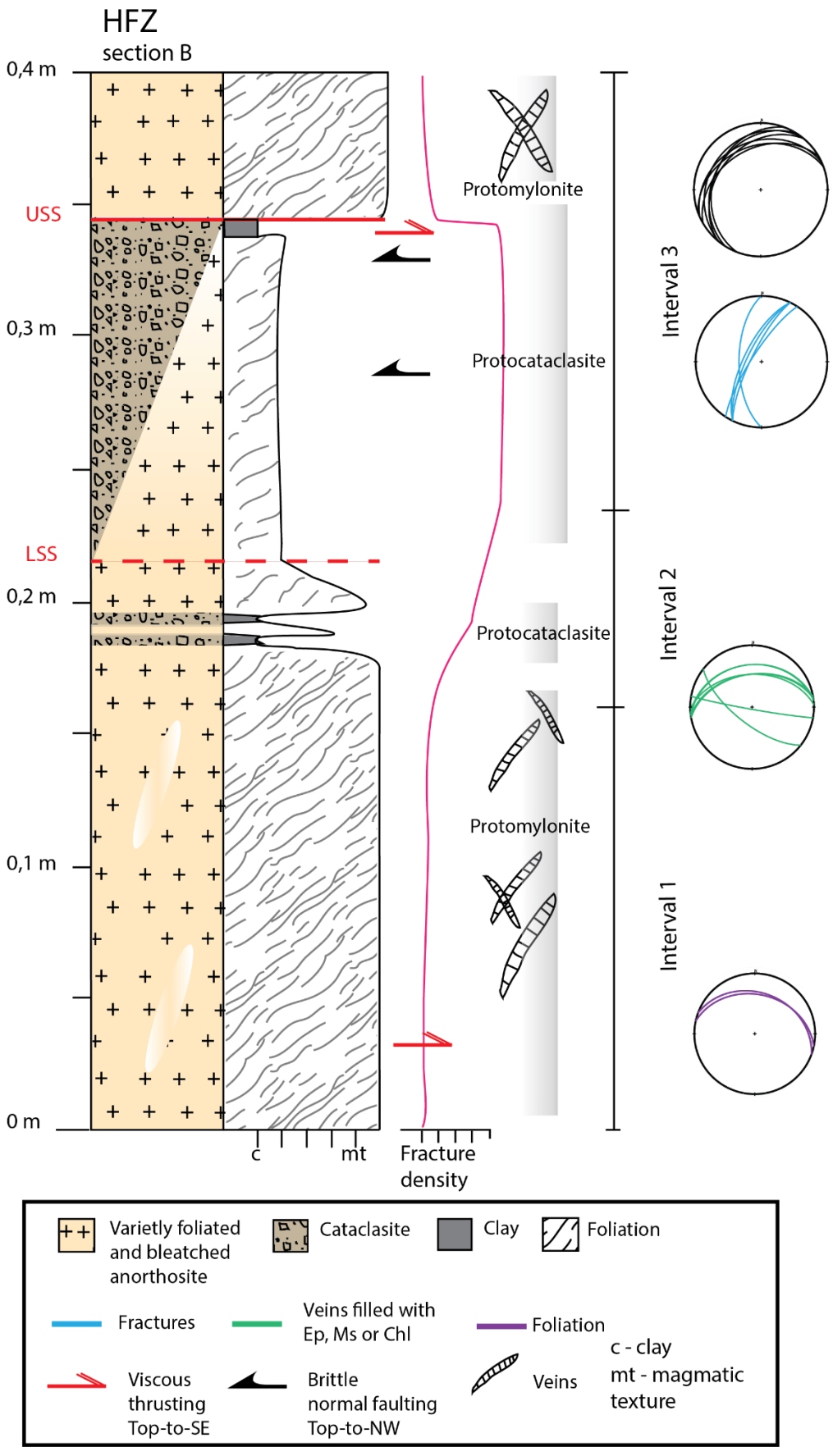

Fig. 4-33: Structural log of section B.

4.3.4 Section C

Section C is located at the southernmost corner of the white house. The fault core is up to 1 m in this section. The main fault plane dips gently toward NW (Fig. 4-26A, Fig. 4-34 A&B). The fault in section C has a very distinct LSS and USS, that allow an easy separation of footwall, hanging wall and fault core. Both the LSS and the USS are comfortably distinguished by the presence of a c. 3 cm clay rich zone (Fig. 4-34C & D). A gouge sample was taken from this section, at the USS, and was dated by K-Ar (Fig. 4-37). In addition, four samples were collected and studied in microscope (Fig. 4-34A&B).

Interval 1

Interval 1 is entirely within the footwall. The footwall is characterized by a penetrative, spaced foliation defined by dark minerals in a pale pink anorthosite matrix indicative (Fig. 4-36B). Just a couple of m away south of the section, the anorthosite is massive, equigranular and lacks evidence of any pervasive planar or linear fabric. This leads to a ductile precursor shear component localized in a fault. Brittle fractures with no mineral infill are arbitrarily distributed in the interval, cutting the viscous component (Fig. 4-36A). Two sets of greisen veins in the footwall have white alteration halos and a dark green core (Fig. 4-35E). Sample AFE_19 is from the intersection between two such veins. The sample is heterogeneous with a phaneritic texture. Purple feldspar dominates the matrix around the two crossing veins, but some feldspar with a distance from the veins has a white-dull color due to sericitization. Mafic enclaves elongated parallel to the foliation decorate the rock in the upper part of the interval.

Interval 2

Interval 2 exhibits an increase in fracture density (Fig. 4-35B) and the color varies between dull pink and dull white. The rock is still coarse-grained but thin zones of cataclastic rock interrupt the more massive rock (Fig. 4-35B). Sample AFE_23 is immediately adjacent to the LSS and characterized by a cataclastic texture. AFE_23 is affected by metasomatic processes with a foliation defined by the alignment of dark green minerals. The sample is heterogeneous and solid but have a poor cohesion due to brittle fractures. In this part of the footwall, close to the LSS, some weak evidence of thrust kinematics are found in the foliation (sigmoidal foliation clasts and gently E-dipping SC planes) indicating an overall top-to-the southeast viscous deformation that predates the brittle deformation (Fig. 4-34Fig. 4-36A). In addition, just a

couple of cm below the USS a mafic enclave is observed in the upper part of this interval extremely transposed parallel to the foliation (Fig. 4-36C). The LSS is characterized by a c. 2 cm thin zone of gouge with a light pink color.

Interval 3

This interval is characterized by a cataclastic texture and interpreted to be the brittle fault core. The rock is of dull white color but is interrupted by thin veins of light green Ep in a crosscutting relationship distributed though out the upper core. Numerous of small veins and fractures are oriented parallel to the fault slip plane and the foliation, indicating a geometric relationship between the foliation and the brittle component (Fig. 4-35A & B, Fig. 4-37). The brittle component is dominant in this part of the fault and the mafic component decreases. Sample AFE_24 is from this brittle fault core. The hand specimen is indurated, despite the many fractures through it. AFE_24 is heterogeneous with a bleached white color clearly altered by sub horizontal veins that goes through the sample.

Interval 4

Interval 4 is the uppermost part of the fault and contains the USS. The viscous fabric, that consists elsewhere of aligned Chl and opaques, is here absent, but appears again in the immediately overlaying hanging wall. The USS is a thin zone of brecciated fragments of the host rock and gouge with subordinate hematite and calcite (Fig. 4-34C & D, Fig. 4-35C). A vein of calcite is located just above the gouge-rich zone. Sample AFE_25 is from 20 cm above USS, the sample is totally metasomatic anorthosite and have a fracture plane parallel to the fault slip plane. The sample is heterogeneous, has a white-dull color and lacked cohesion. Localized metasomatism leads to white halos around some of the veins. The greisen veins appearing in the overhang, close to the USS, demonstrates the high alteration within the rock (Fig. 4-28A). Just north of section C, the fault core attains its minimum thickness, with no more than 20 cm separating LSS and USS (Fig. 4-26, Fig. 4-35A).

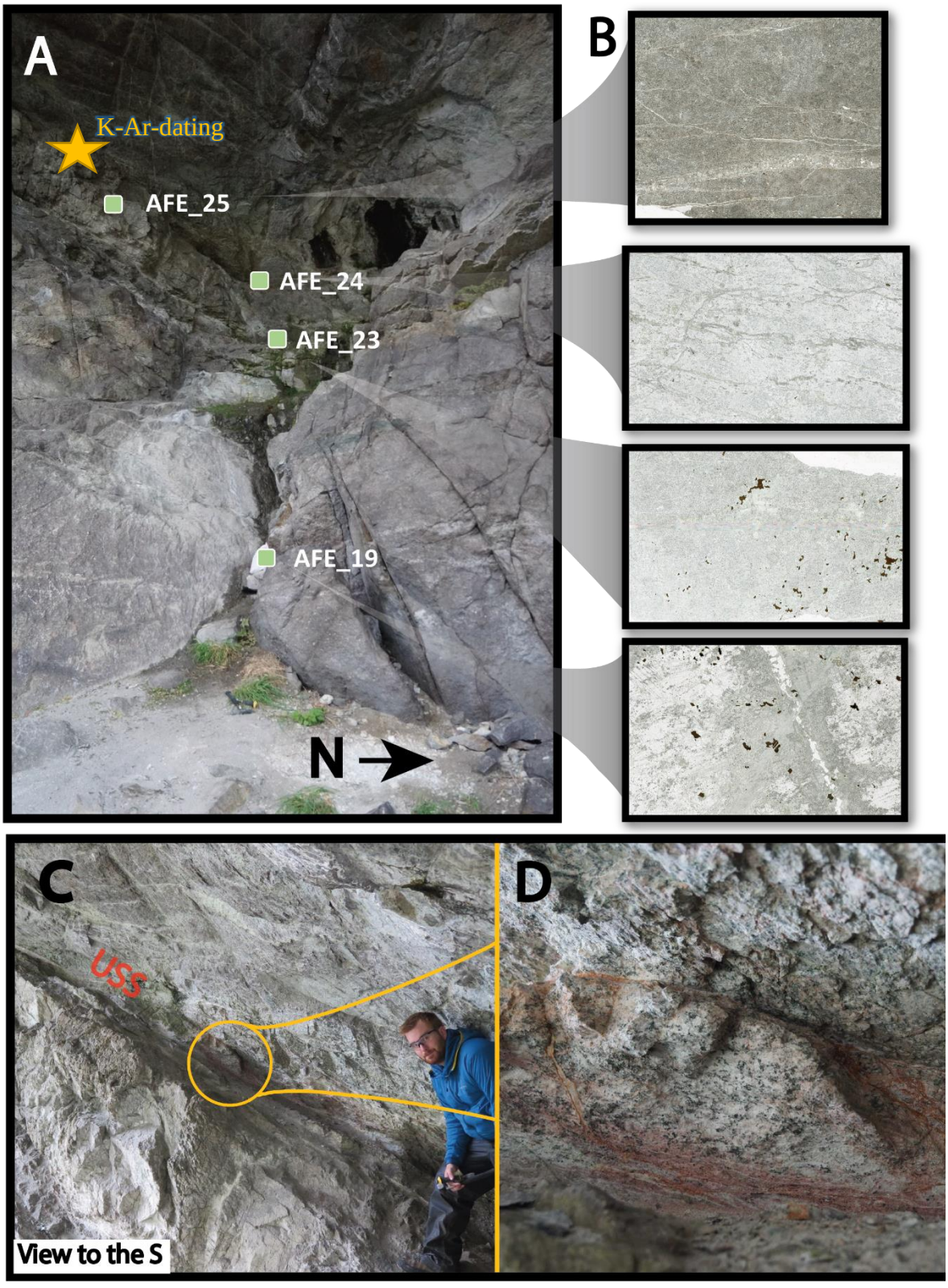

Fig. 4-34:Section C. (A) Sample location along the section. (B) Photo of the four thin sections form Section C, sample AFE_19 to AFE_25. Note that the oxides/opaques are abundant in the two lower samples but are absent in the uppermost samples. (C) Cataclasite with gouge and brecciated fragments a long the USS. (D) Detail of the USS and the cataclasite with subordinate Hem and Cal.

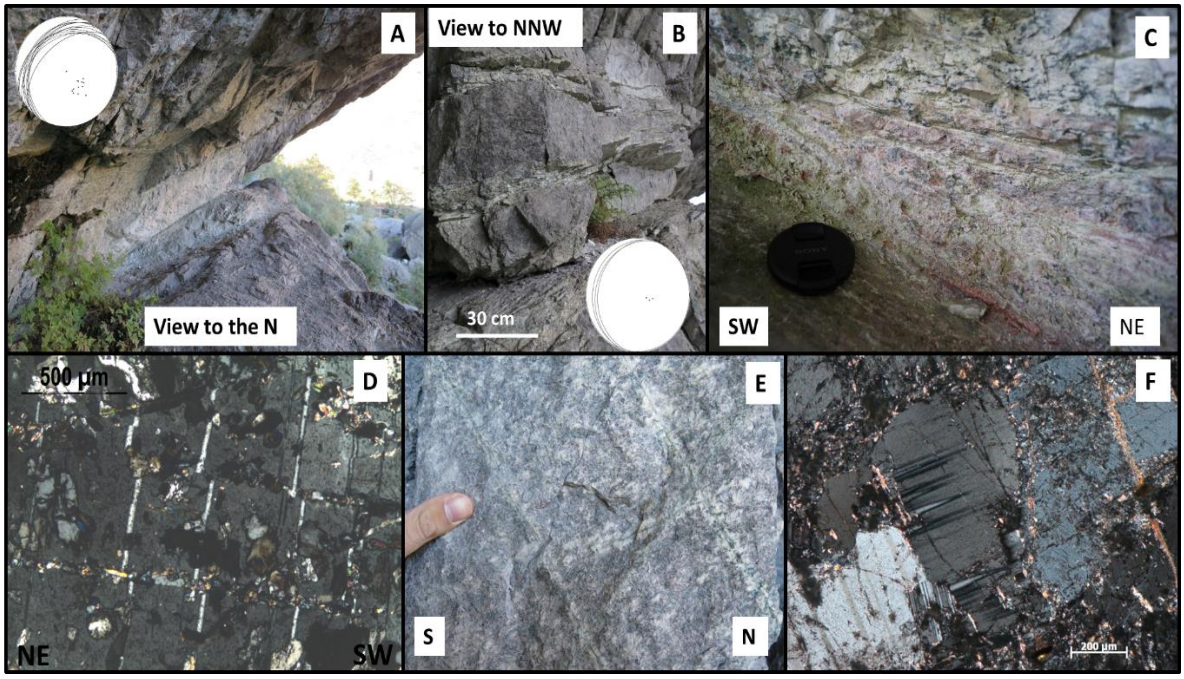

Fig. 4-35: Deformation styles within the HFZ at section C. (A) Detail of brittle the core where it reaches its minimum thickness, view to N. (B) Ductile foliation in interval 2 with localized later fractures that exploit the foliation planes. (C) Closer look at the gouge rich USS with colors varying from dull white, pink and green. (D) Intracrystalline deformation along cleavage, grain scale faulting, sample AFE_24. E) Crossing Ep-Chl veins with a white halo. (F) Deformation twins, sericitization and fractures in sample AFE_19.

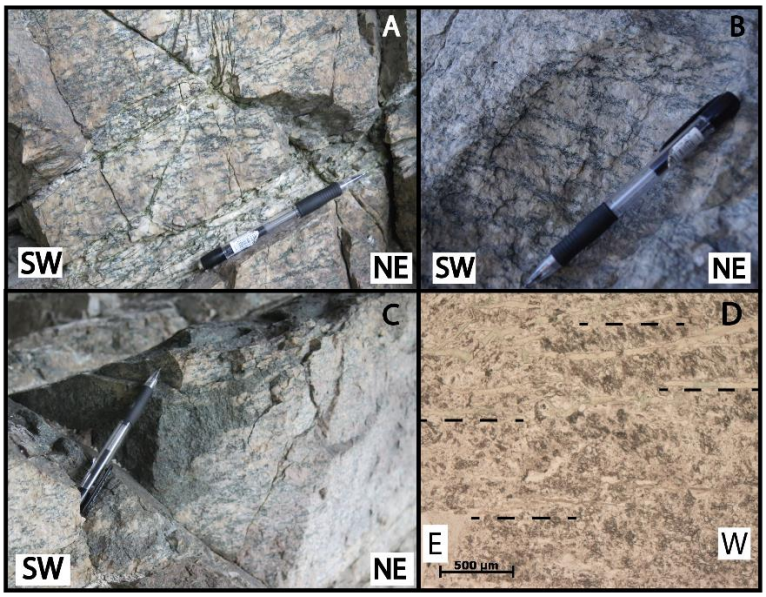

Fig. 4-36: Ductile deformation styles within section C. (A) Ductile penetrative foliation in interval 1 with localized brittle fractures and pervasive alteration of anorthosite from pale pink color to a dull white color concentrated around the brittle fractures. The white color reflects the high content of fluid penetrating though the fault, reflected in pervasive sericitization. (B) Foliation planes defined by the alignment of mafic minerals. (C) Mafic enclaves transposed parallel to the foliation. (D) Sample AFE_23 is illustrating alteration of mafic minerals to Chl, whose spatial orientation defines the foliation seen in (B).

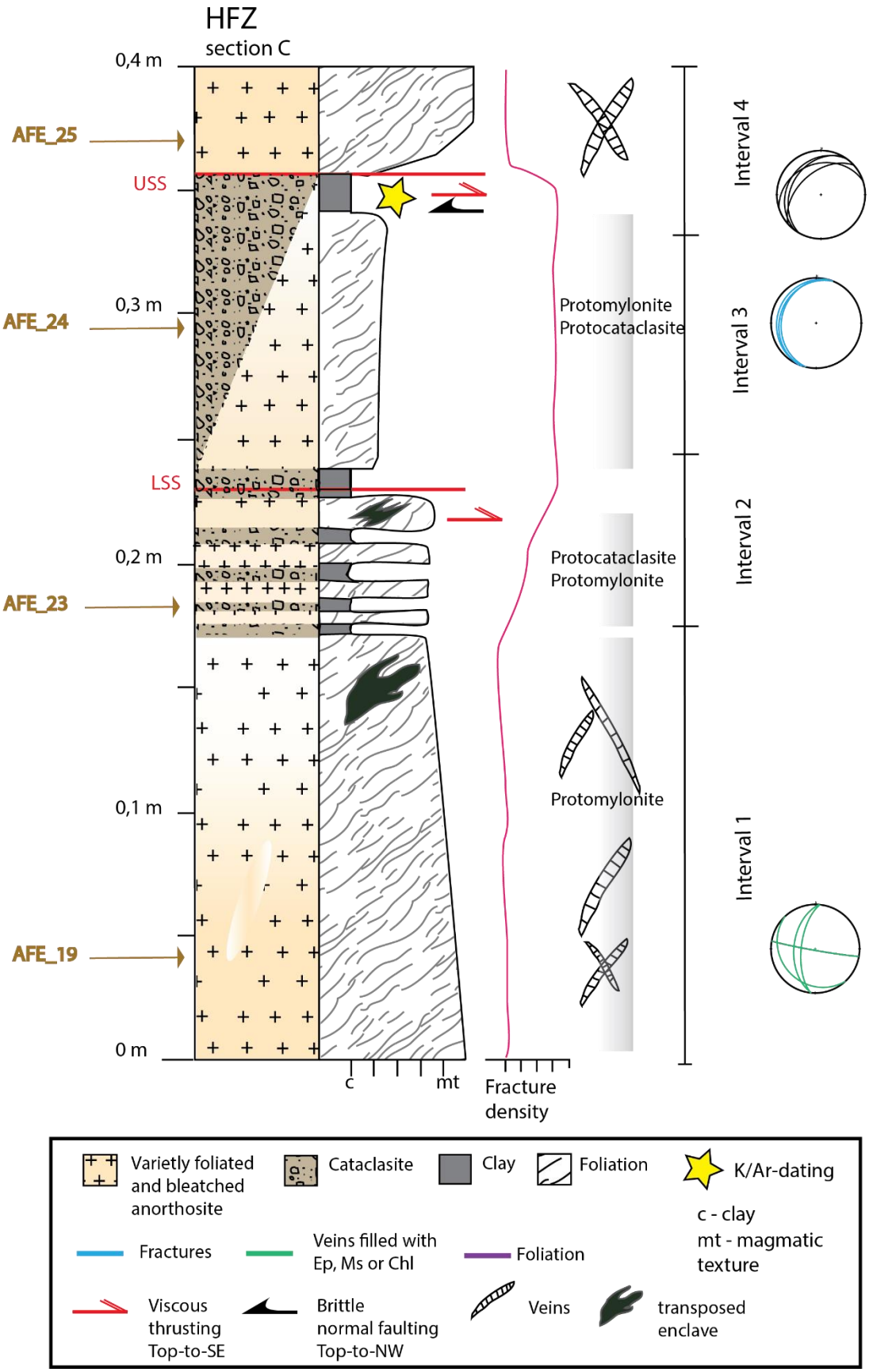

Fig. 4-37: Structural log of section C.

4.3.5 Summary of the structural analysis

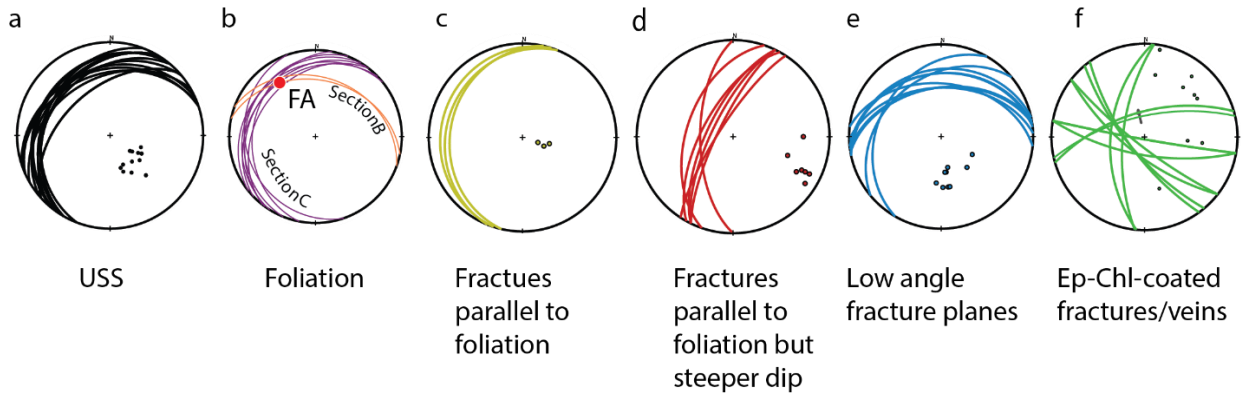

Fig. 4-38: Structural observation measured in field are sorted here according to their characteristics.

To the purpose of this analysis, field observations and structural data from the HFZ are sorted according to their characteristics and plotted in separate stereonets in Fig. 4-38. The stereonets are then used to better understand the structural evolution of the HFZ.

Is the HFZ folded: a closer look at the USS and the foliation

When considering the first stereonet of Fig. 4-38a, it appears that the USS has a distinct and constant dip towards NW throughout the studied section. The USS reflects the brittle reactivation of the HFZ with an overall top-to-the NW normal displacement. The foliation plotted in the second stereonet (Fig. 4-38b), on the other hand, documents an interesting difference between measurements from section B and C, which seems to indicate a folded foliation. The foliation dip changes from NE in section B to W-NW in section C. The foliation plane attitude thus defines an open upright fold with a fold axis oriented towards NW (FA in Fig. 4-38b). Since the foliation is folded, it can be concluded that the ductile deformation that formed the planar anisotropy of the HF occurred prior to the folding event, and, based on the unfolded nature of the USS, that folding predated the last recorded increment of brittle deformation. The folding event is believed to have controlled the overall pinch and swell structure of the fault core.

Brittle extension

Fig. 4-38c and d correspond to smaller fractures within the HFZ. They have the same dip direction, but different dip angle, where Fig. 4-38c has the same dip as the foliation whereas Fig. 4-38d, has a steeper dip. The steeper dipping fracture set can possibly be interpreted as Riedel fractures to the gentler dipping fractures. In that case, they would result from an overall

top-to-NW along the main HFZ oriented like the USS and are interpreted to document a brittle phase of brittle extension oriented NW-SE postdating top-to-SE viscous thrusting. Hence, strain would have concentrated along the weakest planes (foliation planes) and reactivated the foliation in a brittle fashion.

Low-angle fracture planes in Fig. 4-38e are slightly more N-dipping and are mostly observed in section B, where there is a rotation of the foliation towards N(NE) (Fig. 4-38b) due to the folding mentioned above. Since the foliation is bent leading to the pinch and swell structure of the fault, brittle strain concentration would have been the highest in the weak foliation planes and would indeed have generated the low angle fractures parallel to the foliation that are plotted in Fig. 4-38e.

Fig. 4-38f illustrates the Ep-Chl coated fractures/veins observed in the field. These veins have been studied in more detail and results are illustrated in Fig. 4-39. They are mutually crosscutting suggesting two conjugate fracture sets, set I and set II. Set I constrains an extensional stress tensor with extension oriented NNW-SSE. This possibly supports the only slightly misoriented brittle extensional phase of the HFZ oriented NW-SE found in the analysis of the outcrop (Fig. 4-38C & D), and now also confirmed by set I of Ep-Chl-coated veins showing an overall dextral sense of shear along the main HFZ oriented like the USS. Set II is less clear. Due to poor kinematic data, this is proposed only as a possible scenario and is not fully documented.

The structural observations plotted in Fig. 4-38 confirm multiple deformation events accommodated by the HFZ.

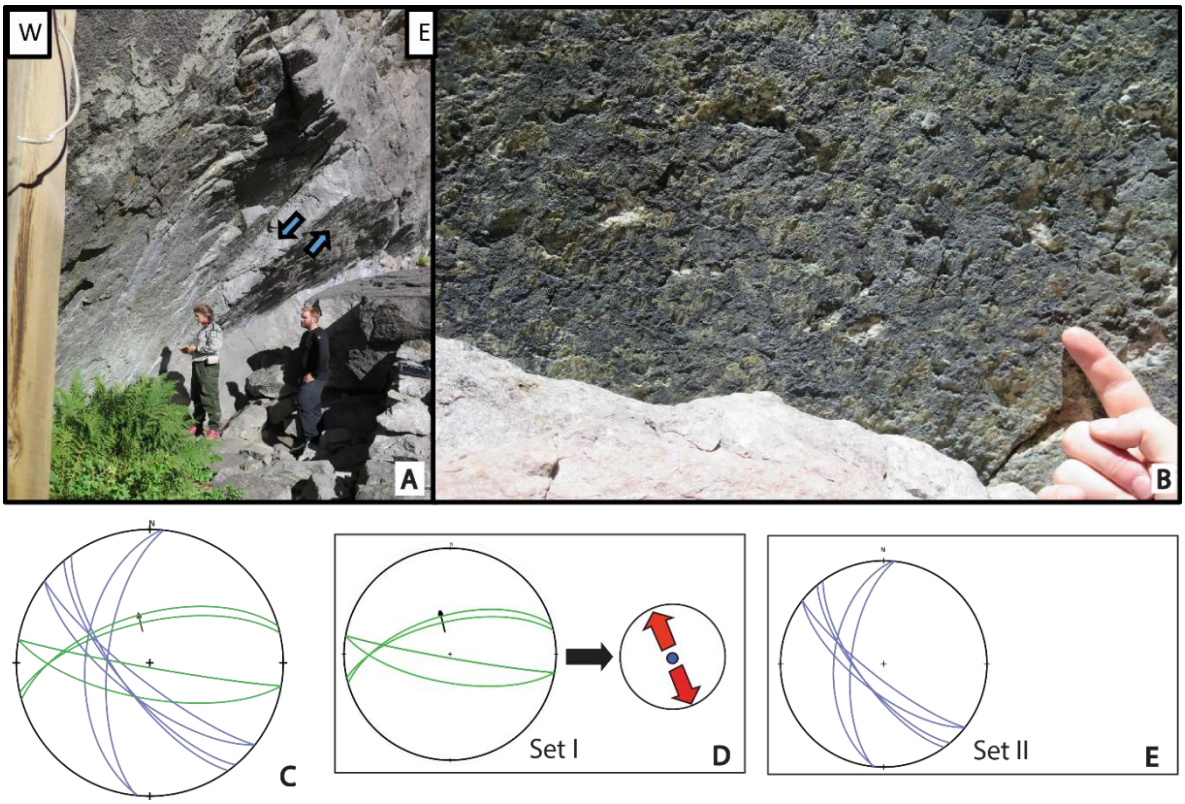

Fig. 4-39: (A) Slip surface with epidote and chlorite coating. Slickensides indicate sinistral sense of shear corresponding to top-to-the NW kinematics. (B) Close-up view of the epidote and chlorite coated surface with faint slickensides. (C) Stereonet of all Ep-Chl coated surfaces observed in the field. (D) Green color indicates set I that is representative for an extensional stress regime. (E) Blue color indicates set II.

4.3.6 Petrography of the HFZ

Field microstructural and petrographic analysis was integrated with observations and analysis based upon the study of eight thin sections from sections A and C (Fig. 4-28 C & D, Fig. 4-34 A). The thin sections contain evidence of both brittle and viscous deformation and are strongly (but variably) affected by metasomatic processes resulting in profound mineralogical transformations of the host anorthosite and localized grain size reduction of the rock. The brittle deformation component is characterized by fractures and veins crossing discordantly the sections, where NE-SW is the most common orientation of the veins. In this section, a detailed account of the microstructural and petrological analysis will be given.

The average mineral composition seen in the thin sections is given by plagioclase with muscovite (Ms), epidote (Ep), chlorite (Chl), zoisite (Zo) and ilmenite (Ilm). Plagioclase varies in grain size from medium to coarse and has a dusty appearance as a result of alteration and metasomatism. It commonly shows evidence of intracrystalline deformation including bent cleavage planes, deformation twins and grain-scale faults (Fig. 4-35D & F). Pl is locally

pervasively altered by metasomatic processes that led to the formation of secondary minerals, such as Ms, Ep, Chl and Zo (Fig. 4-40B). The observed metasomatic processes are due to fluids that flowed along fractures and faults within the anorthosite and thereby interacted with the host rock locally changing its composition (Fig. 4-42D). Veins are the most common microstructure and secondary, metasomatic mineralizations are spatially closely related to these (Fig. 4-40A &D).

There are several alteration styles that are common for the HFZ rocks, such as saussuritization, sericitization and chloritization (Fig. 4-40). Saussuritization leads to extraction of Ca from plagioclase, that reacts with the fluids and allows Zo, Ep, Ms or Cal to form. As Ca reacts with the fluid, Na remains in Pl and forms new albite grains. The mineral product of this process depends on the chemical composition of the fluid and the plagioclase. The veins express saussuritization through halos of altered Pl and a core filled with Zo, Ep, Ms and/or Chl (Fig. 4-40A). Here, Zo generally exhibits fine to medium grain size with anhedral grain shape, it is colorless with anomalous blue interference colors or sometimes 1. order yellow interference colors. Ep has medium grain size, subhedral and equant grain shape, pale yellow color, high relief and high interference colors. Both Zo and Ep are generated within or close to veins and fractures and Zo seems to only appear in veins in the uppermost part of the fault (sample AFE_17,18,24,25).

In addition to saussuritization, sericitization is vastly common in the HFZ whereby sericitization of plagioclase appears typically as millimetric to centimetric halos bordering veins or as overgrowth in Chl and Pl (Fig. 4-40D & F). This process generates sericite characterized as fine grained with a low relief and high interference colors. Chlorite (Chl) results from chloritization of the mafic components and defines the foliation in the more ductilely deformed anorthosites as thin Chl veins or elongated and interconnected levels of individual Chl crystals (Fig. 4-43). This secondary Chl together with altered Ilm appear commonly together, and all the Ilm have a halo of chlorite and epidote (Fig. 4-40E). Ilm and the secondary Chl are absent in the samples close to the USS (AFE_18 and AFE_25), giving the impression that secondary Chl is formed only where the Ilm is preserved in the rock. Two generations of Chl are common, distinguishable by very distinct interference colors, pale green-brown and ink blue. In some areas, the pale green-brown Chl seems to overgrow the ink blue Chl (Fig. 4-40C & D).

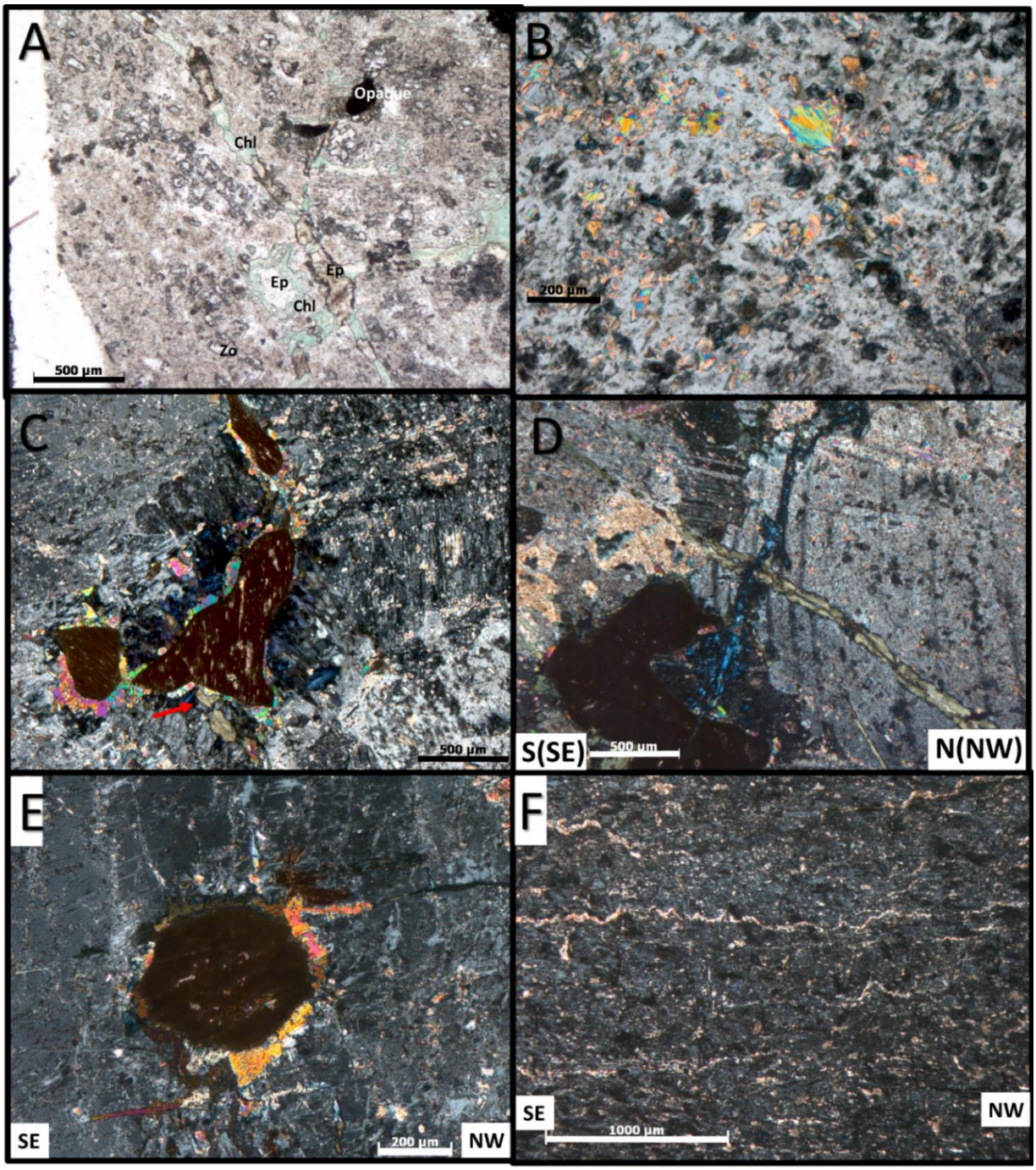

Fig. 4-40: Examples of various types of fault rocks associated with the HFZ. (A) AFE-17: Huge difference in Ep in vein and the one surrounded by Chl (B) Metasomatic processes which generate sericitization: Pl → Clinozoisite and albite AFE_16, 10x, XPL. (C) Oxides surrounded by Ep and dark blue Chl. Iron from the oxide increases the Fe content in the Chl and changes chemistry and color. The red arrow is pointing at Chl with a green-gray color that overprints the surrounding minerals and are very different from the dark blue Chl suggesting two generations of Chl. AFE_16, XPL (D) AFE_17: Zo vein oriented WNW-ESE, crossing a Chl vein, indicating a later infill of the Zo vein. The Chl vein also have an internal lamination, XPL. (E) Oxide surrounded by Ep and Chl mineral growth, AFE_18, XPL (F) Veins oriented parallel to the foliation characterized by (fink)folding and micas in Pl, AFE_18, XPL.

4.3.6.1 Detailed vein mineralogical description

Veins are the most common brittle feature seen in the thin sections from HFZ and were therefore carefully studied. All the main vein sets from the eight thin sections have been analyzed at the microscope and the most important observations will be presented in this section. They are distinguished by petrology and structural properties. The vein infill is influenced by the composition of the host rock and the composition of the fluids percolating though the rock whereby at least four generations of hydrothermal vein deposits are observed and some express polyphase deformation: (1) Ep- Ms veins (2) Zo- Ms veins (3) Chl-veins and (4) Qtz-Ms-Pl-veins. Mineral filling is both massive and fibrous, but the massive minerals are found preferentially in the wider veins.

(1) AFE_16 and AFE_24

AFE_16 is from the lower part of section A (Fig. 4-29) and contains two parallel veins that are continuous throughout the thin section (Fig. 4-42). They dip towards NNE at a steep angle, which is the most common orientation of these types of veins in the HFZ (Fig. 4-45F). These generations of veins mainly contain Ep, Ms and Chl, which varies in grain size from fine grained to elongated medium grained crystals. The northernmost vein has a curvy path, it is c. 1 mm thick and it is distinct throughout the section. The contact to the host rock is rather diffuse with smaller vein shooting out from the major vein causing the secondary mineralization to be diffused over a broad area. These smaller veins often have a halo formed by fine-grained Ms (Fig. 4-42B). The secondary mineralization within the northernmost vein is characterized by fine grained Ms or sericite, fine to medium grained elongated Ep and some medium grained more fibrous Chl. The core of the vein contains mostly fine grained Ms and Ep while the coarser crystals are arranged radially around the vein.

The c. 1 mm thick southernmost vein has a distinct but curvy geometry with smaller veins departing from it and spreading the secondary mineralization over a large area. These smaller veins may represent separate crack-seal events. The core of the vein has a sharp contact to the more diffuse halo of the vein. The vein infill is removed due to polishing but Ep, Ms and some Chl are found around the vein with a decreasing grain size when moving from the lower to the upper part of the thin section. In the lower part, Ilm crystals are situated close to the vein, where we can find the coarsest grained Ep (Fig. 4-42C). It would appear that the secondary mineralization grew faster close to the Ilm. Fig. 4-42D, SEM imaging, shows the upper part of the vein and a texture of secondary minerals (lighter gray color) indicating fluid percolation through the rock along the fracture network. The fluids flowed through an already established

fracture zone in the anorthosite. At the time of fluid infiltration, the fluids started to change the primary chemical and mineralogical composition of the rock, a process known as metasomatism. Both veins described in this paragraph reflect an episode of fluid flow that increased the overall alteration of the rock. Sample AFE_24 shows intracrystalline deformation of coarse-grained Pl through deformation twins, sericitization and fractures, as seen in AFE_16 (Fig. 4-41). Veins in sample AFE_24 are oriented SW-NE appear parallel to the foliation and contain Ep and Ms.

(2) AFE_17

AFE_17 is from the upper part of section A (Fig. 4-29) and contains the generation of veins where Zo precipitated within the vein (Fig. 4-42G). They are characterized by veins with a thickness up to c. 5 mm, a sharp, but curvy contact to the host rock and a vein attitude dipping gently towards NW, oriented parallel to the main fault plane (Fig. 4-42E&F). These veins are filled with fine to medium grained Zo and fine grained Ms/sericite. When moving from their edge towards the center, the mineralogy changes from Zo-rich with an anomalous blue interference color to Ms-rich with a brownish interference color (Fig. 4-42E). There are also local variations of the amount of Zo within these veins, whereby some contain more Ms while others contain only Zo (Fig. 4-42F) and show a much darker anomalous blue interference color. When zooming into the Ms in the center of the vein (Fig. 4-42H&I), one can see that the Ms is finer-grained than the Zo and that Ms precipitated in the center of the vein. Because the Ms is finer-grained than Zo in this part, it can be postulated that Ms precipitated later than the Zo suggesting syntaxial growth generating such spatial relationship. Ms is not located at the exact center of the vein, which may be due to asymmetric growth. Change in fluid pressure may have cause several generations of opening which resulted in precipitation of various minerals such as Zo or Ms. In the uppermost part of the vein there is a transition from the fine-grained Zo to bigger crystals of Zo (Fig. 4-42F). Spikes of finer grained Zo and Ms point into coarser grained Zo indicative of polyphase deformation within the vein (Fig. 4-42F). The contact to the host rock is moderately sharp although thinner veins of Zo propagating from the thick Zo-vein are locally also observed (Fig. 4-42G). These thin veins filled with elongated Zo are perpendicular to the thick vein and pervasive throughout the thin section postdating other structures and overprints other minerals.

Fig. 4-41: Ep-Ms-filled veins and thin levels define the protomylonitic foliation of the HFZ , sample AFE_24 PPL.

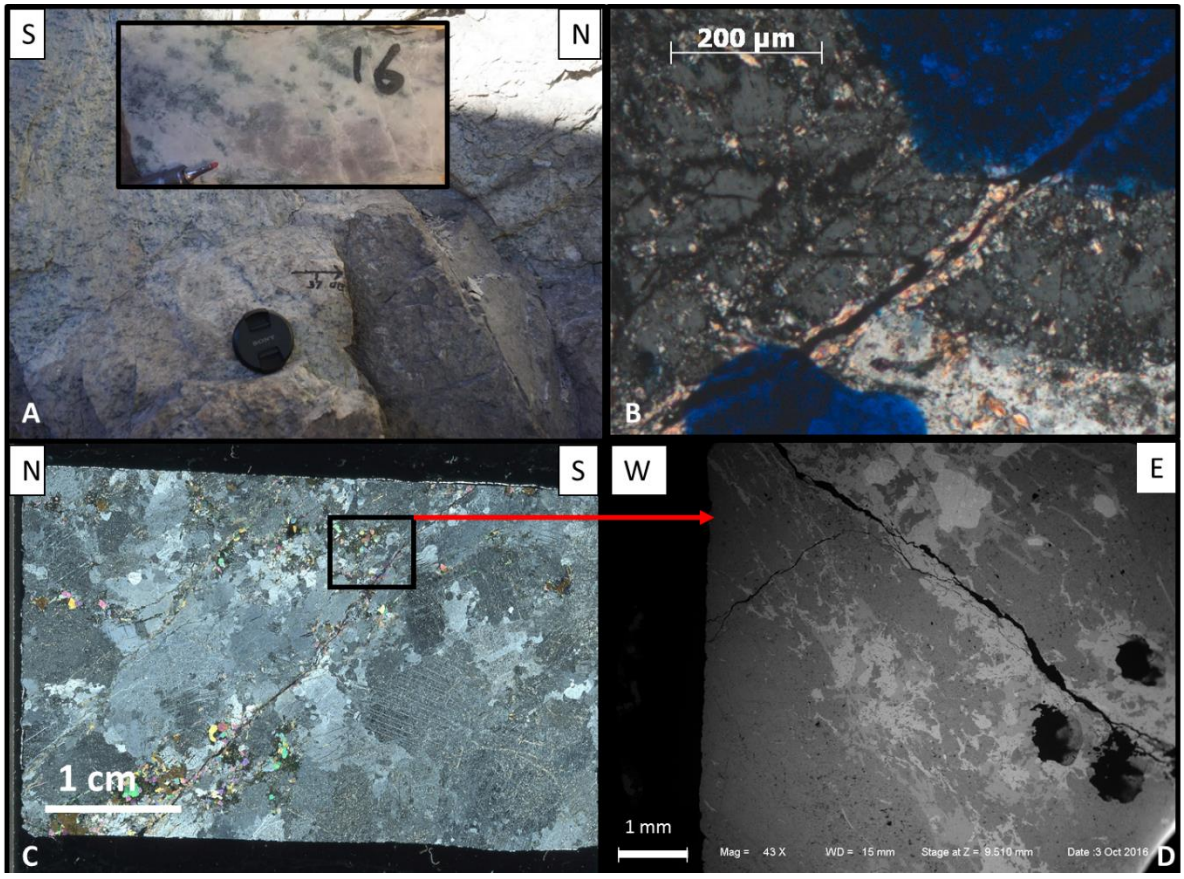

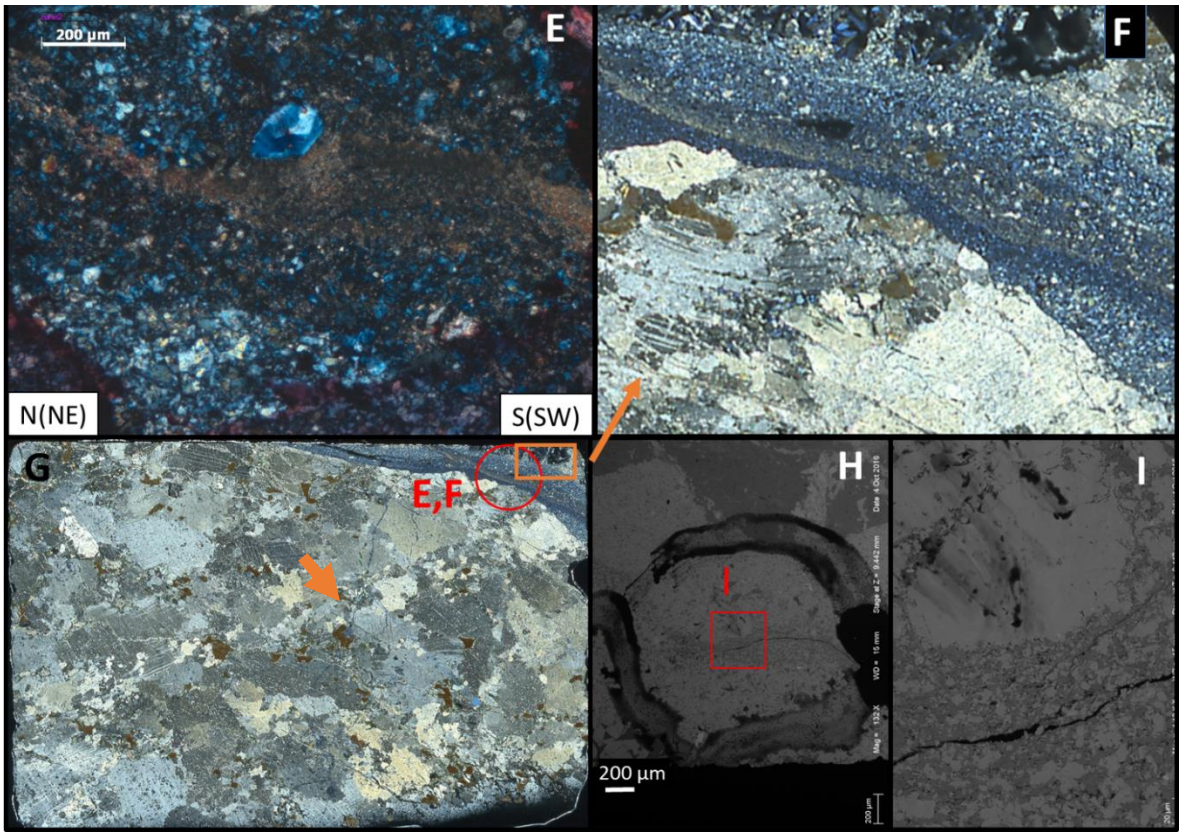

Fig. 4-42: Sample AFE_16 and _17 A-D: (A) Outcrop from where AFE_16 was collected and photo of the hand specimen showing alteration of the anorthosite from purple to pale white/pink. (B) Smaller vein with a halo of sericite spreading out from the major vein, XPL. (C)Thin section of sample AFE_16 in XPL. Two distinct veins or fractures cross the section dipping towards the north and are associated with secondary alteration. (D) SEM- analysis show texture of secondary minerals (lighter gray color) indicating fluid percolation through the rock along the fracture network. E-I = AFE_17 in XPL: (E) Zo vein with two distinct generations of mineralization. Zo is the anomalous blue while brown is Ms/sericite (F) Spikes of fine grained Zo points into the coarser grained Zo. Notice the variations of intense anomalous blue interference color and the areas with more Ms/sericite that have a much lighter interference color within the vein. Change in fluid pressure may have cause several generations of opening and precipitation of various minerals such as Zo or Ms. (G) Thin section AFE_17 where (E) and (F) is marked on the photo the orange arrow points to a perpendicular Zo veins propagating throughout the thin section from the thicker vein. (H, I) H and I are a zoom-in to the core of the vein where the lightest gray color is Zo while the dark gray is Ms/sericite. Note the finer grain size of Ms/sericite.

(3) AFE_18

Thin bands with Chl are commonly distributed throughout the HFZ and define the foliation of the more ductilely deformed anorthosites. They can be elongated and interconnected levels of individual Chl crystals or aggregates close to Ilm crystals. AFE_ 18 from the upper part of section A (Fig. 4-29) contains plenty of evidence in support of this (Fig. 4-43a). These bands have a sharp contact to the host rock and vary significantly in length from millimetric to centimetric scale (Fig. 4-43b) and contain fibrous Chl. Their thickness is often no more than a few millimeters (Fig. 4-43b) except for the Chl close to the Ilm where they can be much thicker.

Fig. 4-43c shows the change in interference colors from the margin of the bands to the inner core. The interference color change from dark brown at the margins to anomalous blue in the core. This might indicate some change in the fluid flow which also has been seen in the Zo-veins in thin section AFE_17 described above. The oldest part of the vein might lay along the edges, while the final composition of the band is in the middle of the vein. Fig. 4-40D show an interesting intersection between the Chl-bearing bands and the Zo veins. The Zo-bearing vein is crossing the Chl-bearing band and predates the Zo- bearing vein.

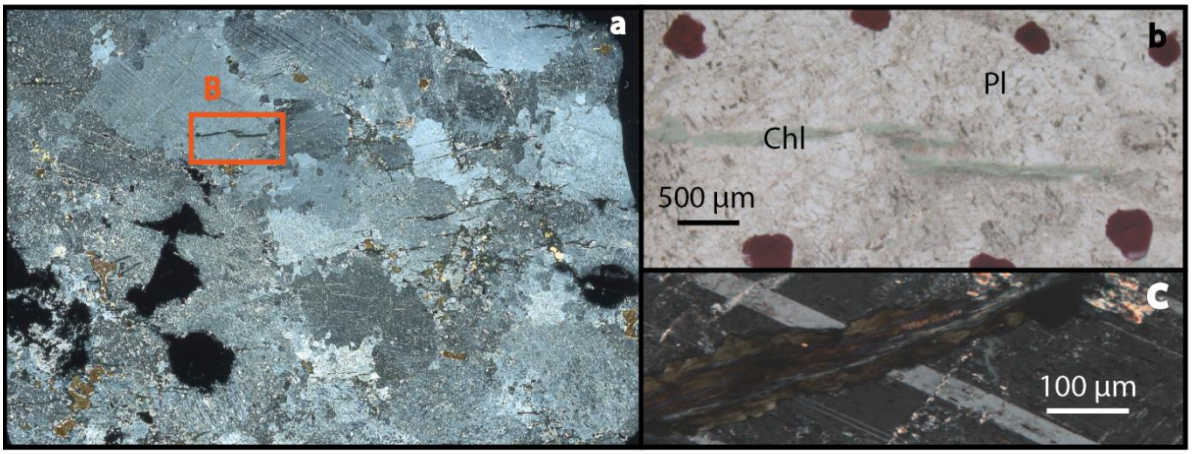

Fig. 4-43: (a) Thin section AFE_18 with the elongated thin veins of Chl distributed throughout the thin section, XPL. (b) Thin vein of Chl that defines the foliation, PPL. (c) A closer look at the vein in (b) where you can see the interference colors changing from the margins into the core, XPL.

(4) AFE_19

Section AFE_19 contains two spectacular veins that cross each other (Fig. 4-44a). AFE_19 is from the footwall of section C (Fig. 4-37) and the Pl is therefore less altered by sericitization. However, both veins caused a halo of sericitized Pl, which confirms the genetic relationship between the vein formation and metasomatic processes. The first vein dips towards E with a steep angle to the main fault plane of HFZ (Fig. 4-26A) and is the only vein of this kind seen in the thin sections. It is characterized by coarse grained, elongated quartz (Qtz) in a matrix of fine grained Pl and Ms (Fig. 4-44c). Qtz shows no evidence of plastic deformation and there is only minor sericitization at the margin of some crystals. The contact between the vein and the host rock is sharp but a light halo of altered Pl surrounds the vein (Fig. 4-44a). The second vein dips towards W with a steep angle and shares the same characteristics as the one described in thin section AFE_16, with mineral infill of Ep, Ms and some Chl. Here, the contact to the host rock is diffuse with smaller veins extending from the main vein. The main vein splits up into two parallel thinner veins in the upper part of the thin section leading to alteration of a bigger

volume of the rock. Secondary metasomatic minerals such as Ep and Ms are not only inside the vein but grew also at the periphery of the vein due to fluid percolation in small veins related to main vein. Several clasts of plagioclase occur in the vein and show that cracking was partly along the vein margins. When zooming into the area where the two veins mutually cross (Fig. 4-44d), one can see that the vein filled with mostly Ep and Ms cuts the one filled with Qtz, which means that the Ep-Ms-vein postdates the Qtz-vein.

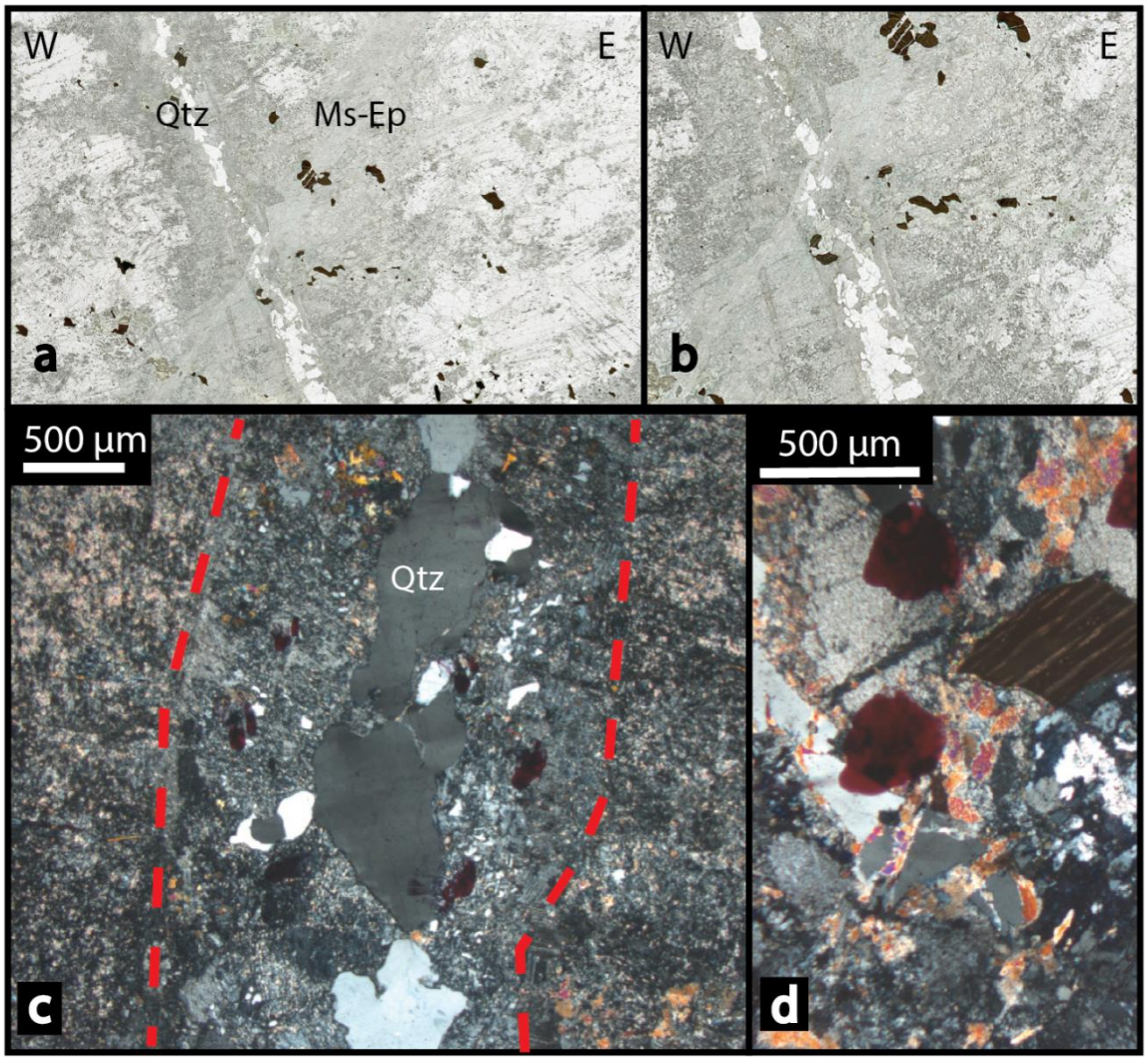

Fig. 4-44: (a) Thin section AFE_19 note the halo of alteration around the two crosscutting veins, PPL. (b) A closer look at the crossing of the two veins where the W-dipping vein postdates the E-dipping vein, PPL. (c) The E-dipping vein filled with Qtz in a matrix of Pl and Ms, XPL. (d) Zoomed in to where they intersect each other. The W-dipping vein overprints the E-dipping vein, XPL.

4.3.6.2 Analysis of veins studied in thin sections

In addition to the field observations, eight thin sections from two sections across the fault were studied (Fig. 4-28,Fig. 4-34) as described previously. All the veins from the thin section were measured and sorted according to their petrological and structural features. The petrological and structural appearance of the veins in thin sections yielded some interesting insights as to the veining history. As shown by field observations, the foliation is folded around a NW-plunging fold axis associated with an open, upright fold geometry. The foliation dips towards the NNE in section B and towards the NW in section C. At the micro scale, the same patterns can be seen. The strike of the analyzed veins is plotted in rose diagrams and the orientation of the veins changes gradually from NW-SE in section A to NE-SW in section C (Fig. 4-45A & B). The veins were then plotted in separate stereonets according to their mineralogical and structural properties. Veins filled with Ep and Ms are plotted in Fig. 4-45f and g, according to which section they belong to. Most of the veins in section A have a WNW-ESE trend and in section C the same veins are oriented NNW-SSE. This is compatible with the folded foliation discussed above (Section 4.3.5) and a change of orientation of both the foliation and the veins (Fig. 4-38, Fig. 4-45A & B). Since many of the veins that contain Ep, Ms and Zo are folded (Fig. 4-45 A, B, f, g) it is reasonable to infer that some of them formed before the viscous folding suggesting a brittle precursor to the viscous deformation.

Bands dominated by chlorite (Chl) are widely distributed in the thin sections (e.g. see; Sample AFE_18). Analysis at the microscope and of hand specimens indicates a strong geometric relationship between the foliation and these veins (Fig. 4-45e). They are subparallel the foliation and can be separated into two generations, where generation 1 is characterized by opaques, Chl and some Ep, whereas generation 2 thin elongated bands of Chl at an angle to generation 1 (Fig. 4-45A &B). Generation 2 is thin long veins not following any specific grain boundaries or mineral cleavage|. In addition, generation 2 change interference color from green-brown at the margins to dark ink-blue towards the center of the veins (Fig. 4-43c). The foliation plotted in the stereonets in Fig. 4-45a and b, suggest generation 1 trending NNW-SSE. Generation 2 varies more but show an average NE-SW-trend and are parallel to the foliation.

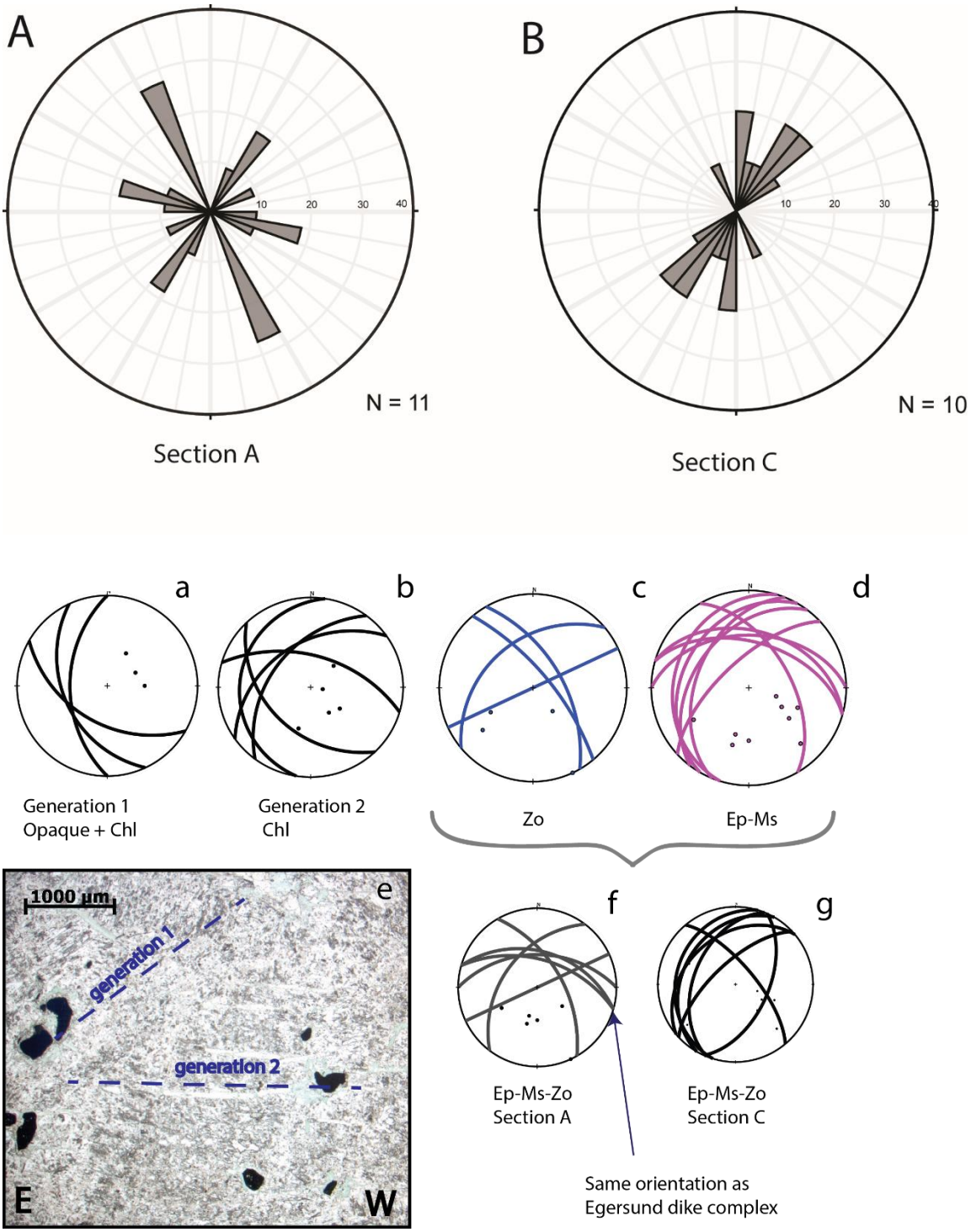

Fig. 4-45: Vein orientations separated by their geological properties. (A) is all the veins from the four thin sections from section A, showing a main trend NW-SE. (B) shows the same as (A) only with the thin sections from section C. Here, the veins have a NE-SW- trend. (a) are all generation 1 veins filled with Chl-Ilm with a dip towards SW. (b) show generation 2 veins dipping generally towards NW. (c) Vein with Zo with no clear patterns (d) Veins filled with Ep and Ms that have two trends, NNE-SSW and NW-SE, respectively, that are parallel to the foliation. (f) and (g) separate the Ep-Ms-Zo-veins from section A and C, respectively. Notice the change from NE dipping veins in section A to NW dipping veins in section C, the same pattern seen for the foliation. These relationships can be used to conclude that some of the veins filled with Ep, Ms and Zo are older than the folding of the outcrop and so that part of the brittle deformation history predates viscous deformation.

4.4 K-Ar-dating

Radiometric dating has recently become a reliable tool for the absolute dating of brittle faults (Zwingmann et al., 2010; Viola et al., 2013; Torgersen et al., 2014). Among the many successfully dated fault, there are several fault rocks constraining the Scandinavian Caledonides formation and the later the Mesozoic evolution (Eide et al., 1997; Fossen et al., 2016; Viola et al., 2016). Structural and stratigraphic evidence together with $^{40}Ar/^{39}Ar$ cooling ages have suggested a main extensional phase of Early Devonian age connected with the late orogenic collapse of the Caledonides (e.g. Fossen, 2000). However, no absolute deformation ages have been obtained yet that can be directly linked to that early Devonian extensional event. To try to fill this gap, we have studied in detail the HFZ, which, on the basis of its structural characteristics, seems to be a possible late Caledonian extensional fault. Sampling for gouge dating was thus carried out from the HFZ USS in Sokndal (Fig. 4-46). In addition to the HFZ, two other samples were dated in the area, GVI_14 from the Jøssingfjord Pass Fault and OFR_3 from Dydland quarry (Fig. 4-46).

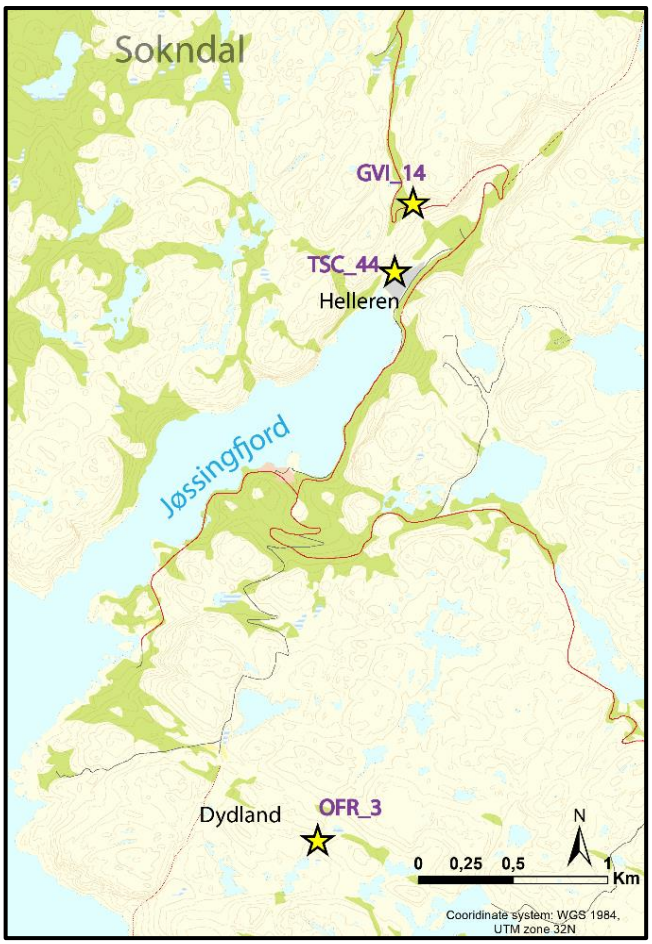

Fig. 4-46: Location of the three gouge samples collected in the field area and later dated with the K/Ar-method

The three field locations for these samples are described in the previous chapters, whereas the XRD-data constraining their mineralogical composition are presented in Table 4-3. It is important to characterize the mineral phases to interpret the K-Ar- ages correctly. This is because we need to identify and possibly quantify the K-bearing minerals and how they are present in the various grain sizes, potentially affecting the obtained age. The HFZ (TSC_44) consists primarily of interstratified illite/smectite, illite/mica and chlorite, but also some feldspars, laumonite and trace of hematite and quartz. XRD-data from sample GVI_14 are poor,

but illite/mica is the K-bearing phase and dioctahedral smectite, stilbite and laumonite also occur. OFR_3 differs from the other samples by a higher content of kaolin and dioctahedral smectite, but has less albite/anorthite and illite/mica. The coarsest fraction contains some calcite as well.

A total of thirteen ages were obtained from the three analyzed samples (Table 4-4) from grain size fractions between <0.1 and 6-10 μm. Ages vary from 532.6 ± 10.7 Ma to 170.58 ± 5.86 Ma (Table 2 and Fig. 4-47). The three samples have a grain size- dependent age, wherein the greater the grain size, the older the age. This relationship and its physical meaning have been recently discussed in detail by, for example, Torgersen et al. (2014), Torgesen et al. (2015) and Viola et al. (2016). The K content varies among the three samples and the HFZ sample has a generally higher K content (2.54% to 2,27%) while K is significantly lower for GVI_14 and OFR_3 (0.594% to 0.195%). This correlates with the amount of K-bearing mineral phases identified by XRD in the samples. Radiogenic ^{40}Ar content ranges from 99.1% to 46.2% , which resulted in reliable age determinations.

The results from the three faults in this thesis are shown and interpreted in Fig. 4-47 in an age versus grain size spectra. These fault ages spread from the Cambrian to the Mesozoic. From these data, four periods of deformational or thermal events have been identified. (1) Thermal anomaly in the Cambrian (~533 Ma) related to the pre- collisional phase of the Caledonian orogeny or it could be a mixed age. (2) Growth of authigenic illite during the extensional phase of Caledonian Orogeny (~403Ma) (3) New period of activity during the Carboniferous (~354-310 Ma) and (4) period of renewed faulting in the Late Triassic/Early Jurassic ((225 Ma) 170-180Ma).

Table 4-3: XRD-data from the three dated samples

Sample ID	Fraction [µm]	Quartz	K-feldspar	Albite/Anorthite	Illite/Mica 2M1	Chlorite	Kaolin	Dioctahedral smectite	Interstratified illite/smectite	Hematite	Stilbite	Laumontite	Calsite
TSC_44	< 0.1	Not avalible											
	0.4-0.1				36	21			41			2	
	2-0.4		4	4	13	24			53	trace		2	
	6-2	1	6	5	11	22			49	1		5	
GVI_14	< 0.1	Not avalible											
	0.4-0.1				xx			xx			xx	xx	
	2-0.4				11			46			29	14	
	6-2				19			29			39	13	
OFR_3	< 0.1						9	91					
	0.4-0.1			2	5		28	65					
	2-0.4			6	3		25	66					
	6-2			9	3		21	62					5

Table 4-4: K/Ar results.

Sample ID	Fraction [µm]	K [%]	Rad. 40Ar [mol/g]	Rad. 40Ar [%]	Age* [Ma]	Error [Ma]
TSC_44	<0.1	2,47	1,936E-09	92,2	403,2	10,1
	<0.4	2,54	2,316E-09	96,0	461,3	9,3
	<2	2,31	2,298E-09	97,5	498,0	10,2
	2-6	2,27	2,439E-09	99,1	532,6	10,7
GVI_14	<0.1	0,195	6,578E-11	46,2	184,7	17,6
	<0.1	0,195	8,122E-11	57,1	225,4	8,0
	<0.4	0,232	1,364E-10	75,4	310,7	7,0
	<2	0,268	1,729E-10	80,9	338,2	7,3
	2-6	0,253	1,520E-10	79,3	316,7	6,9
OFR_3	<0.1	0,204	6,330E-11	65,72	170,58	5,86
	<0.4	0,434	1,908E-10	77,53	237,22	7,98
	<2	0,594	3,548E-10	90,72	315,16	6,64
	2-6	0,558	3,789E-10	95,21	354,29	7,26

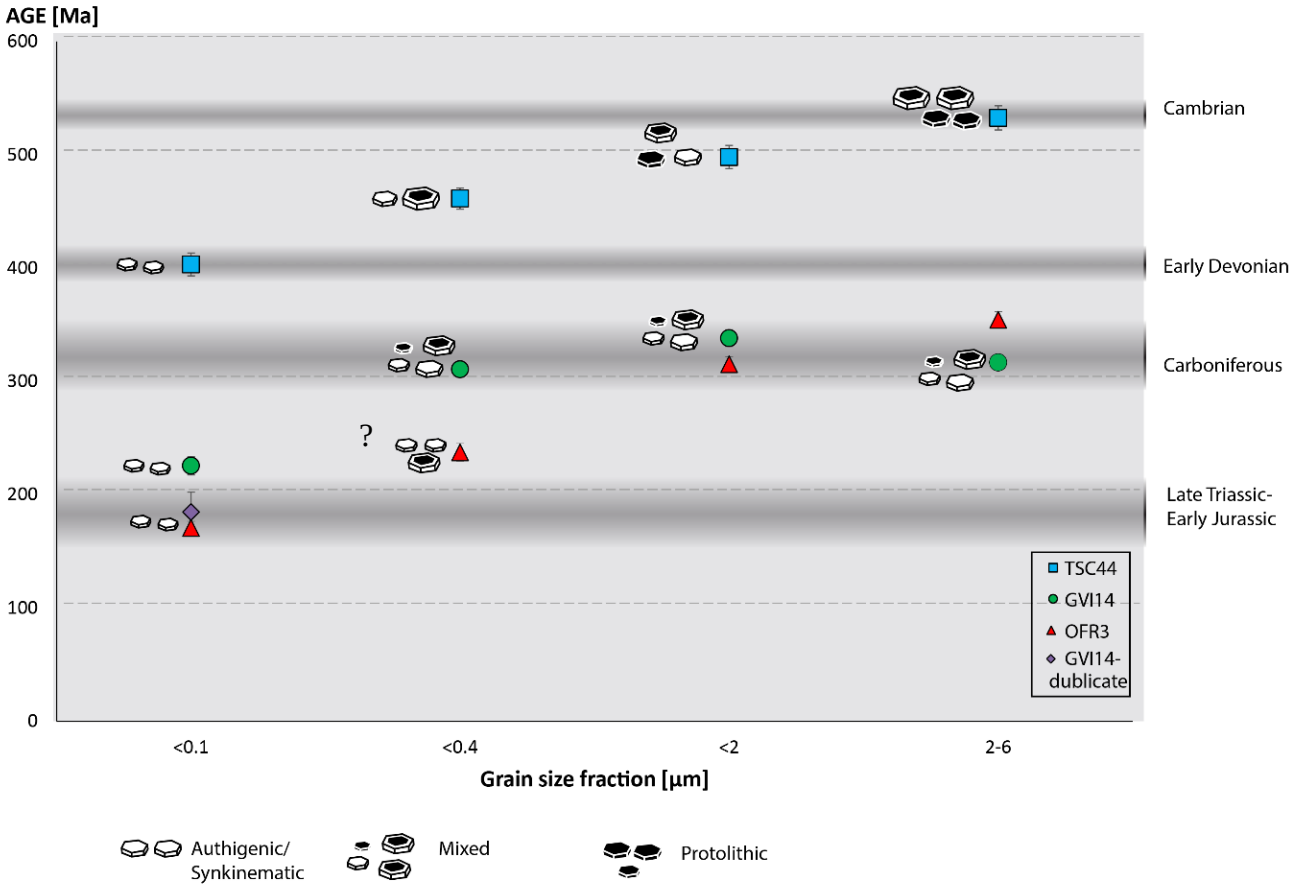

Fig. 4-47: Age versus grain size spectra. The gray horizontal bars define periods with anomalous thermal conditions, faulting or alteration episodes. The Cambrian event is interpreted to represent low greenschist facies conditions due to the Caledonian influence in the area. During the Early Devonian, reactivation occurred as a consequence of post-collisional extension of the Caledonian orogen. In the Carboniferous faulting activated GVI14 and OFR3 in the waning stage of the extensional Caledonian phase. The youngest dated ages in the three samples attest to continuation of the North Sea rifting , as reported from the Egersund Basin (Tvedt et al., 2013).

4.5 Palaeostress analysis

In highly faulted and fractured rocks, such as Åna-Sira anorthosite, it is necessary to identify fault subsets according to their mechanical characteristics. These subsets are associated with different stress tensors that reveal different stress fields through time. To separate these fault sets, field structural observations, kinematic data, mineralization and chronology is used to constrained reliable datasets.

The field observations presented above are assembled in this chapter and subdivided into different fracture sets based on geometric and kinematic criteria (Fig. 4-48.) Unfortunately, due to few complete fault-slip data that could be measured in the field, results from the palaeostress

analysis are generally poor, but are nonetheless considered as an additional tool to unravel the complex brittle history in the area.

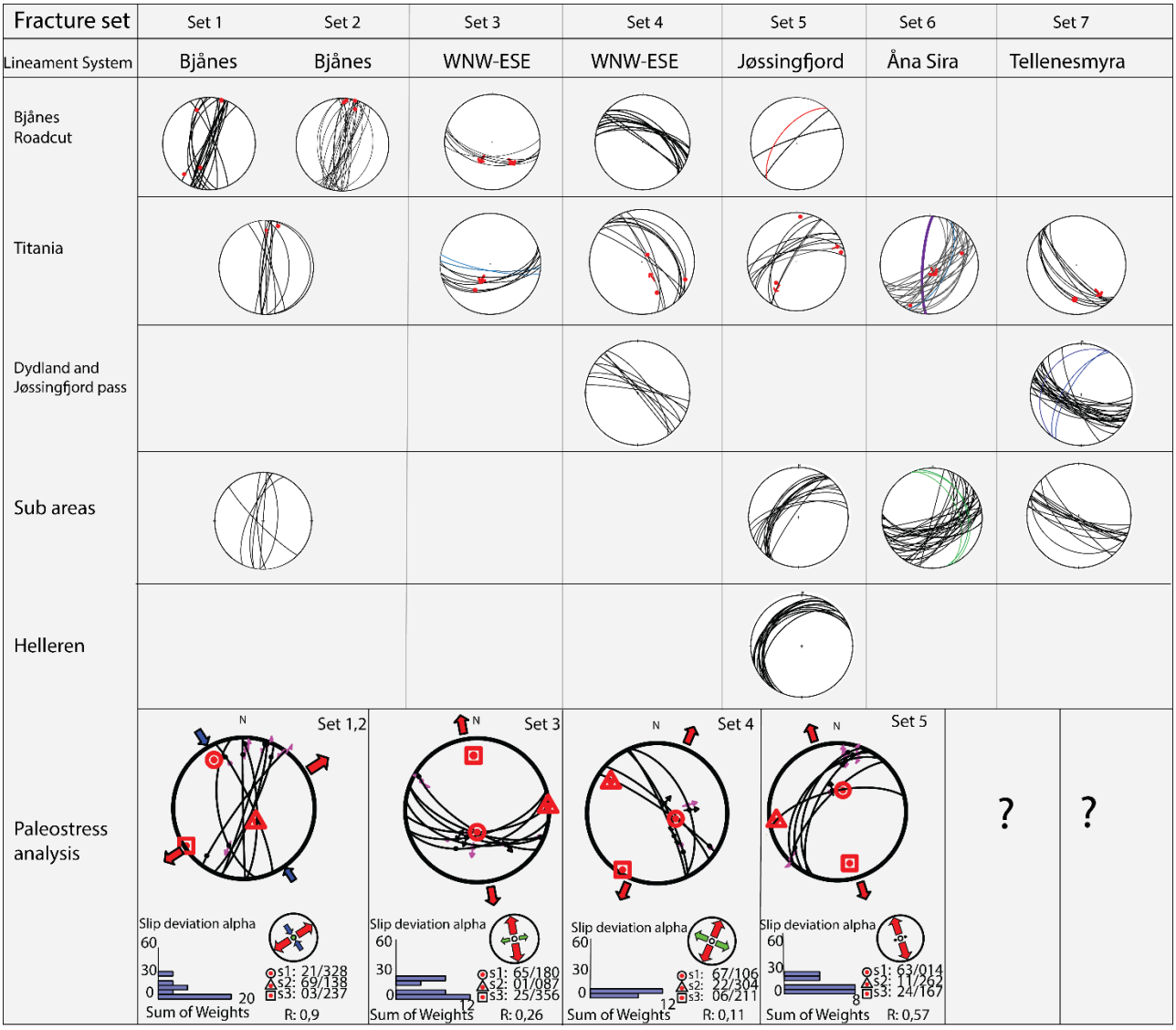

Fig. 4-48: Structural observations suggest seven distinct events of brittle deformation, each corresponding to a different paleostress field. Inversion of fault-slip data with the WinTensor software (Delvaux and Sperner, 2003) has permitted the reconstruction of four reduced tensors derived from fracture sets 1 & 2, 3, 4 and 5. The stress ratio, R, varies from 0,11 to 0,9 corresponding to a transtensive stress regime for all the calculated stress tensors.

Set 1 Set 2 The key/type locality for fractures assigned to set 1 and set 2 is the Bjånes roadcut. Those faults have a subvertical dip and a N-S strike, are dominantly brittle and are characterized by high fracture density, by zones with gouge typically defining the borders of the deformation zone and a core containing fragments of crushed and brecciated host rock. Secondary minerals such as Ep-Chl-Hem are common and are located within the damage zone or along thin, striated

fault planes. In addition, ductile deformation structures are revealed in some of the faults (Section 4.2.1.1, 4.2.1.3 & 4.2.1.4), suggesting multiple deformation episodes and brittle localization along earlier ductile precursors. The reduced palaeostress tensor indicates a transpressional stress regime oriented NW-SE. The many fractures of set 1 and 2 that lack striations and thus do not permit a full inversion procedure, are nonetheless geometrically compatible with this solution. Possible age on the last deformation phase in this set could be the transtensive extension during the Cretaceous as these structures cut E-W trending structures.

Set 3 Set 3 contains E-W trending structures with a moderate to high dip (40°-80°). Crosscutting relationships suggest that they are cut by set 1 and 2 (Section 4.2.1.6 and 4.2.1.7: Bjånes zone 6 and zone 7). Geometrically the Egersund Dike Swarm can be assigned to this WNW-ESE trending set. The reduced palaeostress tensor indicates an NNW-SSE extensional regime. Data from Montalbano et al. (2016) suggest a sinistral oblique extension and a NNE-SSW transtenional stress field for the emplacement of the Egersund Dike Swarm and, based on the fact that Montalbano and coauthors used a much larger dataset, it is therefore likely that their solution is more appropriate for this fracture set.

Set 4. Set 4 strikes WNW-ESE with a steep to moderate dip towards NE. Set 4 is characterized by discrete fractures but lacks major fault zones. Only a handful of striated fault planes was available for the inversion procedure, which yielded c. NE-SW extension with a low stress ratio.

Set 5 dips moderately towards NW. Its fault zones are very distinct and contain gouge and cataclasites; the Helleren Fault Zone belongs to this set and is used as key locality. Overall NW-SE extension is constrained by the inversion. Along the Bjånes road cut, E-W striking structures cut the NW dipping structures of Set 5. These structures are well developed near the coast.

Set 6. Set 6 is related to the pervasive Åna-Sira lineament system and the major Tellenesvatn lineament. These are very distinct in the Titania A/S open pit. Not enough fault-slip data were measured to invert a reduced stress tensor.

Set 7. Set 7 strikes NW-SE with a steep to moderate dip towards SW. Its structures are related to Tellenesmyra Lineament System and its major fault zones in the area such as the Tørkeanlegget Fault Zone, the Jøssingfjord Pass Fault and the Dydland gully (Section 4.2.2.5, 4.2.3 & 4.2.4). Faults in this set are characterized as brittle faults with multiple deformation episodes containing gouge and cataclastic-brecciated rock. No inversion could be attempted.

5 Discussion

This section discusses the complex structural evolution of the Åna-Sira anorthosite by assembling the results obtained from the multiscalar approach discussed above, by then elaborating on the implications of the structural evolution of the HFZ and, finally, by creating a conceptual evolutionary model of the tectonic and structural evolution of the anorthosite body and SW Norway.

5.1 Lineament mapping

The goal of utilizing manual lineament mapping of the bedrock through remote sensing was to identify the main lineament trends in the highly fractured anorthosite. There are several pitfalls when using this method as the number, orientation and length of the mapped lineaments will vary significantly as a function of numerous boundary conditions of the "picking exercise", making the reproducibility of the output generally poor (Scheiber et al., 2015). However, for the purpose of this study, the obtained data are helpful indicators to understand the brittle deformational history and possible correlations with other regional studies. In addition, the lineament maps were useful to correlate the spatially limited field observations to the greater picture.

The number of mapped lineaments varies with the scale of the image used for the remote sensing interpretation. The smaller the scale, obviously, the more lineaments are mapped. The bigger the scale, the higher the number of large regional structures. Large-scale lineaments may also be large-scale faults with high strain localization controlling the deformation of the rock at a greater scale than smaller structures.

Some of the lineament systems constrained by remote sensing are locally more pervasive than others. For example, the Åna Sira and Jøssingfjord lineament systems are most distinct close to the coast. This is also documented by field observations near the coast that reveal a majority of structural trends parallel to Jøssingfjord and Åna Sira lineament system. These two lineament systems are continuing off-shore and will be discussed Chapter 5.5.

When looking at the rose diagrams obtained from regional lineament mapping (Ch. 4.1), some trends are more commonly distinguished than others, such as lineament trends N-S (Bjånes LS) and NE-SW (Jøssingfjord LS or Åna-Sira LS). Karlsen (1997), who did a similar lineament mapping exercise in the Åna-Sira anorthosite but on aerial photographs, revealed these two trends as two of the most pervasive lineament sets of the area, although he did not consider the influence of scale and illumination azimuth. A regional lineament mapping in

southwestern Norway (Gabrielsen et al., 2002) correlates subordinate NE-SW trending structures with large scale faults such as the Hardangerfjord Shear Zone and Møre-Trøndelag Fault Complex (Fig. 2-3), initiated during the Caledonian extensional phase and reactivated several times during the Mesozoic. The Jøssingfjord and Åna Sira lineament systems might therefore be correlated with paroxysms of the Caledonian tectonism, as they share the same lineament trend and are more frequently observed close to coast. However, the Åna Sira system indicates an offset of some of the dikes that intruded together with the Fe-Ti deposits, suggesting that the Åna-Sira system was active much earlier than the Jøssingfjord system. The Egersund Dike Swarm cuts through these features and is not affected by the deformation of the two lineament systems (Fig. 4-4 and Fig. 4-8).

When considering the prominent N-S trending lineaments that characterize the region, it is worth noting that they are commonly recognized on the Norwegian mainland and on the continental shelf, with the highest density in the Oslo-Trondheim, Bergen and Finnmark region (Gabrielsen et al., 2002), with the Bergen area as the most relevant area for this study. Here, N-S lineaments parallel to the western coast of South Norway incorporate a system of faults (Braathen, 1999) as well as intrusion of dikes of Permo-Triassic age (Fossen and Dunlap, 1999). Major off-shore faults with this structural trend, such as the Øygarden Fault Complex, reflect the presence of deep, basement-involved precursor faults nucleated during the Permo-Triassic and multiply reactivated during the Mesozoic (Fossen et al., 2016). Some of the strands of the Øygarden Fault Complex offset Tertiary sequences (Gabrielsen et al., 2002). These rifting events have possibly also affected the Åna-Sira anorthosite. The distinct N-S pattern in the rose diagrams together with field observation reveal large brittle fault zones suggesting nucleation in relation to Permo-Triassic rifting, but also later reactivations.

The Crusher, Tellenesmyra and the WNW-ESE lineament systems are very similar and not easy to divide exclusively based on field evidence. The Egersund Dike Swarm (EDS) is used to separate the WNW-ESE system from the Tellenesmyra and Crusher lineament systems. The EDS is an important marker for tectonic activity in the area, regarded as a crucial time marker connected to the opening of Iapetus Ocean (Montalbano et al., 2016). The fracture rose diagrams, especially in the case of the ÅS, show a lineament frequency peak oriented WNW-ESE, which might be related to this Precambrian event. WNW-ESE oriented lineaments seen in the Fennoscandian basement farther east are likely to be of Precambrian origin as well (Gabrielsen et al., 2002). The Tellenesmyra and Crusher lineament systems are well developed close to Tellenes Ore deposit, suggesting a relationship to the intrusion of the mineralized

norites and the Tellenes Fe-Ti deposit (Schärer et al., 1996). Possible later reactivation during the Mesozoic is discussed farther down.

5.2 Geochronology – the origin of illite in the dated gouges

The dynamic life of faults may express multiple periods of tectonic activity, each reflecting different processes such as friction, fluid flow and rheological changes causing spatial and temporal changes in the fault architecture, especially in old terrains. This results in a complex history of structural domains whose texture, composition, physical and isotropic characteristics reveal different stages of the faults history. The temporal dimension of a multiply reactivated fault can therefore be overlooked because it is hidden behind the varied structural feature that reflect this complexity. By utilizing K-Ar ages from authigenic and synkinematic illite separated from brittle fault rocks, brittle faults can be accurately dated and can thus become useful time markers to unravel long and complex brittle deformation histories (Viola et al., 2016).

An interesting issue when dating faults with the K-Ar method is what the ages of the different grain size fractions actually mean. The origin of the dated K-bearing minerals that are found in each of the size fractions is essential to answer this question. Zwingmann et al. (2010), Torgersen et al. (2014) and Viola et al. (2016) studied this issue in detail and established a conceptual model accounting for the observed relationship between grain size and K/Ar age. Deformation along the fault generates growth of new, fine authigenic illite grains that will mix with protolithic illite/muscovite that contains a different radiogenic Ar signature than the authigenic grains (Eide et al., 1997; Viola et al., 2013; Torgersen et al., 2014; Viola et al., 2016). If protolithic illite/muscovite is absent within a fault, all the grain size fractions will yield the same age, representing one single deformation phase where older phases are overprinted or never existed. However, this is rarely the case (especially in old faults), and protolithic illite/muscovite and authigenic illite grains are often mixed together thus generating mixed ages. The recent conceptual understanding of the relationships between grain size and K-Ar ages, especially why the age decreases with decreasing grain-size, suggests that the K-Ar ages of the <0.1μm (finest) illite fraction date the latest episode of deformation recorded by the fault rock through growth of synkinematic and authigenic illite during faulting. The intermediate grainsizes are interpreted as reflecting a mixed assemblage of authigenic synkinematic illite and protolithic illite/muscovite. The coarsest fraction is instead generally interpreted as a protolithic component, i.e. an inherited input to the fault rock derived from the host rock. The radiogenic Argon signature of the dated fraction changes therefore because of contamination of K-bearing

mineral phases derived from mineral components which did not crystallize during faulting. Careful analysis is therefore necessary to correctly identify the source of the radiogenic Ar in the dated fraction.

The Helleren Fault Zone (HFZ), dated by sample TSC44, stands out with the oldest age for all dated fractions (Fig. 4-47). This means that the coarsest grain size in GVI14 and OFR3 are likely not protolithic (that is, inherited from the host rock, because they would otherwise have the same Cambrian age), but represent a later episode of deformation or a mixed age. The coarsest grain size for TSC44 could be a cooling age connected to the shallow emplacement of the anorthosite. Previous isotropic studies (Summerized in Boven et al., 2001; Vander Auwera et al., 2011) in the area suggest, however, that the Cambrian event (Fig. 4-47) might be due to Caledonian metamorphism. From the coarsest grain size to the finest, the ages decrease progressively defining an inclined age spectra and are therefore considered as mixed ages reflecting authigenic growth of younger illite on older protolithic nuclei and those ages are this devoid of any geological meaning. The finest fraction (<0.1μm) is a groundbreaking result as the dated authigenic and synkinematic illite represents the latest deformation phase of the Helleren Fault Zone and is the only late Caledonian age to date that constrains directly the collapse of the orogen. According to Fossen (2000), the onset of the post-orogenic extensional phase started at c. 405 Ma, as indicated by amphibole Ar^{40}/Ar^{39} cooling ages.

GVI14 and OFR3 share the same horizontal age-distribution pattern, with one significant offset only for the intermediate fraction (<2μm) (Fig. 4-47). If these faults are related to the same deformation event, the variations in intermediate ages might be due to mixing of multiple populations of illite/mica. This means that the intermediate fractions might contain some older population of illite, which produces an age older than the real deformation age of OFR3. If that is the case, hydrothermal activity might have partly reset the isotropic system, as possibly indicated by the high kaolin content in the sample (see XRD-data table 4-2), which reflects deep alteration. However, if they are truly independent, it means that we have two deformation events in a short period of time during the Carboniferous (~ 354-310 Ma). Carboniferous illite ages have also been reported from the Bergen area, representing continued brittle deformation during the waning stages of Caledonian Orogeny (Table 5-1) (Viola et al., 2016; Ksienzyk et al., 2016). Furthermore, a rapid age change happens for fraction <0.4 μm to <0.1 μm, indicating a new formation of authigenic illite during the Early-Middle Jurassic (170-180 Ma) interpreted to represent the continued rifting following the Permo-Triassic North Sea rifting (Fossen and Dunlap, 1999), seen in the Egersund Basin and in the Bergen area (Tvedt

et al., 2013; Ksienzyk et al., 2016). The structural background of the samples is also important when comparing these two samples. GVI14 is from the Jøssingfjord Pass Fault and is comprised of a gouge-rich zone from within a highly-fractured fault core with a sharp contact to the anorthosite. OFR3 is from the Dydland gully, which is an earlier kaolin-mine much more affected by alteration with an ambiguous contact to the host rock. These differences in structural characteristics can influence the relative small variations between the two data sets.

Table 5-1: Data from dating of Fault Rocks from Southwestern Norway (K/Ar)

Locality	Source	Orientation	Age (Ma)
Nordfjord Sogn Detachment	Eide et al. (1997)	NE-SW	260 144
Bergen-Rolvsnes Granodiorite	Scheiber et al. (2016) (Ar/Ar)	WNW-ESE Top-to-NNW thrust	450
Bergen-Rolvsnes Granodiorite-Goddo fault	Viola et al. (2016)	NNW-SSE dipping c. 45 E	260 200 125
Bergen	Ksienzyk et al. (2016)		>340 305-270 215-180 120-110
Åna-Sira Anorthosite	This study	NE-SW, dips 30-40° to NW NW-SE dipping 70 SW	403 184 170

5.3 Helleren Fault Zone (HFZ)

Helleren represents one of the most significant structures in the Åna-Sira Anortosite massif and is therefore a very important feature to consider when trying to unravel the brittle evolution of the area. The detailed analysis done in Chapter 4.3 has revealed multiple episodes of deformation, starting with brittle precursors controlling subsequent ductile deformation, which, in turn, was itself later reactivated in the brittle regime. This study constrains a temporal evolution of the complex, multiply-reactivated brittle-ductile Helleren Fault Zone by a detailed fault architectural analysis and K-Ar dating of synkinematic illite.

The occurrence of initial brittle structures (veins and joints) playing a key role for nucleation and localization of ductile shear zones is recognized in coarse-grained rocks in other areas, including, the Italian Alps (Guermani and Pennacchioni, 1998), Sierra Nevada, California and Northern Spain (Segall and Simpson, 1986). The role played by brittle precursors in controlling subsequent ductile deformation is not fully understood, partly because brittle deformation is

likely erased by ductile overprint and partly because they often are overlooked. However, this approach is relevant to fully understand the nucleation of faulting. Guermani and Pennacchioni (1998) studied the Mont Blanc granite in the Alps aiming to understand such brittle-to-ductile deformation history. They defined a sequence of events starting with formation of (1) joints and veins followed by (2) cataclasites and (3) mylonites and foliated granites. The brittle precursor had a strong influence on the way ductile deformation zone nucleated and further localized. They recognized five structural features that documented such sequence of events; (1) strong localization of ductile deformation; (2) high lateral continuity of mylonitic horizons; (3) sharply bounded discontinuous ductile shear zones; (4) high intersection between mylonites; and (5) mylonites with cataclastic lenses and not vice versa. The preservation of all these features and the exact same sequence is not the case for HFZ. However, some of these features can be recognized and may record the existence of a precursor brittle episode.

Brittle cooling joints/veins

The Åna-Sira Anorthosite locally shows coexisting brittle and plastic structures. Their coexistence, however, is not resulting from the classic superposition of brittle on ductile during exhumation to the surface. The carefully studied HFZ is characterized by both brittle and ductile deformation in a totally intra-anorthositic shear zone. The earliest tectonic structures are suggested to be joints and veins formed due to the rapid cooling of the magma (Boven et al., 2001). In the HFZ, some of these veins steered the development of the protomylonitic foliation that formed during the nucleation of the ductile HFZ, a ductile top-to-the SE thrust. Viscous localization during thrusting exploited zones of severe grain size reduction in the anorthosite due by the sericitization that was caused by metasomatism linked to fluid flow along the early cooling joints and fractures (Fig. 4-40c & d). Thin section analysis shows how veins diffuse into subordinate veins which make it possible for later viscous deformation to affect not only one vein plane but a larger volume of metasomatized anorthosite (Fig. 4-42D). The structural analysis has shown that some of the veins were folded and rotated by a younger episode of diffuse viscous deformation (Fig. 4-45) confirming that brittle veins predate the ductile deformation phase of HFZ. These brittle structures thus weakened the anorthosite by grain size reduction by frictional deformation, fluid infiltration and metasomatism and acted as effective precursors to the localization of the later viscous deformation.

Viscous fabric exploiting cooling joints- Thrusting top-to-SE

Later viscous deformation exploited the cooling joints. A transition from brittle to viscous behavior in rocks requires an increase in temperature, confining pressure and/or water content or a decrease of the strain rate. The inherited zones of brittle structures derived from the pluton cooling provided rheological discontinuities in the anorthosite and viscous deformation focused along these weaker zones without affecting the surrounding anorthosite. For the HFZ this model is supported by (1) the fact that viscous deformation is localized along fractures and joints that are parallel to the present HFZ and that were optimally oriented during the viscous deformation phase but are instead absent in the surrounding anorthosite and (2) by the documented grain size reduction by metasomatism and sericitization along the cooling joints investigated in the thin sections that shows that the earlier brittle features are oriented parallel to the foliation (AFE_16 & AFE_24, Fig. 4-41). This is interpreted to be related to the early subduction and accretion in the Caledonides that affected region c. 460-445 Ma ago (Roberts, 2003; Scheiber et al., 2016), as indicated by regional metamorphism considerations (Boven et al., 2001).

Folding

Folding of the HFZ is recognized by the rotation of the foliation and the veins that express an open upright fold with a fold axis plunging towards NW (Fig. 4-38). The foliation changes its planar attitude in response to the overall pinch and swell structure of the outcrop representing a fold. This is known from field observation and rotation of veins seen in thin section analysis (Fig. 4-38, Fig. 4-45). Folding is hypothetically assigned to shortening of Caledonian age.

Brittle reactivation, extensional normal faulting top-to-NW

The fault that was later cut by a brittle extensional phase producing a planar upper slip surface (USS) characterized by a c. 5 cm thick zone with gouge dated by the K-Ar - method to 403 ± 10 Ma. This latest NW-SE brittle extensional phase is supported by regional stress inversion and a number of brittle kinematic indicators at the outcrop. Studies in the Caledonian orogen (Fossen, 2000) have dated the onset of the extensional history related to the orogeny collapse indeed to c. 405 Ma, which correlates good with our data.

This proposed model of Helleren Fault Zone (Fig. 5-1) reveals in summary evidence of a set of precursor brittle structures that localized later viscous top-to-SE thrusting before the fault was again reactivated in a full brittle fashion with top-to-NW extensional kinematics during the collapse of the Caledonian orogen.

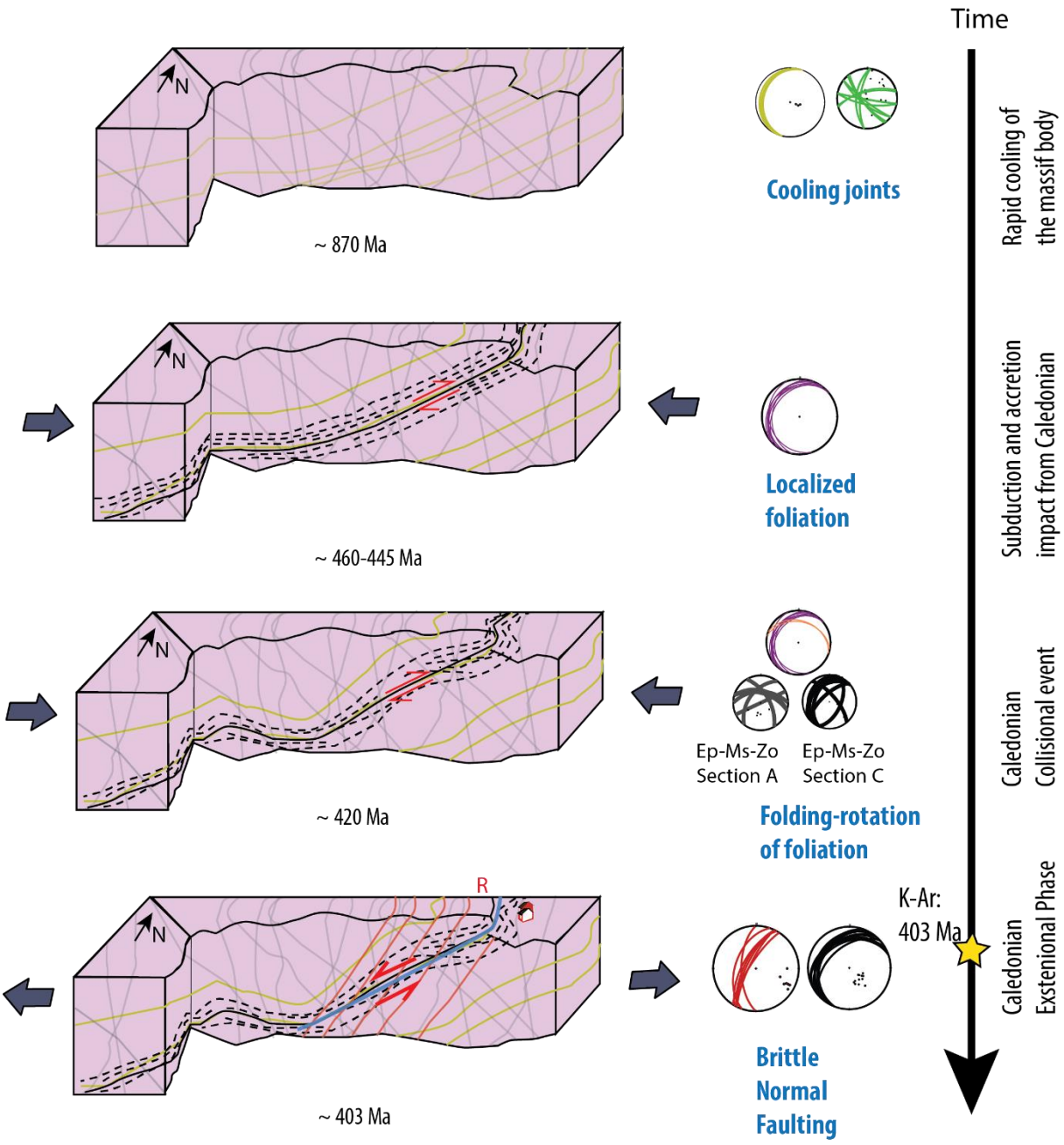

Fig. 5-1: Conceptual evolution scheme of the Helleren Fault Zone. The four indicated stages are proposed based on field observations, thin section analysis and radiogenic dating. Further description of the stages is described in the text. It is important to note that a brittle precursor, genetically linked to the cooling of the anorthosite, is envisaged to the subsequent localization of viscous deformation. –the kinematics of the fault is complex: it nucleated as a top-to-the SE ductile thrust, which exploited earlier brittle fractures to localize, followed by a fully brittle top-to-the NW extensional reactivation. Whereas the age of the ductile phase is only speculatively assigned to the early Caledonian compressional phases, the age of the brittle extensional reactivation is constrained by K-Ar dating of synkinematic illite separated from a fault gouge related to the extensional phase.

Other major NE-SW trending fault zones outside study area

Many major structures that are related to the same period of the extensional phase of the HFZ, share the same spatial orientation of the HFZ. The Hardangerfjord Shear Zone (Fossen and Hurich, 2005), the Nordfjord Sogn Detachment (Smethurst, 2000), the Møre-Trøndelag Fault Zone (Fossen, 1992) are among them. Unlike the HFZ, though, these deformation zones are all described as ductile shear zones during the extensional phase and not as brittle faults. This difference might be due to the geographic location of HFZ, which remained in a marginal and far position to the active orogen, and thus did not experience the deformational event to same extent as the other fault zones. The Lærdal-Gjende Fault Zone farther inland is described as the brittle extension of the Hardangerfjord Shear zone (Larsen et al., 2003), indicating a change from ductile to brittle deformation conditions. Other sets of NE-SW trending faults are also recognized in Northern Norway related to Caledonian activity (Gabrielsen et al., 2002) and some to the Proterozoic basement evolution.

5.4 Brittle evolution of southern Norway

In this section results from structural analysis in the Bergen area and from the North Sea are charted together and discussed considering structure observation in the Åna-Sira Anorthosite. Similar spatial trend does not necessary imply that these structures have a common age and origin. However, structures deformed under same stress regime tends to behave similarly.

5.4.1 NW-SE and NE-SW trending structures (Jøssingfjord and Tellenesmyra lineament system, set 5 and set 7)

Offshore relations. Tvedt et al. (2013) studied faults off-shore in the Egersund basin (a basin initially formed in response to Carboniferous-to-Permian rifting) by 3D seismic data and fault throw analysis. They concluded that a combination of basement faulting and salt (re-)mobilization are the driving mechanisms behind fault activation and reactivation in the basin. Early Triassic rifting triggered salt layers and activated old basement faults affecting the nucleation and localization of NE-SW trending faults in the cover layers. Further, throw analysis revealed a high density of reactivated NE-SW striking normal faults in the Egersund Basin initiated during subsequent rifting in the Middle Jurassic. During this study, structures with this trend are mapped onshore, such as the Helleren Fault Zone (HFZ) and the Jøssingfjord lineament system, which are most pervasive close to the coast. The radiometric dating of the

last increments of strain of the onshore component of the HFZ yielded an age of 403± 10 Ma, which is interpreted as being related to the extensional phase of Caledonian Orogeny. These features might have initiated the nucleation and localization of younger faults offshore that were active in the early Triassic and middle Jurassic.

Sørensen et al. (1992) and Tvedt et al. (2013) reported major NW-SE-striking normal faults in the Egersund Basin also restricted to tectonic activity from the Early Triassic and Middle Jurassic periods. This can be correlated onshore to dike intrusions in the Sunnhordland region, which are dated to the Early Triassic and Middle Jurassic and have the same structural trend (NNW-SSE; (Færseth et al., 1976) of the normal faults mapped in the Egersund Basin. NW-SE trending structures in the Åna-Sira anorthosite is Tellenesmyra lineament system, the Tørkeanlegget Fault and Jøssingfjord Pass Fault. The Tørkeanlegget Fault is highly brecciated with three major zones with differently-colored gouge, whereas the Jøssingfjord Pass Fault is less brecciated and less gouge-rich but contain secondary mineral phases. The authigenic synkinematic illite from the Jøssingfjord Pass Fault yielded an age of 185 ± 18 Ma and can be correlated to the Middle Jurassic rifting phase revealed offshore. This relationship suggests active rifting onshore and offshore. In the Åna-Sira anorthosite, faults oriented NW-SE can be traced all the way back to 920 ± 3 Ma and the intrusion of the Tellenes dike containing norite and the great Fe-Ti deposit which is believed to intrude along a tectonically weak zone (Schärer et al., 1996). This suggests that the Jøssingfjord Pass Fault and Tørkeanlegget Fault were last reactivated in the Middle Jurassic, but were originally related to an earlier tectonic event, maybe as early as the intrusion of the noritic dikes, c. 920 Ma ago.

In summary, the older faults in the Åna-Sira anorthosite (initiated by norite dike intrusion and Caledonian tectonics) have affected the nucleation and localization of the younger NE-SW and NW-SE trending faults of Triassic and Jurassic age.

Caledonian relations. Not far north from the Rogaland Anorthosite Province, in the Bergen area (Fig. 2-3), outcrop rock sequences of the Caledonian nappes. Here, there are made significant discoveries of major structures oriented NE-SW controlling the postcollisional extension of the Caledonian Orogen and later extensional faulting in the Mesozoic due to a change from convergent to divergent plate motion (e.g. Fossen and Rykkelid, 1992; Eide et al., 1997; Andersen et al., 1999; Larsen et al., 2003; Gabrielsen et al., 2010; Viola et al., 2016; Scheiber et al., 2016). Among them is the brittle Lærdal-Gjende Fault System with its continuation into Hardangerfjord Shear Zone. Hardangerfjord Shear Zone (HSZ) is described as a fundamental extensional shear zone cutting through the Caledonian nappes and basement

exposing the basement-cover contact with about 4 km of displacement along the shear zone. HSZ is related to Devonian divergence between “Laurentia” and “Baltica” which resulted in stretching of the basement and major basal shear zones cutting the nappes (Fossen, 1992; Fossen and Rykkelid, 1992). Basement-involved faults initiated during the Permo-Triassic and Jurassic are recognized and interpreted in a seismic section from the North Sea across the continuation of Hardangerfjord Shear Zone (Andersen et al., 1999) which is in correlation with observations from the Egersund basin (Tvedt et al., 2013) discussed above. Further investigation by Andersen et al. (1999) of the Lærdal-Gjende Fault System (brittle continuation of HSZ) revealed different stages of reactivation (Permo-Triassic and Jurassic) affecting a much wider region in southern Norway than only in the main rift segments (North Sea and Oslo Rifts). In the Åna-Sira anorthosite, Dydland Fault and Jøssingfjord Pass Fault was active during Jurassic age emphasizing Andersen et al. (1999) model suggesting regional impact of Jurassic rifting.

As for the interest of this study, structural features in the Caledonian nappes share the same structural features as some of the structures recognized in the Åna-Sira anorthosite. The most important is the Helleren Fault Zone (HFZ) sharing the same NE-SW trend and contains both ductile and brittle deformation as seen in a greater scale in Hardangerfjord Shear Zone (Fossen and Hurich, 2005) and Lærdal-Gjende Fault System. Radiometric dating of HFZ, giving a Devonian age, confirms the extensional phase of Caledonian Orogeny also affecting the Åna-Sira anorthosite. Other major structures further north in the Caledonian nappes nucleated during the Devonian extensional phase such as Nordfjord-Sogn Detachment (Smethurst, 2000) (later reactivated in latest Permian and Latest Jurassic Early-Cretaceous; Eide et al. (1997)) and Møre-Trøndelag Fault Zone (Gabrielsen et al., 1999) sharing the same trend as HFZ. K-Ar-data from HFZ and constraints provided by regional geology emphasizes a consistent relationship between NE-SW structures in the study area and the Devonian extensional phase of Caledonian Orogeny.

5.4.2 WNW-ESE LS- Egersund Dike Swarm

The Egersund Dike Swarm have N110-120E trends with steep dip usually >70° and is an important time marker for the brittle evolution of the area due to previous studies that implies that Egersund dike swarm is a syn-rift precursor of the opening of Iapetus Ocean, an early stage of Rodinia breakup. The statement is supported by palaeostress analysis (using anisotropy of magnetic susceptibility (AMS) technique) and geochronologic (U-Pb) age of the dike intrusion (Bingen et al., 1998b; Montalbano et al., 2016). The AMS imply that the rifting occurred in a

context of oblique extension, characterized by a sinstral, strike—slip component in an overall NNE-SSW extensional regime. Geochronology gave a U-Pb intrusive age of 616 ± 3 Ma which corresponds well with the breakup of Rodinia (Li et al., 2008). WNW-ESE trending structures in the study area (such as Bjånes Fault Zone 6 and 7; Section 4.2.1.6 and 4.2.1.7) are characterized as faults with a dominant mafic component and are therefore suggested to be developed during this major event. Earlier and later phases of tectonic or magmatic activity might have activated/reactivated these structures further.

5.4.3 N-S trending structures (Bjånes lineament system)

Structures oriented N-S is recognized in several areas of Norway (Bryhni and Sturt, 1985; Gabrielsen et al., 2002). In the Southwestern Norway, these structures are well known at the continental shelf as general trends in the Sveconorwegian orogen to be N-S to NNW-SSE (Bryhni and Sturt, 1985). Studies done in the Bergen area (Braathen, 1999) show a population of N-S trending structures characterized by breccia or cataclasites with sub vertical dip. These basement related structures transect all rocks in the region, structures that led to propagation of structures into the overlying rocks (Braathen, 1999). Geochemistry done on dikes oriented N-S in the Bergen area conclude with dike ages that fall in groups of Permian (246-270Ma), Triassic (220-241 Ma) and Middle Jurassic (162-179Ma) ages (Færseth et al., 1976; Fossen and Dunlap, 1999; Valle et al., 2002). Viola et al. (2016) used K/Ar dating to reveal four phases of activation/reactivation of the NNW-SSE striking Goddo fault in the Rolfnes granodiorite close to Bergen, indicating Devonian- Early Carboniferous, Permian, Triassic-Early Jurassic and Early Cretaceous deformation. NNW-SSE and N-S trends are also associated with some of the major basins off-shore, such as Viking graben that developed during Jurassic which overprint NE-SW trending structures of Hardangerfjord Shear Zone (Smethurst, 2000; Fossen and Hurich, 2005). Just north of Bergen, off-shore, is the Øygarden Fault Zone (of Permo-Triassic origin), with master N-S faults located immediately west of the coast (in the Sunnfjord region). Bathometry of Øygarden Fault Zone indicate deep basement involved faults affecting sequences up to Tertiary time (Smethurst, 2000; Gabrielsen et al., 2002). All these structures share similar characteristics as the N-S trending structures seen in the Åna-Sira anorthosite (e.g. Bjånes road cut). It is therefore reasonable to emphasize that the dominant population of N-S structures in the Åna-Sira anorthosite have been active during some or during all of these periods. Subordinate NW-SE (Set 4 in Fig. 4-48) trending fractures are often found in relation to N-S trending structures in the study area (Bjånes roadcut) and Braathen (1999), Smethurst (2000) and Valle et al. (2002) found the same relationship in the Bergen area.

5.5 Conceptual model of the evolution of the Åna-Sira Anorthosite

In an effort to make the structural history manageable, the results from structural analysis proposed in the Bergen area and fault analysis from the North Sea (Egersund Basin) are charted together with the interpretation proposed in this MSc suggesting a possible interpretation of the brittle deformation history of the Åna-Sira anorthosite. Based on the field data it is evident that the Åna-Sira anorthosite has experienced at least eight deformation episodes. The following post-Sweconorwegian stages have been documented below and illustrated in Fig. 5-2:

(1) The rapid cooling of the 930 Ma anorthosite caused numerous cooling joints. These were later exploited by later tectonic events, such as the deformation episode that formed the Helleren Fault Zone. The c. 10 Ma younger intrusion of the mineralized norite-jotunite-quartz mangerite dike (c. 920 Ma) containing the great Fe-Ti ore deposit did most likely exploit the anisotropy in the anorthositic massif caused by the joints (Schärer et al., 1996). Fracture set 7 might still be inherited from this intrusion and evolved trough later tectonic activity. Offset/displacement of the norite-jotunite-quartz-mangerite dikes but not of the 616 Ma old Egersund Dike Swarm (Bingen et al., 1998b) by fracture set 6 (Åna-Sira lineament system) indicates that fracture set 6 formed between the intrusion of the ÅS (c. 930 Ma; Schärer et al., 1996) and the opening of Iapetus ocean (c. 615-570 Ma; Bingen et al., 1998b; Li et al., 2008; Montalbano et al., 2016) .

NE-SW oblique extension

(2) Subsequent slow cooling followed from c. 870 Ma (Bingen et al., 1998a) until the precursor stage of the opening of Iapetus ocean started with the intrusion of the Egersund dike swarm during NE-SW oblique extension at 616 Ma (Bingen et al., 1998b; Montalbano et al., 2016). Fracture set 3 and 4 might have formed during this event.

N*NW-SSE compression*

(3) The initial stages of the Caledonian Orogeny were associated with magmatic activity and subduction of oceanic crust (c.480-450; (Roberts, 2003). In the Åna-Sira anorthosite the activity farther north led to formation of foliation localized on earlier brittle features, in an overall NNW SSE compressional stress regime, as recognized in Helleren Fault Zone. A brittle precursor is thus suggested for the localization of viscous deformation in the area.

N*W-SE compression*

(4) Large lateral movements during NW-SE compression and continent-continent collision are recorded in the Precambrian basement with local thrusts, folding and the associated

metamorphism at 450-400 Ma (Bryhni and Sturt, 1985; Roberts, 2003). As for the Åna-Sira anorthosite, the Helleren Fault Zone was folded during this stage.

N*W-SE extension*

(5) Extensional collapse of the Caledonian belt associated with crustal thinning and the origin of large-scale detachment zones with top-to-NW extension affected southwestern Norway (Andersen et al., 1999; Fossen, 2000). The offshore continuation of the extensional structures had significant control on the structures and basin geometries in the North Sea (Tvedt et al., 2013). The last deformation of the Helleren Fault Zone is related to this event (403 Ma, K-Ar illite age) and fracture set 5 are interpreted as having developed during this stage.

W-E extension

(6) The Permo-Triassic rifting is well known off-shore, responsible for forming structures accommodating large amounts of petroleum. Studies off-shore indicate major normal faults inherited from deformation episode **(5)** (Tvedt et al., 2013). In addition, important faults trending N-S (fracture set 1,2) (Sørensen et al., 1992) were generated in this period. These structures are also recognized in the Bergen area, e.g. the Øygarden Fault Zone in the North Sea (Smethurst, 2000). Dyke oriented N-S are correlated to this event (Færseth et al., 1976; Fossen and Dunlap, 1999). Fracture sets 1 and 2 were therefore probably active during this stage. K-Ar ages of the coarsest illite fraction of sample GVI_14 (Jøssingfjord Pass Fault) and OFR_3 (Dydland) indicate a period of deformation at that time for fracture set 7.

NE-SW extension

(7) During the Late Triassic-Jurassic southwestern Norway underwent crustal stretching and fault reactivation was the norm. This is documented off-shore by active faults oriented NE-SW and NW-SE (Sørensen et al., 1992; Tvedt et al., 2013) and documented onshore by the direct dating of faults to this time (Eide et al., 1997; Viola et al., 2016; Ksienzyk et al., 2016). Some N-S trending dykes also emplaced during the Middle Jurassic. Dating of synkinematic illite from Jøssingfjord Pass Fault and Dydland gully yielded ages of Middle Jurassic age and were therefore active during the crustal stretching during the Late Triassic-Jurassic. Fracture Set 3, 4, and 7 are therefore believed to have been active during this period.

WNW-ESE extension

(8) Crustal extension attained its climax at the transition from the Jurassic to the Cretaceous before fast sediment infill of the basins and transgression covered southwest Norway. However, faulting in the early Cretaceous is documented in the Bergen area (Viola et al., 2016; Ksienzyk

et al., 2016) and therefore fracture sets 1 and 2 in the Åna-Sira anorthosite might also have been active at this time. These N-S structures cut across E-W structures observed at Bjånes roadcut, suggest a young reactivation of N-S structures.

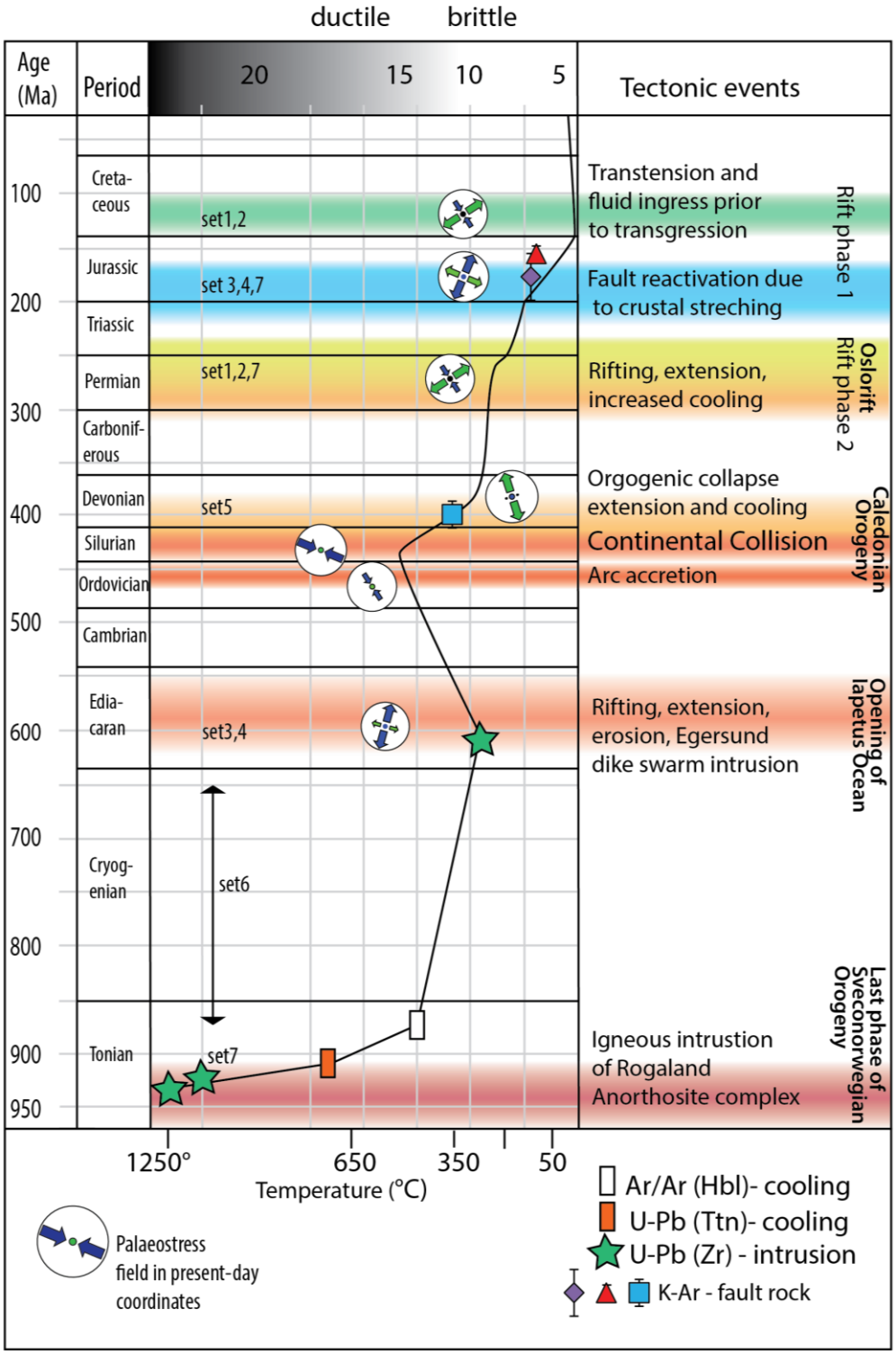

Fig. 5-2: Time-constrained structural evolutionary model of the Åna-Sira anorthosite spanning between the Neoproterozoic and the Cretaceous.

6 Conclusions

This thesis present results from remote sensing analysis, field mapping, microstructural analysis and radiometric dating (K-Ar of synkinematic illite) of the Åna-Sira anorthosite massif. The massif is part of the Rogaland Anortosite Province that intruded during the final stage of Sveconorwegian orogeny 930 Ma ago and has undergone several deformation phases after intrusion generating a highly fractured and faulted basement.

The structural evolution of the Åna-Sira anorthosite is followed by these phases:

1. Early Neoproterozoic – Rapid cooling of the anorthosite caused cooling joints, followed by a Fe-Ti- noritic intrusion. Initiation of fracture set 7.
2. Middle Neoproterozoic – Activation of fracture set 6, proved by displacement of ÅS (930 Ma) and not Egersund Dike Swarm (616 Ma).
3. Late Neoproterozoic – Activation fracture set 3, 4 and intrusion of Egersund dike swarm.
4. Cambrian/Ordovician – Increasing temperature due to Caledonian compressional activity. Foliation localized at Helleren Fault Zone
5. Silurian – Local folding due to Caledonian continent-continent collision
6. Devonian – Activation fracture set 5 caused by collapse of Caledonian Orogeny
7. Permo-Triassic – Active fracture set 1,2,7 due to extensional rifting.
8. Triassic-Jurassic – Active fracture set 3, 4, 7 and active rifting in the North Sea
9. Cretaceous - Waning of extensional rifting, but some activity in fracture set 1 and 2.

K/Ar dating made it possible to get strong temporal control of three faults in the study area, constraining deformation events related to Devonian (C. 403 Ma; Helleren Fault Zone) and Jurassic time (c. 170-180 Ma; Dydland and Jøssingfjord Pass Fault). Helleren Fault Zone stand out as an important structure regarding the evolution of the area and detailed mapping of the three sections A, B and C of Helleren Fault Zone led to a structural history of the fault, which can be divided into four phases:

- A brittle precursor, genetically linked to the cooling of the anorthosite in the Neoproterozoic, is envisaged to the subsequent localization of viscous deformation.
- Top-to-the-SE ductile thrusting, generating localized foliation following already established joints/ veins, during the initial compressional stage of Caledonian orogeny in Cambrian.

- Folding occurred as a consequence of continent-continent collision of Caledonian Orogeny.
- Fully brittle top-to-the NW extensional reactivation of HFZ along USS. The age of the brittle extensional reactivation is constrained by K-Ar dating of synkinematic illite to 403 Ma and the extensional phase of Caledonian orogeny.

Structural evidence for these four phases are:

- Veins parallel to foliation and a precursor for the foliation. Observed in field and in the microscope.
- Folded foliation.
- Microstructural observation of veins; Veins as a precursor to metasomatism and important contributors to alteration and mechanical weakening of the rock.
  Reactions causing alteration of the anorthosite:
  - Saussuritization
  - Sericitization
  - Chloritization
- Riedel fractures, striations, cataclasite and gouge are caused by brittle normal faulting.

This study show that multiscalar investigation of highly fractured and faulted crystalline rocks allow recognition of several deformation episodes.

7 Perspectives

- Further understanding of the development of brittle fractures and veins as a precursor for further deformation of the anorthosite and HFZ. Available geochemistry of chlorite from four of the thin section across HFZ would be of interest.
- Further microstructural analysis of the thin section from Bjånes roadcut could improve the understanding of the mechanisms between ductile and brittle deformation in the area.
- In order to improve the model of structural evolution of the anorthosite more specific field work will be necessary. By direct radiometric dating of faults within each fracture sets a better model may be constrained. Typical good fault rocks for dating would be Tørkeanlegget Fault Zone, Bjånes roadcut and Titania Fault Zone 1 or 2 as they possibly represent long lived faults reactivated several of times.
- Improvement of the palaeostress analysis would strengthen the model further.

References

Andersen, T. B., Torsvik, T. H., Eide, E. A., Osmundsen, P. T. & Faleide, J. I. 1999. Permian and Mesozoic extensional faulting within the Caledonides of central south Norway. *Journal of the Geological Society,* 156**,** 1073-1080.

Angelier, J. 1994. Fault slip analysis and paleostress reconstruction. *In:* HANCOOK, P. (ed.) *Continental deformation.* University of Bristol, UK: Pergamon Press 101-120.

Awdal, A., Braathen, A., Wennberg, O. & Sherwani, G. 2013. The characteristics of fracture networks in the Shiranish Formation of the Bina Bawi Anticline; comparison with the taq taq Field, Zagros, Kurdistan, nE Iraq. *Petroleum Geoscience,* 19**,** 139-155.

Barnichon, J.-D., Havenith, H., Hoffer, B., Charlier, R., Jongmans, D. & Duchesne, J.-C. 1999. The deformation of the Egersund–Ogna anorthosite massif, south Norway: finite-element modelling of diapirism. *Tectonophysics,* 303**,** 109-130.

Bingen, B., Andersson, J., Soderlund, U. & Moller, C. 2008a. The Mesoproterozoic in the Nordic countries. *Episodes,* 31**,** 29-34.

Bingen, B., Boven, A., Punzalan, L., Wijbrans, J. R. & Demaiffe, D. 1998a. Hornblende 40 Ar/39 Ar geochronology across terrane boundaries in the Sveconorwegian Province of S. Norway. *Precambrian research,* 90**,** 159-185.

Bingen, B., Demaiffe, D. & Breemen, O. V. 1998b. The 616 Ma old Egersund basaltic dike swarm, SW Norway, and late Neoproterozoic opening of the Iapetus Ocean. *The Journal of Geology,* 106**,** 565-574.

Bingen, B., Nordgulen, O. & Viola, G. 2008b. A four-phase model for the Sveconorwegian orogeny, SW Scandinavia. *Norsk Geologisk Tidsskrift,* 88**,** 43.

Bingen, B., Stein, H. J., Bogaerts, M., Bolle, O. & Mansfeld, J. 2006. Molybdenite Re–Os dating constrains gravitational collapse of the Sveconorwegian orogen, SW Scandinavia. *Lithos,* 87**,** 328-346.

Bingen, B. & Van Breemen, O. 1998. U-Pb monazite ages in amphibolite-to granulite-facies orthogneiss reflect hydrous mineral breakdown reactions: Sveconorwegian Province of SW Norway. *Contributions to Mineralogy and Petrology,* 132**,** 336-353.

Bolle, O., Besse, M. & Diot, H. 2010. Magma flow and feeder chamber location inferred from magnetic fabrics in jotunitic dykes (Rogaland anorthosite province, SW Norway). *Tectonophysics,* 493**,** 42-57.

Bolle, O. & Duchesne, J.-C. 2007. The Apophysis of the Bjerkreim–Sokndal layered intrusion (Rogaland anorthosite province, SW Norway): A composite pluton build up by tectonically-driven emplacement of magmas along the margin of an AMC igneous complex. *Lithos,* 98**,** 292-312.

Boven, A., Pasteels, P., Kelley, S., Punzalan, L., Bingen, B. & Demaiffe, D. 2001. 40 Ar/39 Ar study of plagioclases from the Rogaland anorthosite complex (SW Norway); an attempt to understand argon ages in plutonic plagioclase. *Chemical Geology,* 176**,** 105-135.

Braathen, A. 1999. Kinematics of post-Caledonian polyphase brittle faulting in the Sunnfjord region, western Norway. *Tectonophysics,* 302**,** 99-121.

Bryhni, I. & Sturt, B. 1985. Caledonides of southwestern Norway. *In:* GEE, D. G. S., B. A. (ed.) *The Caledonide Orogen—Scandinavia and Related Areas.* . Wiley 89-107.

Celerier, B. 1988. How much does slip on a reactivated fault plane constrain the stress tensor? *Tectonics,* 7**,** 1257-1278.

Clauer, N. & Chaudhuri, S. 2012. *Clays in crustal environments: isotope dating and tracing*, Springer Science & Business Media.

Dalrymple, G. B. & Lanphere, M. A. 1969. Potassium-argon dating: Principles, techniques and applications to geochronology. *(Freeman) San Francisco, California.* 258.

Delvaux, D. & Sperner, B. 2003. New aspects of tectonic stress inversion with reference to the TENSOR program. *Geological Society, London, Special Publications,* 212**,** 75-100.

Demaiffe, D., Weis, D., Michot, J. & Duchesne, J.-C. 1986. Isotopic constraints on the genesis of the Rogaland anorthositic suite (southwest Norway). *Chemical Geology,* 57**,** 167-179.
Eide, E. A., Torsvik, T. H. & Andersen, T. B. 1997. Absolute dating of brittle fault movements: Late Permian and late Jurassic extensional fault breccias in western Norway. *Terra Nova,* 9**,** 135-139.
Fossen, H. 1992. The role of extensional tectonics in the Caledonides of south Norway. *Journal of structural geology,* 14**,** 1033-1046.
Fossen, H. 2000. Extensional tectonics in the Caledonides: Synorogenic or postorogenic? *Tectonics,* 19**,** 213-224.
Fossen, H. 2010. *Structural geology*, Cambridge University Press.
Fossen, H. & Dunlap, W. J. 1999. On the age and tectonic significance of Permo-Triassic dikes in the Bergen-Sunnhordland region, southwestern Norway. *Norsk Geologisk Tidsskrift,* 79**,** 169-178.
Fossen, H. & Hurich, C. A. 2005. The Hardangerfjord Shear Zone in SW Norway and the North Sea: a large-scale low-angle shear zone in the Caledonian crust. *Journal of the Geological Society,* 162**,** 675-687.
Fossen, H., Khani, H. F., Faleide, J. I., Ksienzyk, A. K. & Dunlap, W. J. 2016. Post-Caledonian extension in the West Norway–northern North Sea region: the role of structural inheritance. *Geological Society, London, Special Publications,* 439**,** SP439. 436.
Fossen, H. & Rykkelid, E. 1992. Postcollisional extension of the Caledonide orogen in Scandinavia: Structural expressions and tectonic significance. *Geology,* 20**,** 737-740.
Fredin, O., Viola, G., Zwingmann, H., Sørlie, R., Brönner, M., Lie, J.-E., Grandal, E. M., Müller, A., Margreth, A. & Vogt, C. 2017. The inheritance of a Mesozoic landscape in western Scandinavia. *Nature Communications,* 8**,** 14879.
Færseth, R., Macintyre, R. & Naterstad, J. 1976. Mesozoic alkaline dykes in the Sunnhordland region, western Norway: ages, geochemistry and regional significance. *Lithos,* 9**,** 331-345.
Gabrielsen, R., Odinsen, T. & Grunnaleite, I. 1999. Structuring of the Northern Viking Graben and the Møre Basin; the influence of basement structural grain, and the particular role of the Møre-Trøndelag Fault Complex. *Marine and Petroleum Geology,* 16**,** 443-465.
Gabrielsen, R. H., Braathen, A., Dehls, J. & Roberts, D. 2002. Tectonic lineaments of Norway. *Norsk Geologisk Tidsskrift,* 82**,** 153-174.
Gabrielsen, R. H., Faleide, J. I., Pascal, C., Braathen, A., Nystuen, J. P., Etzelmuller, B. & O'donnell, S. 2010. Latest Caledonian to Present tectonomorphological development of southern Norway. *Marine and Petroleum Geology,* 27**,** 709-723.
Gilkes, R., Scholz, G. & Dimmock, G. 1973. Lateritic deep weathering of granite. *Journal of Soil Science,* 24**,** 523-536.
Grohmann, C. H. & Campanha, G. OpenStereo: open source, cross-platform software for structural geology analysis. AGU Fall Meeting abstracts, 2010.
Guermani, A. & Pennacchioni, G. 1998. Brittle precursors of plastic deformation in a granite: an example from the Mont Blanc massif (Helvetic, western Alps). *Journal of Structural Geology,* 20**,** 135-148.
Henderson, I. 2001. 3D-Mapping in the Tellenes Mine. *NGU Report: 2001.118.* Trondheim, Norway: Geological Survey of Norway.
Henderson, I. 2002. Updating of 3D structural mapping of Tellenes Mine. *NGU report: 2002.116.* Trondheim, Norway: Geological Survey of Norway.
Karlsen, T. 1997. Geometry of fracture zones and their influence on the ore quality at the Tellnes ilmenite mine, Rogaland. *NGU report, 97.031*. Trondheim, Norway: Geological Survey of Norway.
Kartverket 2013. http://data.kartverket.no/download/content/digital-terrengmodell-10-m-utm-32. *Downloaded: 06/2016*.
Krause, H., Gierth, E. & Schott, W. 1985. Ti–Fe deposits in the South Rogaland igneous complex with special reference to the Åna-Sira anorthosite massif. *Norges geologiske undersøkelse Bulletin,* 402**,** 25-37.
Ksienzyk, A. K., Dunkl, I., Jacobs, J., Fossen, H. & Kohlmann, F. 2014. From orogen to passive margin: constraints from fission track and (U–Th)/He analyses on Mesozoic uplift and fault reactivation in SW Norway. *Geological Society, London, Special Publications,* 390**,** SP390. 327.

Ksienzyk, A. K., Wemmer, K., Jacobs, J., Fossen, H., Schomberg, A. C., Süssenberger, A., Lünsdorf, N. K. & Bastesen, E. 2016. Post-Caledonian brittle deformation in the Bergen area, West Norway: results from K–Ar illite fault gouge dating. *Norwegian Journal of Geology*, 96.

Larsen, Ø., Fossen, H., Langeland, K. & Pedersen, R.-B. 2003. Kinematics and timing of polyphase post-Caledonian deformation in the Bergen area, SW Norway. *Norwegian Journal of Geology/Norsk Geologisk Forening*, 83.

Lee, J.-Y., Marti, K., Severinghaus, J. P., Kawamura, K., Yoo, H.-S., Lee, J. B. & Kim, J. S. 2006. A redetermination of the isotopic abundances of atmospheric Ar. *Geochimica et Cosmochimica Acta*, 70**,** 4507-4512.

Li, Z.-X., Bogdanova, S., Collins, A., Davidson, A., De Waele, B., Ernst, R., Fitzsimons, I., Fuck, R., Gladkochub, D. & Jacobs, J. 2008. Assembly, configuration, and break-up history of Rodinia: a synthesis. *Precambrian research*, 160**,** 179-210.

Mangerud, J., Gyllencreutz, R., Lohne, Ö. & Svendsen, J. I. 2011. Glacial history of Norway. *Quaternary glaciations - extent and chronology*. Elsevier 279-298.

Marker, M. 2013. Berggrunnskart SOKNDAL 1311 IV, M 1:50 000. *Norges geologiske undersøkelse*.

Marker, M., Schiellerup, H., Meyer, G. B., Robins, B. & Bolle, O. 2003. Geological map of the Rogaland Anorthosite Province. *NGU Special Publication 9 - Plate 1*

Mattila, J. & Viola, G. 2014. New constraints on 1.7 Gyr of brittle tectonic evolution in southwestern Finland derived from a structural study at the site of a potential nuclear waste repository (Olkiluoto Island). *Journal of Structural Geology*, 67**,** 50-74.

Montalbano, S., Diot, H. & Bolle, O. 2016. Asymmetrical magnetic fabrics in the Egersund doleritic dike swarm (SW Norway) reveal sinistral oblique rifting before the opening of the Iapetus. *Journal of Structural Geology*, 85**,** 18-39.

Munro, M. A. & Blenkinsop, T. G. 2012. MARD—A moving average rose diagram application for the geosciences. *Computers & Geosciences*, 49**,** 112-120.

Möller, C., Andersson, J., Lundqvist, I. & Hellström, F. 2007. Linking deformation, migmatite formation and zircon U–Pb geochronology in polymetamorphic orthogneisses, Sveconorwegian Province, Sweden. *Journal of Metamorphic Geology*, 25**,** 727-750.

Pasteels, P. & Michot, J. 1975. Geochronologic investigation of the metamorphic terrain of southwestern Norway. *Norsk geologisk tidsskrift*, 55**,** 34.

Raharimahefa, T. & Kusky, T. M. 2009. Structural and remote sensing analysis of the Betsimisaraka Suture in northeastern Madagascar. *Gondwana Research*, 15**,** 14-27.

Roberts, D. 2003. The Scandinavian Caledonides: event chronology, palaeogeographic settings and likely modern analogues. *Tectonophysics*, 365**,** 283-299.

Rød, J. K. 2015. *GIS-Verktøy for å forstå verden* Trondheim, Norway, Fagbokforlaget.

Scheiber, T., Fredin, O., Viola, G., Jarna, A., Gasser, D. & Łapińska-Viola, R. 2015. Manual extraction of bedrock lineaments from high-resolution LiDAR data: methodological bias and human perception. *GFF*, 137**,** 362-372.

Scheiber, T., Viola, G., Wilkinson, C. M., Ganerød, M., Skår, Ø. & Gasser, D. 2016. Direct 40Ar/39Ar dating of Late Ordovician and Silurian brittle faulting in the southwestern Norwegian Caledonides. *Terra Nova*.

Schärer, U., Wilmart, E. & Duchesne, J.-C. 1996. The short duration and anorogenic character of anorthosite magmatism: U Pb dating of the Rogaland complex, Norway. *Earth and Planetary Science Letters*, 139**,** 335-350.

Segall, P. & Simpson, C. 1986. Nucleation of ductile shear zones on dilatant fractures. *Geology*, 14**,** 56-59.

Smethurst, M. 2000. Land–offshore tectonic links in western Norway and the northern North Sea. *Journal of the Geological Society*, 157**,** 769-781.

Smith, M. & Pain, C. 2009. Applications of remote sensing in geomorphology. *Progress in Physical Geography*, 33**,** 568-582.

Sæter, H. S. B. 2006. *Fault-slip inversion and palaeostress analysis above and below a post-Caledonian Extensional Detachment.* Master thesis, Norwegian University of Science and Technology.

Sørensen, S., Morizot, H. & Skottheim, S. 1992. A tectonostratigraphic analysis of the southeast Norwegian North Sea Basin. *Structural and Tectonic Modelling and its Application to Petroleum Geology***,** 19-42.

Torgersen, E., Viola, G., Zwingmann, H. & Harris, C. 2014. Structural and temporal evolution of a reactivated brittle–ductile fault–Part II: Timing of fault initiation and reactivation by K–Ar dating of synkinematic illite/muscovite. *Earth and Planetary Science Letters,* 407**,** 221-233.

Tvedt, A. B., Rotevatn, A., Jackson, C. a.-L., Fossen, H. & Gawthorpe, R. L. 2013. Growth of normal faults in multilayer sequences: a 3D seismic case study from the Egersund Basin, Norwegian North Sea. *Journal of Structural Geology,* 55**,** 1-20.

Valle, P., Færseth, R. B. & Fossen, H. 2002. Devonian-Triassic brittle deformation based on dyke geometry and fault kinematics in the Sunnhordland region, SW Norway. *Norwegian Journal of Geology/Norsk Geologisk Forening,* 82.

Vander Auwera, J., Bolle, O., Bingen, B., Liégeois, J.-P., Bogaerts, M., Duchesne, J.-C., De Waele, B. & Longhi, J. 2011. Sveconorwegian massif-type anorthosites and related granitoids result from post-collisional melting of a continental arc root. *Earth-Science Reviews,* 107**,** 375-397.

Vidal, G. & Moczydłowska, M. 1995. The Neoproterozoic of Baltica—stratigraphy, palaeobiology and general geological evolution. *Precambrian Research,* 73**,** 197-216.

Viola, G., Henderson, I., Bingen, B. & Hendriks, B. 2011. The Grenvillian–Sveconorwegian orogeny in Fennoscandia: Back-thrusting and extensional shearing along the "Mylonite Zone". *Precambrian Research,* 189**,** 368-388.

Viola, G., Kounov, A., Andreoli, M. & Mattila, J. 2012. Brittle tectonic evolution along the western margin of South Africa: more than 500Myr of continued reactivation. *Tectonophysics,* 514**,** 93-114.

Viola, G., Scheiber, T., Fredin, O., Zwingmann, H., Margreth, A. & Knies, J. 2016. Deconvoluting complex structural histories archived in brittle fault zones. *Nature Communications,* 7.

Viola, G., Venvik Ganerød, G. & Wahlgren, C. H. 2009. Unraveling 1.5 Ga of brittle deformation history in the Laxemar-Simpevarp area, southeast Sweden: A contribution to the Swedish site investigation study for the disposal of highly radioactive nuclear waste. *Tectonics,* 28.

Viola, G., Zwingmann, H., Mattila, J. & Käpyaho, A. 2013. K-Ar illite age constraints on the Proterozoic formation and reactivation history of a brittle fault in Fennoscandia. *Terra Nova,* 25**,** 236-244.

Westphal, M., Schumacher, J. C. & Boschert, S. 2003. High-temperature metamorphism and the role of magmatic heat sources at the Rogaland anorthosite complex in Southwestern Norway. *Journal of Petrology,* 44**,** 1145-1162.

Will, G. 2006. *Powder diffraction: The Rietveld method and the two stage method to determine and refine crystal structures from powder diffraction data,* Springer Science & Business Media.

Wise, D. U., Funiciello, R., Parotto, M. & Salvini, F. 1985. Topographic lineament swarms: clues to their origin from domain analysis of Italy. *Geological Society of America Bulletin,* 96**,** 952-967.

Zwingmann, H., Mancktelow, N., Antognini, M. & Lucchini, R. 2010. Dating of shallow faults: New constraints from the AlpTransit tunnel site (Switzerland). *Geology,* 38**,** 487-490.

Appendix A: K-Ar – dating method

K-Ar- dating is a radiometric dating method used in geochronology. The method is based on radioactive decay of potassium (^{40}K) into Argon (^{40}Ar). Potassium is a common element in the Earth crust and are present in many minerals, such as clays and micas. Brittle fault rocks have a high content of clays and this method therefore offers the potential to generate absolute timing of faulting. This method is based Dalrymple and Lanphere (1969) and procedures at the laboratory at NGU.

K

Potassium have a half-life of 1.25 Ma and decays to ^{40}Ar. Because of the long half-life of ^{40}K, it allows the method to calculate absolute age of rock or clay samples. To find the concentration of K, minimum 30 mg of clay is dissolved in $LiBO_4$ at 800°C. Further, HNO_3 is added and dissolves the sample completely with a solution of all the major elements and trace elements. The wt% of ^{40}K is then measured and converted into moles.

$$\frac{K\ wt\%}{Total\ wt\%}$$

Convert into moles:

$$\frac{K\ wt\% * Abundance\ of\ 40K\ in\ total\ K}{100 * molar\ mass\ of\ total\ K} = {}^{40}K\ \left(\frac{g}{mol}\right)$$

Where abundance of ^{40}K in total K is a constant, molar mass of total K is known and K wt% is measured by the method.

Ar

Argon is a noble gas and due to the complete electron shelf, it rather stays alone than reacting with other atoms or molecules. This property makes it easy for argon to release from potassium while heating. The three main isotopes of argon found on Earth are ^{36}Ar, ^{38}Ar and ^{40}Ar. In air there is a constant relationship between these three isotopes (Lee et al., 2006);

$$\left(\frac{40_{Ar}}{36_{Ar}}\right)_{Air} = 298.56$$

$$\left(\frac{36_{Ar}}{38_{Ar}}\right)_{Air} = 0.189431$$

The concentration of Ar in the sample is measured by a special designed mass spectrometer build at NGU and managed by Roelant van der Lelji:

The sample is enfolded in molybdenum and placed in vacuum to obtain a closed system as possible. Then, the heat from a furnace heats the sample up to 1400°C and the argon gas, together with other gases, vaporizer and goes through a system of valves to make sure the gas is completely mixed. Getters is used to remove all the undesirable gases. A chemical reactive

cell in the getters removes the undesirable gases from the system leaving only the noble gases behind. To be able to measure the actual radioactive ^{40}Ar in the sample, a known amount of $^{38}Ar_{Trace}$ is mixed into the gas as a reference. Further, valves close to the furnace are locked and the valves with gas close to the mass spectrometer are isolated from the rest of the instrument. Two last getters remove the rest of the gases except argon. The mass spectrometer is underpressured to avoid atmospheric argon into the spectrometer. The underpressured pump is then closed and a valve is opening to let the sample gas into the mass spectrometer for 70 seconds. During this time, the mass spectrometer does not measure any signals. An electromagnetic field consisting of two plates with high differential voltage focuses the gas, then, a beam shoots the atoms with electrons which charges the atom positively. This process is explained by Lorentz Law:

$$\vec{F} = q\vec{V}x\vec{B}$$

Where q= the electron, B=magnetic field, V= the velocity of the particle and F=the force applied on the particle. The atoms go through a magnet and a signal from the atoms is measured. The mass spectrometer measure voltage as time goes. To get the voltage at t_0, a regression line is calculated. All the three isotopes are measured by the mass spectrometer to assess how much of the total argon is of atmospheric origin. The concentration of ^{40}Ar this found by these calculations.

$$^{40}Ar_{Air} = {}^{36}Ar_{Sample}\left(\frac{40_{Ar}}{36_{Ar}}\right)_{Air} \quad , \quad {}^{38}Ar_{Air} = {}^{36}Ar_{Sample}\left(\frac{38_{Ar}}{36_{Ar}}\right)_{Air}$$

$$^{40}Ar_{Sample} = {}^{40}Ar_{Air} + {}^{40}Ar^* \rightarrow {}^{40}Ar^* = {}^{40}Ar_{Sample} - {}^{36}Ar_{Sample}\left(\frac{40_{Ar}}{36_{Ar}}\right)_{Air}$$

$$^{38}Ar_{Sample} = {}^{38}Ar_{Air} + {}^{38}Ar_{Trace} \rightarrow {}^{38}Ar_{Trace} = {}^{38}Ar_{Sample} - {}^{36}Ar_{Sample}\left(\frac{38_{Ar}}{36_{Ar}}\right)_{Air}$$

Then, $^{40}Ar^*$ is divided by the known $^{38}Ar_{Trace}$:

$$\frac{40_{Ar*}}{38_{Ar}Trace} = {}^{40}Ar_{Sample} - {}^{36}Ar_{Sample}\left(\frac{40_{Ar}}{36_{Ar}}\right)_{Air} / {}^{38}Ar_{Sample} - {}^{36}Ar_{Sample}\left(\frac{38_{Ar}}{36_{Ar}}\right)_{Air} \rightarrow$$

$$\underline{^{40}Ar^*} = ({}^{40}Ar_{Sample} - {}^{36}Ar_{Sample}\left(\frac{40_{Ar}}{36_{Ar}}\right)_{Air} / {}^{38}Ar_{Sample} - {}^{36}Ar_{Sample}\left(\frac{38_{Ar}}{36_{Ar}}\right)_{Air}) * {}^{38}Ar_{Trace}$$

Voltage is converted to moles:

$\frac{40_{Ar*}\,(Volts)}{38_{Ar}Trace\,(Volts)} * 38_{Ar}Trace\,(mol) = 40_{Ar*}(mol)$, where $38_{Ar}Trace\,(mol)$ is known from the tracer.

Now both ^{40}K (mol) and ^{40}Ar (mol) is known and the Age equation is used to find the absolute age of the sample.

$$t(yr) = 1.80408 * 10^9 * \ln\left[9.540445 * \frac{40_{Ar*}}{40_K} + 1\right]$$